JAERI-Conf
95-020

PROCEEDINGS OF THE MEETING ON TUNNELING REACTION AND LOW TEMPERATURE CHEMISTRY, 95 JULY

July 31~August 1, 1995, Tokai, Japan

October 1995

(Eds.) Tetsuo MIYAZAKI* and Yasuyuki ARATONO

日本原子力研究所
Japan Atomic Energy Research Institute

本レポートは，日本原子力研究所が不定期に公刊している研究報告書です。

入手の問合わせは，日本原子力研究所技術情報部情報資料課（〒319-11 茨城県那珂郡東海村）あて，お申し越しください。なお，このほかに財団法人原子力弘済会資料センター（〒319-11 茨城県那珂郡東海村日本原子力研究所内）で複写による実費頒布をおこなっております。

This report is issued irregularly.

Inquiries about availability of the reports should be addressed to Information Division, Department of Technical Information, Japan Atomic Energy Research Institute, Tokai-mura, Naka-gun, Ibaraki-ken 319-11, Japan.

編集兼発行　日本原子力研究所
印　　刷　いばらき印刷㈱

The Meeting on Tunneling Reaction and Low Temparature Chemistry, 95 July - Tunneling Reaction and Cryotechnique-

July 31 ~ August 1, 1995

Japan Atomic Energy Research Institute
Tokai, Japan

Sponsored and Organized
by
Advanced Science Research Center,
Japan Atomic Energy Research Institute

Japanese Society of Radiation Chemistry

Supported
by
Chemical Society of Japan

JAERI-Conf 95-020

Proceedings of the Meeting on Tunneling Reaction and Low Temperature Chemistry, 95 July

July 31 - August 1, 1995, Tokai, Japan

(Eds.) Tetsuo MIYAZAKI* and Yasuyuki ARATONO

Advanced Science Research Center
Japan Atomic Energy Research Institute
Tokai-mura, Naka-gun, Ibaraki-ken

(Received September 14, 1995)

Tunneling reaction that is caused by quantum tunneling of atoms or molecules is a new type of chemical reactions. Since tunneling reaction takes place at ultralow temperature below 77K, it has destroyed the common knowledge that any chemical reactions cannot occur at ultralow temperature where atoms and molecules are completely frozen and thus it has opened a new field of low temperature chemistry.

Tunneling reaction and low temperature chemistry are related to many problems in different fields, such as physical chemistry, radiation chemistry and photochemistry, radiation physics, and solid state physics. Studies on tunneling reaction need special cryotechnique. Thus, we have organized the meeting on tunneling reaction and its related problems as well as cryotechnique by attendance of specialists from different fields. The number of participants in this meeting is 35 and 14 invited lectures are presented there. We believe that the proceedings of the meeting will contribute to understanding of tunneling reaction and its related problems.

The editors wish to thank Mr. Takayuki Kumada, of low temperature chemistry research group of Advanced Science Research Center, for his assistance in preparation of the meeting and in editing the proccedings.

Keywords: Tunneling Reaction, Low Temperature Chemistry, Cryotechnique, Radiation Chemistry

---

* Nagoya University

JAERI-Conf 95-020

トンネル反応および低温化学についての研究会報告集
1995年7月31日－8月1日、東海村

日本原子力研究所先端基礎研究センター
（編）宮崎　哲郎*・荒殿　保幸

（1995年9月14日受理）

トンネル反応とは原子または分子のトンネル効果によって引き起こされる反応で新しい型の化学反応と言える。トンネル反応は77K以下の極低温でも反応が起こり、極低温では化学反応は起こり得ないと考えられていた従来の概念を覆すものである。またトンネル反応は低温化学と言う新しい分野を誕生させた。

トンネル反応と低温化学は様々な分野の問題とも関連している。特に物理化学、放射線化学、光化学、低温有機化学、放射線物理学、物性物理学などとは関係が深い。極低温でトンネル反応を研究するためには、特別の実験技術が必要となる。今回、トンネル反応と関連課題さらに極低温実験技術について研究会を開催した。研究会の出席者は35名で種々の分野の専門家から成っている。14件の講演がなされ、その概要を報告集としてまとめた。この報告集がトンネル反応およびその関連課題の解明の一助になれば幸いである。

なお、本研究会の開催および報告集の編集にあたっては、先端基礎研究センター、原子トンネル反応研究グループの熊田高之氏に多くの助力をお願いした。

記して感謝する。

日本原子力研究所：〒319－11　茨城県那珂郡東海村白方白根2－4
＊名古屋大学

Contents

目　　次

Preface

New Era in Tunneling Science

Muneyuki Date

Director of Advanced Science Research Center, JAERI

Tunneling, it is a typical quantum mechanical phenomenon and the first example was the α-decay from a radioactive nucleus around 1930. This means that the α-particle in a nuclear potential escapes through the potential barrier and the phenomenon has been understood by considering the wavy nature of the particle with exponential tails toward outside.

The second progress has been achieved in condensed matters. The electron tunneling through semiconductor barriers by Esaki, superconducting tunneling through the gap by Giaever and discovery of the Josephson effect in a superconducting link have been reported around 1960 and they got the Nobel Prize.

The third stage of the quantum tunneling has come now in the field of chemistry. It is quite natural that the basic physical principle soon transfers into chemistry and biology.

There is an increasing interest in the application of the quantum tunneling to chemical reactions. The tunneling just discussing is classified into the atomic tunneling. Light atoms such as proton have large amplitude of the zero-point vibration even at low temperatures so that the reaction probabilities through the molecular potential still remains at liquid helium temperatures where usual chemical reactions are believed to be inactive. Moreover, the rate of the tunneling reaction is expected to be enhanced by decreasing temperature because the atomic arrangement becomes regular at low temperatures. Accordingly one can anticipate the opening of an age of low temperature chemical reactions induced by the quantum tunneling of light atoms.

It is also emphasized that the tunneling reactions is not limited in the in-door science. Recently, it is reported that the interstellar chemical reaction rate is unbelievably fast if only usual reaction processes are taken into account. This should also be explained by introducing the tunneling reactions.

Professor Miyazaki, a pioneer of the chemical tunneling reactions, has organized a research group of this field in the Advanced Science Research Center, JAERI and the systematic study is going on. I hope that a new era of the tunneling science is achieved with novel findings in the low temperature chemical reactions.

Importance of Tunneling Reactions

Tetsuo Miyazaki, Chairman of the Meeting

It has been accepted generally that chemical reactions take place by passing over the potential energy barrier for a reaction (cf. a classical reaction in Fig. 1). A hydrogen atom, a proton, or a hydrogen molecule can be considered as quantum particles because of their small mass that can pass through a potential energy barrier by a quantum-mechanical tunneling caused by a wave character of them. Recently it has been found that the reaction of transfer of a hydrogen atom, a proton, or a hydrogen molecule take place at low temperatures by passing through the potential energy barrier for a reaction by a tunneling effect (cf. Fig. 1). Since the classical reaction in Fig. 1 is suppressed completely below 77 K, we can study only tunneling reactions at low temperature.

Tunneling reactions have the following characteristic points. First, the activation energy for the reaction is nearly zero. Thus, the reaction occurs at very low temperature, giving birth to the new field of low-temperature-chemistry. A part of organic substances in cosmos that are related to the origin of life may be formed by tunneling reactions in dark clouds at very low temperature. Second, a high selectivity and a large isotope effect are observed in the tunneling reaction. The high selectivity in reactions will give a fascinating process in organic synthesis. The large isotope effect may be used for separation of hydrogen isotopes in nuclear-fusion technology. Third, since a tunneling reaction is caused by a wave character of an atom, it is an universal chemical reaction, creating a new paradigm in the theory of a chemical reaction. A tunneling of an atom in a reaction is related to recent topics of solid-state-physics, such as a quantum diffusion of muons and hydrogen atoms. Most of biological reactions in cells are hydrogen-atom(or proton)-transfer reactions of free radicals, in which tunneling reactions may play an important role . Therefore, the tunneling reactions are related to topics of physics, biology, astronomy, and nuclear fusion in addition to chemistry(cf. Fig. 2).

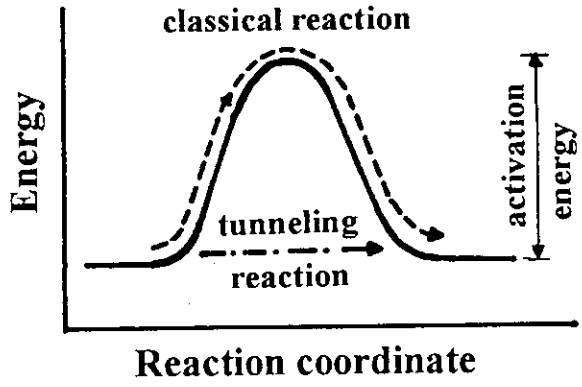

Fig. 1. Energy along the reaction coordinate

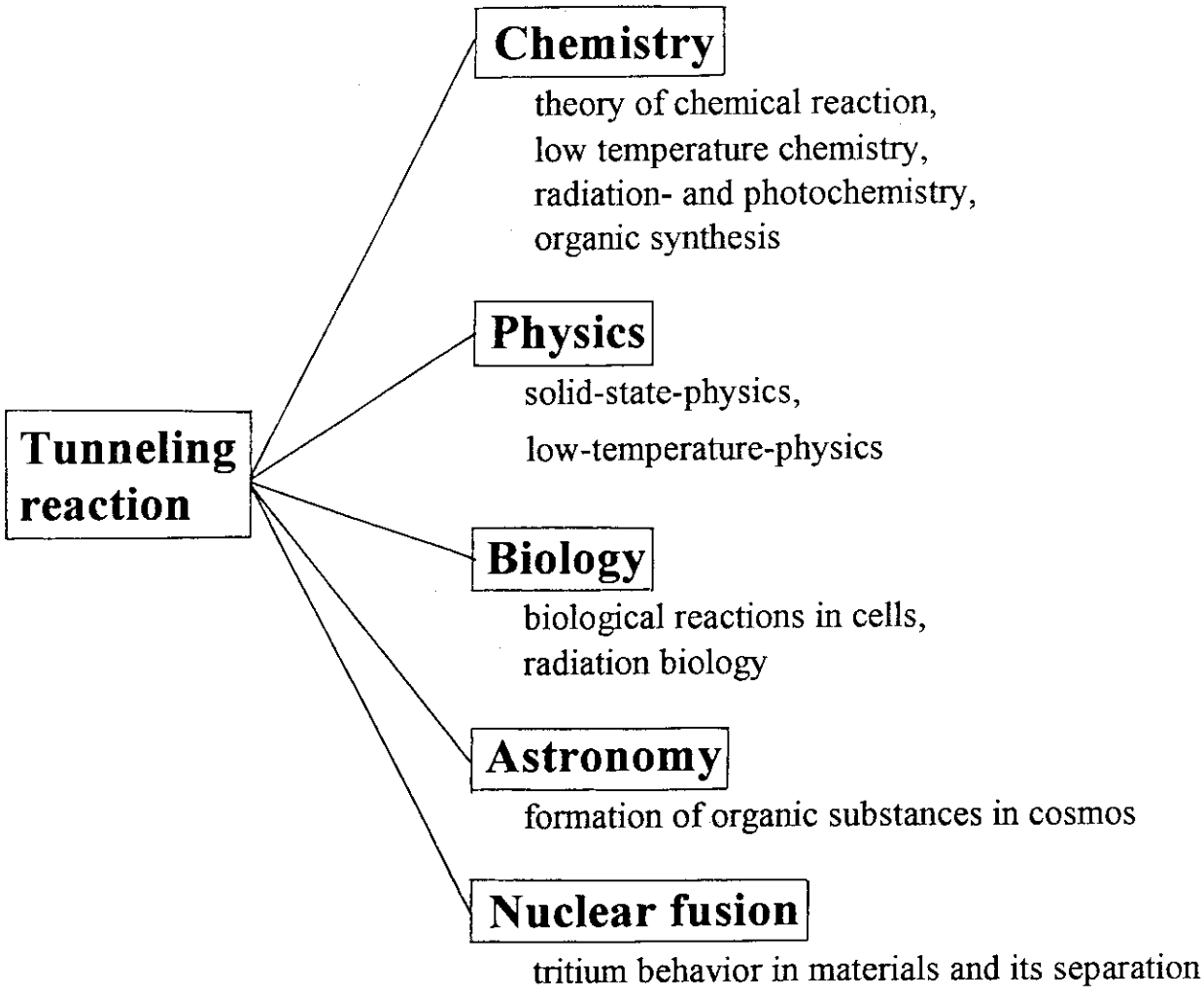

Fig. 2. Tunneling reaction and its related fields

1. Tunneling Reactions Studied by ESR and Pulse Radiolysis at Very Low Temperatures

Tetsuo Miyazaki

Department of Applied Chemistry, School of Engineering,
Nagoya University, Chikusa-ku, Nagoya 464-01, JAPAN

Research Group for Tunneling Reaction,
Advanced Science Research Center,
Japan Atomic Energy Research Institute,
Tokai-mura, Ibaraki 319-11, JAPAN

Introduction

Chemical reactions caused by a quantum-mechanical tunneling of an atom or a molecule can be studied at ultralow temperature below 77 K, since the general reactions that take place by passing over the potential energy barrier for a reaction are suppressed completely at this temperature. In this report experimental methods for study of tunneling reactions are described briefly and the examples of the tunneling reactions studied by these methods are summarized.

Experimental methods

1. ESR cryostat for storage of long time at ultralow temperature

Tunneling reactions of free radicals, atoms, or ions that were produced at first by irradiation with γ-rays or UV-light can be studied by ESR spectroscopy. In the reaction of hydrogen atoms with hydrogen molecules in solid hydrogen below 4.2 K, some type of tunneling reactions takes place in about 100 hr. Thus, the irradiated samples should be stored in liquid helium for more than 100 hr. Figure 1 shows an ESR cryostat used for storage of more than 100 hr at 4.2 K. The quartz cryostat was made by Eikosha Co. (Osaka, Japan). The cryostat consists of two parts; one for liquid helium and the other for liquid nitrogen. The cryostat for liquid helium is evacuated by a vacuum pump during the storage of sample.

2. Pulse radiolysis at very low temperature

When a tunneling reaction takes place fast, the pulse radiolysis is an useful technique. Figure 2 shows a setup of pulse radiolysis at very low temperature. The

temperature of the sample was controlled by the use of an Oxford CF 1204 cryostat using liquid helium. Pulse irradiations were made by using 2-MeV electron beams generated with a Febetron 707 accelerator. The pulse duration was 20 ns. The radiation dose delivered by each pulse is about 0.6 kGy. One severe requirement for this study is that the sample should be transparent even at very low temperature.

Results

Since a number of studies on tunneling reactions have been reported by us, the studies are classified into several types of reactions.

1. Tunneling reactions H(D) + H_2(HD, D_2)[1,2]

The conclusive evidences for tunneling reactions of H(D) atoms with H_2(HD, D_2) molecules at ultralow temperatures were obtained. The absolute rate constants for the reactions, measured experimentally, were compared with theoretical values calculated by others.

2. Effect of rotational quantum states (J=0, 1) on tunneling reactions H(T) + H_2[3]

The ratio of the rate constant for the tunneling reaction H(T) + H_2(J=0)→ H_2(HT) + H to that for the tunneling reaction H(T) + H_2(J=1) → H_2(HT) + H was estimated experimentally as about 4.

3. High selective hydrogen-atom-abstraction reaction by H atoms deduced by tunneling effect[1,4]

When H atoms are produced by the γ-radiolysis of solvent alkane or by the photolysis of HI in the alkane mixtures at 77 K, the H atoms abstract hydrogen atoms very selectively from alkane solutes at low concentratrion, caused by tunneling. The selective hydrogen-atom-abstraction was confirmed both by ESR measurement of free radicals and by the analysis of final products.

4. Tunneling detachment of H_2 molecule from dimethylbutane cation[5]

H_2-molecule-elimination from 2,3-dimethylbutane(h-DMB) cations, produced by γ-irradiation of h-DMB-SF_6 mixtures at 70 K, forms fast tetramethylethylene cations at 77K.

$(CH_3)_2CHCH(CH_3)_2^+ \rightarrow (CH_3)_2C{=}C(CH_3)_2^+ + H_2$

D_2-molecule-elimination from 2,3-dimethylbutane-2,3-d_2 cations, however, takes place very slowly at 77 K. The significant isotope effect (k(H_2-elimi)/k(D_2-elimi) $=1.7\times10^4$) was explained in terms of a model of the tunneling elimination of a hydrogen molecule from a DMB^+ ion.

5. Tunneling proton-transfer-reaction from ethanol to benzene anion[6]

When ethanol-benzene mixtures are irradiated by γ-rays or pulse electrons at 77 K, cyclohexyl radicals are produced by the following proton transfer reaction.

$$C_6H_6^- + C_2H_5OH \rightarrow C_6H_7 + C_2H_5O^-$$

The reaction is retarded in deuterated ethanol. The large isotope effect ($k(C_2H_5OH)/k(C_2D_5OD) \geq 100$) was ascribed to a tunneling effect on the reaction.

References

1. T. Miyazaki, Radiat. Phys. Chem., *37*, 635 (1991).
2. T. Miyazaki, S. Kitamura, H. Morikita, and K. Fueki, J. Phys. Chem., *96*, 10331 (1992).
3. Y. Fujitani, T. Miyazaki, N. M. Masaki, Y. Aratono, and E. Tachikawa, Chem. Phys. Lett., *214*, 301 (1993).
4. B. Tilquin, C. Gourdin-Serveniere, T. Miyazaki, and K. Fueki, Bull. Chem. Soc. Jpn., *57*, 2029 (1984).
5. T. Miyazaki, S. Kitamura, Y. Kozono, and H. Matsunaga, J. Phys. Chem., *98*, 10767 (1994).
6. T. Miyazaki, T. Shiba, K. Fueki, and Y. Kamiya, J. Phys. Chem., *95*, 9115 (1991).

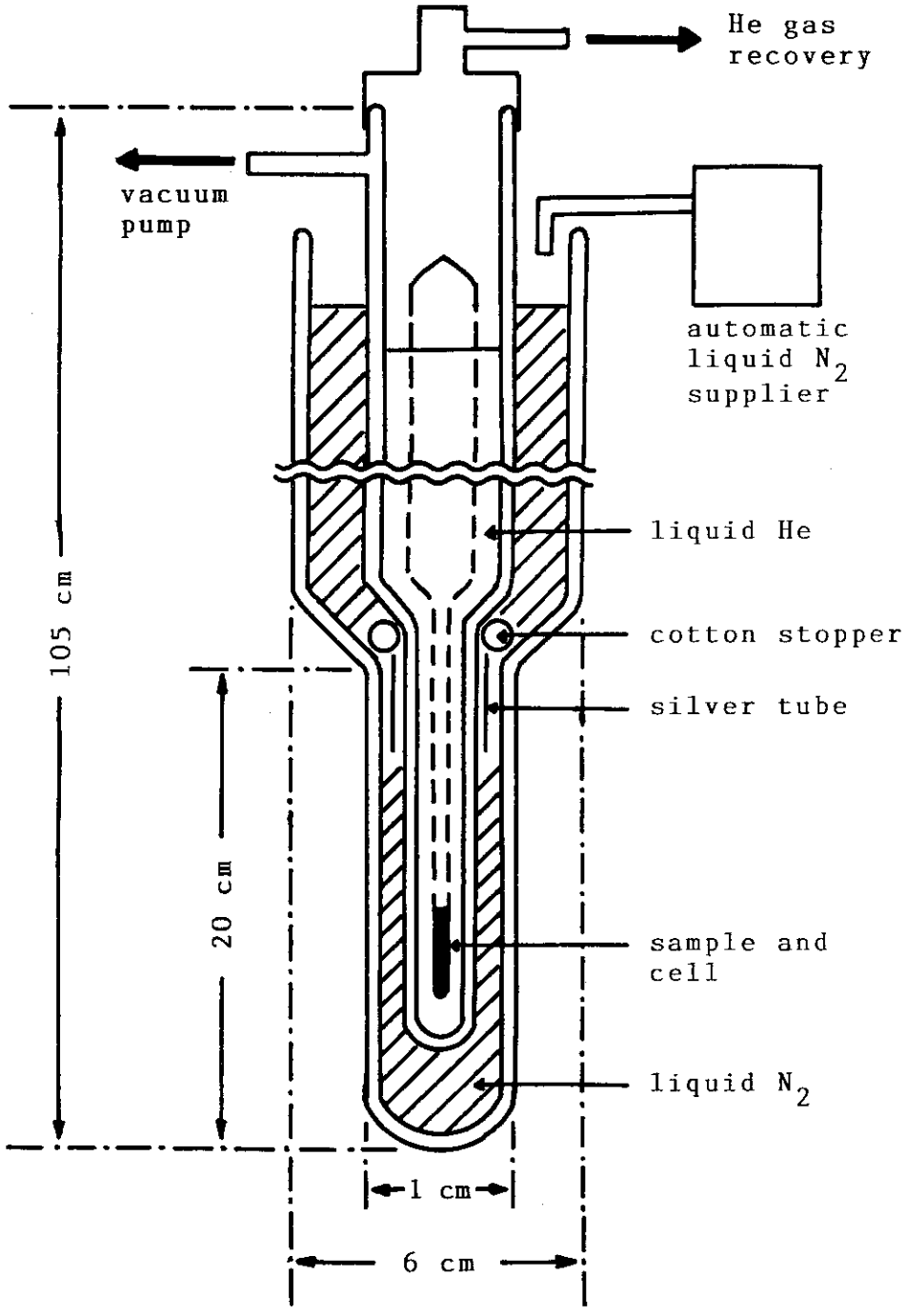

Fig. 1. ESR cryostat used for storage for more than 100 hr at 4.2 K.

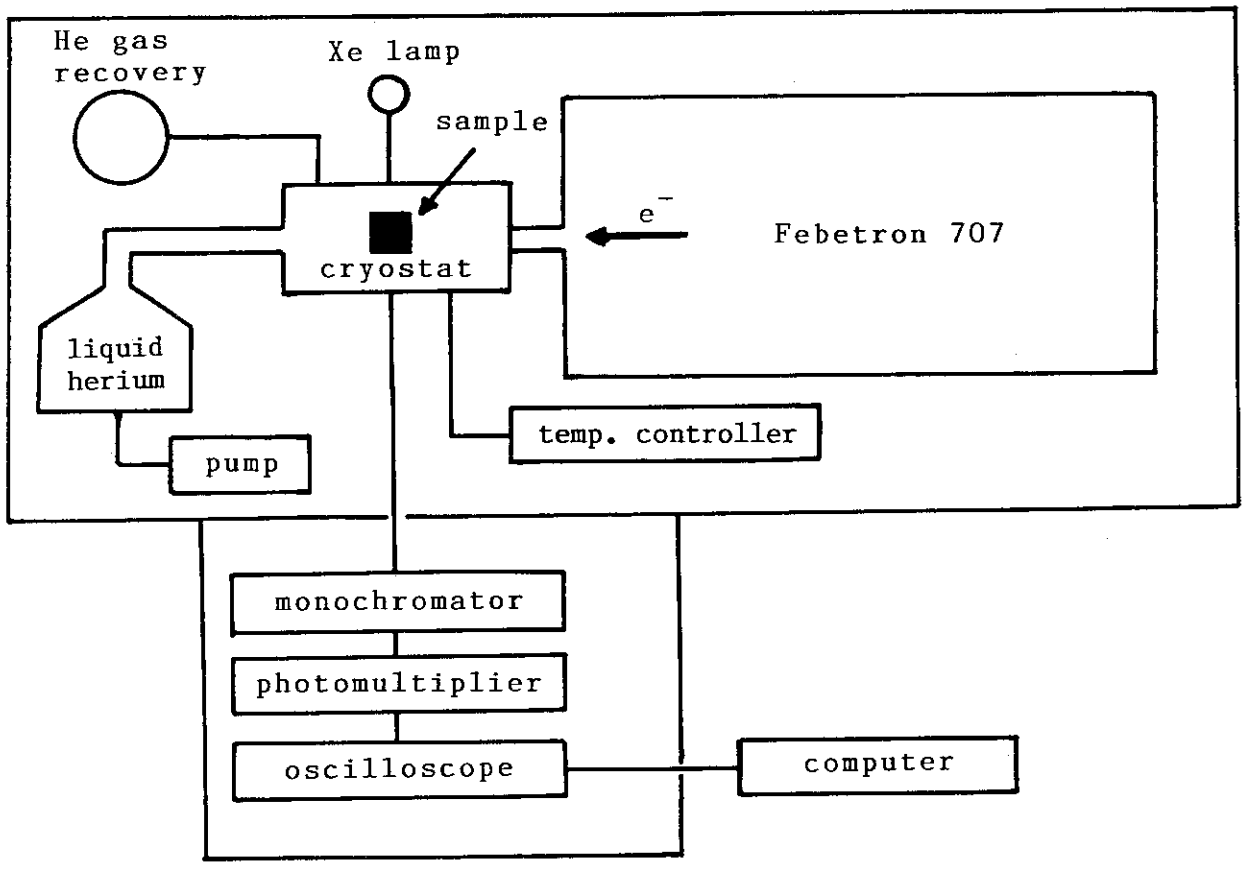

Energy of electron : 2 MeV
Dose of one pulse : 0.6 kGy
Electron-pulse duration : 20 ns
Temperature : 5 - 300 K

Fig. 2. Setup of pulse radiolysis at very low temperature.

2. ESR Studies on the Radiolysis of Crystalline Materials at Cryogenic Temperatures

National Industrial Research Institute of Nagoya,
Hirate-cho, Kita-ku, Nagoya, 462 Japan
Kaoru Matsuura, Takeshi Kusumori, and Hachizo Muto*

ABSTRACT

Presently we report our recent works on the radiolysis of crystalline materials that were studied mainly by ESR spectroscopy. They include A) hydrocarbon radiolysis using hydrocarbon mixed crystals with hydrocarbon having a different molecular chain length, alkenes, and with alkynes, B)the structure and reactions of extremely unstable ions of alkenes, alkynes, and halogenated alkanes trapped in crystalline matrices at cryogenic temperatures, and C)transfer and reactions of electrons, holes, and H atoms, and H/D isotope effects in the radiolytic reactions of hydrocarbons and H_2O/ D_2O mixed crystals.

INTRODUCTION

The transfer of small particles such as electrons, holes, and H atoms plays an important role in the solid state reactions, especially at low temperatures, since molecules and large fragments are difficult to diffuse. The transfer and reactions of these particles may differ from those in glassy solids and may depend on the crystalline structures. The study of the structure dependencies would provide a better understanding for the solid state reactions including the radiolysis of hydrocarbons. Hydrocarbon is one of the most fundamental and important organic compounds and the radiolysis mechanism is still open to question.[1,2] These circumstances have stimulate us to investigate the above subject A) and C) including H/D isotope effect and tunneling reactions.[3-14] Low-temperature solids serve as suitable matrices for trapping and studying unstable reaction intermediates such as trapped electrons and radical ions. However, the studies were carried out mainly using glassy solids such as 3-methylpentane, tetrahydrofuran, and alkali glass rather than crystalline matrices, because of the high solubility of solute molecules. One of the authors(H.M.) had studied the low-temperature radiolysis of succinic acid single crystals doped with an impurity amount of fumaric acid having a similar molecular frame work. It was found that the latter molecules efficiently trapped the radiation-induced electrons.[15] Besides, on the way studying subject A), we found that the electrons were stably trapped in the crystalline defects of binary hydrocarbon mixed crystals having different chain lengths.[3] From these results, we have

* The correspondence should be addressed.

studied the above subject B) in order to trap and to investigate the anion and cation of alkenes and alkynes using alkane crystalline matrices with a similar molecular frame.[7-12] These ions were never detected because of their extreme instabilities. Similar radiolysis studies by aide of single crystal analysis have been carried out for halogenated alkanes including carbon tetrachloride,[16-21] which radiolysis mechanism was not clarified in spite of being one of the most useful electron scavengers in radiation chemistry.

A)Radiolysis of hydrocarbon mixed crystals

In normal hydrocarbon crystals, molecules are oriented and packed by making molecular layer structures as shown in Fig.1. The n-hydrocarbons with carbon number $6 \leq m \leq 9$ have a triclinic crystal structure, and in C_{10}-C_{25} alkanes, those with the even number of carbons have also a triclinic structure and those odd numbers have an orthorhombic structure.[3] Two kinds of crystals have different molecular packing and boundary width in the layer boundary regions.

First, we studied the low-temperature radiolysis and the role of defects of binary n-hydrocarbon mixed crystals with different chain lengths. Evidence has been obtained to show that the radiation-induced electrons are trapped in the mixed crystals at 77 and 4.2 K in contrast to the absence of trapped electrons in the neat n-alkanes (Fig.2) together with the following results on the trapping site.[3] The ESR line width(ΔH_{msl}) of trapped electrons (reflecting the effective defect size) correlates with the chain-length difference(Δm) between two n-alkanes (Fig.3). An increase of

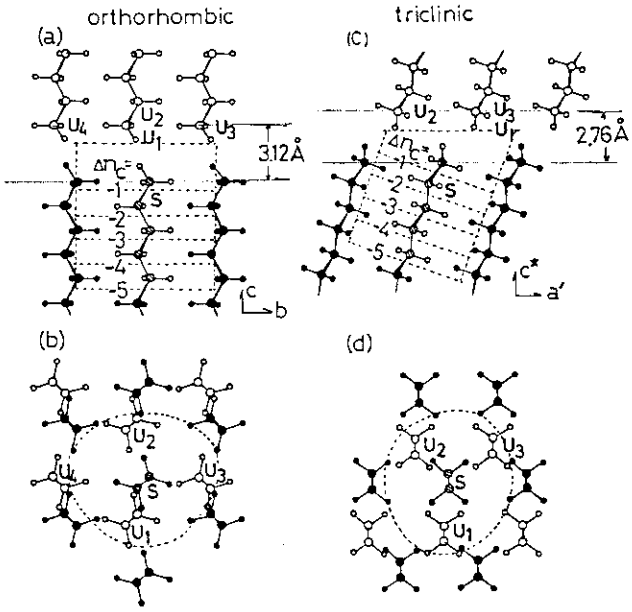

Fig.1 Crystal structures of (a), (b) orthorhombic and (c), (d) triclinic *n*-alkanes. (b) and (d) are the projections along the molecular chain axis. The areas enclosed by dotted lines show (a), (c) the longitudinal section and (b), (d) the radial section of the cylindrical void expected in the case where the position designated by S is occupied by the solute molecule having shorter chain length by Δn_c than the matrix one.

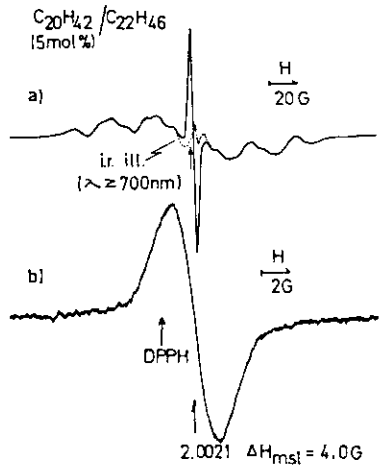

Fig.2 ESR spectra of (a) $C_{20}H_{42}$ (5 mol %)/$C_{22}H_{46}$ mixed crystal irradiated and observed at 77 K and (b) the trapped electrons. (b) is obtained by subtracting the spectrum after photobleached by IR light from (a).

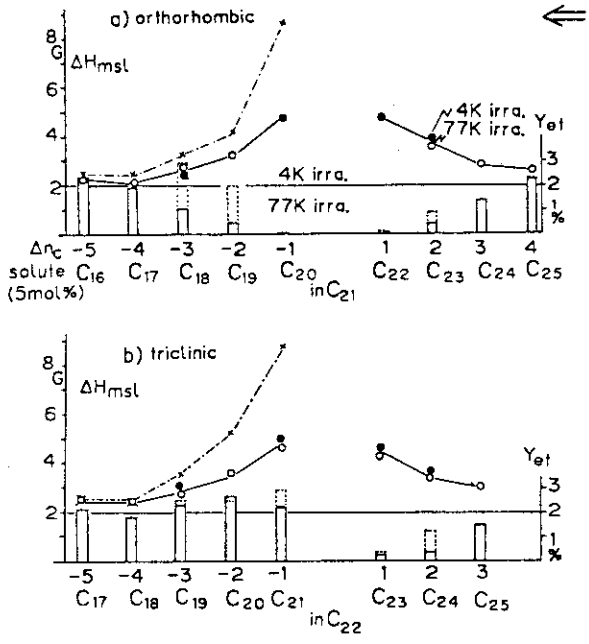

Fig.3 Dependences of the yield Y_{te} and the ESR line width ΔH_{msl} of trapped electrons on the difference (Δn_c) between the number of carbons of solute and matrix molecules in mixed crystals of binary *n*-alkanes. (a) $C_{21}H_{44}$ and (b) $C_{22}H_{46}$ are employed as the matrices with orthorhombic and triclinic structures, respectively. Solid and dotted bars represent the observed yield Y_{te} by the 77 and 4 K irradiations, and ○ and ● represent the observed width ΔH_{msl} at the irradiation temperatures, respectively. x indicates the calculated width (see text).

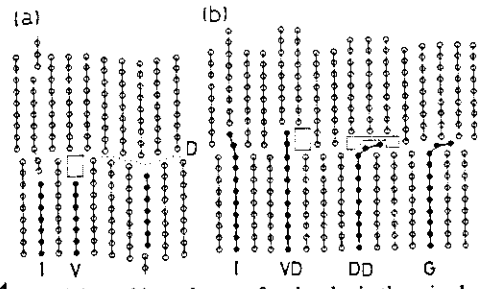

Fig.4 Possible packing schemes of molecules in the mixed crystal of binary *n*-alkanes having orthorhombic structure in the cases with (a) shorter and (b) longer solute molecules (black sticks) than the matrix. V, D, and I indicate the schematic drawing of void, dislocation, and the interweaving of the molecular chain ends without the creations of voids, respectively. DD and VD in (b) show the possible defect and void created by dislocations around the longer solute molecules at the layer boundary.

Δm gives a higher yield of the trapped electrons probably because of a stabilization due to an expansion of the defect size. The number of defects accessible to the electrons at 77 K depends on the crystal structures, being slightly larger in triclinic crystal than in orthorhombic crystals. The effect of deuteriation of the molecules on ΔHmsl (C_8-d/C_{10}-h, C_8-h/C_{10}-d, C_8-d/C_{10}-d) in addition to the above results suggests that the trapping site is a crystalline lattice defect created by inhomogeneous contacts of the different chain-length molecules at the layer boundary, and that pre-existing defects such as voids are necessary for electrons to be trapped in crystalline n-alkanes(Fig.4). The amount of the trapped electrons was about 3 % or less of the total radical yield, indicating that free electrons which have escaped from the geminate recombination are trapped.

Secondly, the radiolysis study of C_mH_{2m+2} (m=7-12; 1 mol%)/$C_{10}D_{22}$(m=7-12) mixed crystals of binary n-alkanes was studied by ESR spectroscopy to understand the role of defects and H/D isotope effect in the radical formation in crystalline organic compounds.[4] Efficient (10-25 %) and selective formation of the protiated solute radicals depending on the carbon-chain difference Δm between solute and matrix molecules was found in the mixed crystals(Δm=-3~ +2) irradiated at 77 K. The terminal type of radical (I) is formed only in the mixed crystals with shorter solute molecules than the matrix(m<10: Δm<0) and is the only solute radical in the case of $\Delta m \leq -2$ (Fig.5).

$C'H_2$-CH_2-CH_2- (I)

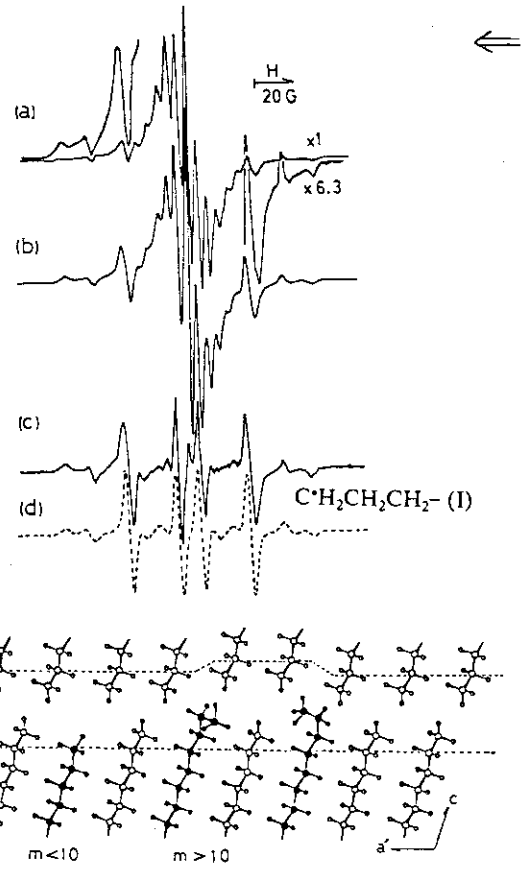

Fig. 7 Possible molecular packing schemes in $C_mH_{2m+2}/C_{10}D_{22}$ mixed crystals (having a triclinic crystal structure) with (a) shorter ($m < 10$) and (b) longer solute molecules ($m > 10$) than the matrix molecules (see text).

Fig.5 Observed ESR spectra for (a) C_7H_{16} (1 mol %)/$C_{10}D_{22}$ and (b) C_8H_{18} (1 mol %)/$C_{10}D_{22}$ mixed crystals irradiated at 77 K. (c) ESR spectrum of the solute radicals, which is obtained by subtracting the matrix spectrum from (b). (d) ESR spectral simulation for $C^{\bullet}H_2CH_2CH_2-$ radical (see text).

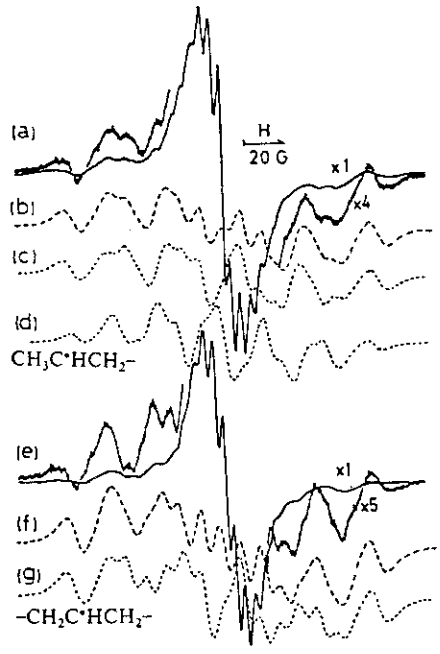

Fig.6 Observed ESR spectra for (a) $C_{11}H_{24}$ (1 mol %)/$C_{10}D_{22}$ and (e) $C_{12}H_{26}$ (1 mol %)/$C_{10}D_{22}$ mixed crystals irradiated at 77 K. (b) and (f) show the simulated ESR spectra for the protiated solute radicals formed in the mixed crystals. (b) and (f) are obtained by adding the simulated component spectra for (d) $CH_3C^{\bullet}HCH_2-$ to those for (c) and (g) $CH_2C^{\bullet}HCH_2-$ radicals in the two mixed crystals, respectively (see text).

Penultimate type radicals(II) and interior type radicals(III) are formed selectively in the case of $\Delta m \geq 0$(Fig.6).

CH3C'HCH2- (II) -CH2C'HCH2- (III)

This efficient and selective formation was neither observed in the mixed crystals irradiated at 4 K nor in those of the protiated-alkane matrix C10H22) irradiated at 77 K or 4 K.

The details of this process are concluded as follows. Deuterium atoms radiolitically produced from the matrix molecules can diffuse and some of them escape to the boundary regions at 77 K. They can migrate for some distance in the regions(with looser molecular packing than those in the bulk regions; see Fig.1) and efficiently abstract a H atom from a protiated solute molecule via a tunneling reaction with a large isotope effect. In the case of $m \leq 8$, the escaped D atoms can react with only the terminal CH3-groups of the solute molecule in the boundary regions, forming selectively solute radical(I). The selective formation of radicals II and III in the case of $m \geq 10$ is due to the exposure of the penultimate- and interior-type secondary C-H bonds(with lower bond strengths than the primary CH3 bond), in addition to the exposure of the CH3 bonds to the boundary regions

(Fig.7). While, the D atoms produced at 4.2 K are converted to $C_{10}H_{21}$ radicals by abstraction of D atom from a neighboring matrix molecule, since they are suppressed to diffuse and can not encounter with the solute molecules of small content. These results strongly imply the participation of hydrogen atom reaction in the neat-alkane radiolysis itself.

In order to confirm further H atom reaction mechanism in hydrocarbon radiolysis, a radiolysis study was made for 1-alkyne(0.5-7.0 mol%)/n-C_mH_{2m+2} (m=10-13).[5] A vinyl type radical(Rv: $CH_2=C'-CH_2-CH_2-$) was efficiently produced by H-atom addition to 1-alkyne(~20%) in orthorhombic mixed crystals, but not in triclinic crystals having even carbon numbers (Fig.8). For pure n-alkanes, the terminal type alkyl radical I: $C'H_2CH_2CH_2-$ is formed(~25%) only in the former crystals along with II and III radicals. Triclinic crystals produce only II and III as described above(Fig.9). The yield of Rv radicals increases and the radical I yield concomitantly decreases with increase in the solute concentration(Fig.10). The sum of their yield was almost constant, indicating the same precursor for both radicals. These results can be understood only by H atom reactions

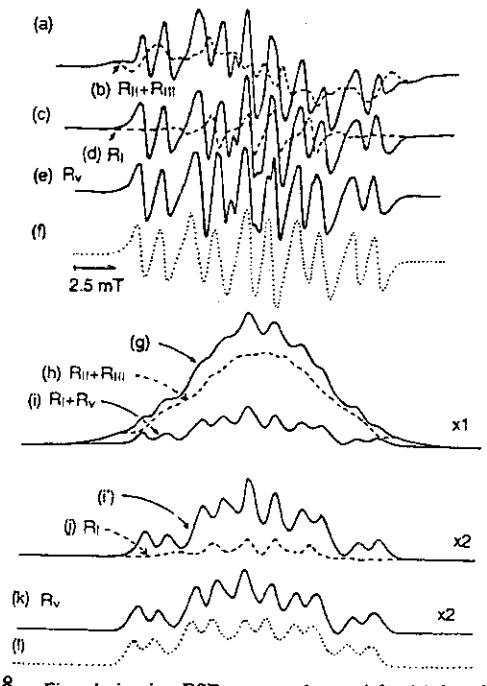

Fig.8 First-derivative ESR spectra observed for (a) 1-undecyne-(5.0 mol %)/n-$C_{11}H_{24}$ mixed crystals and (b) n-$C_{13}H_{28}$(5.0 mol %)/n-$C_{11}H_{24}$ mixed crystals irradiated at 77 K. The spectrum of (a) is composed of four kinds of radicals; $CH_2-CH_2-C_9H_{19}$ (R_I), $CH_3-CH-CH_2-C_8H_{17}$ (R_{II}), and $-CH_2-CH-CH_2-$ (R_{III}) and a vinyl-type radical, $CH_2=C-C_9H_{19}$, formed by H atom addition to 1-undecyne molecules. (c) Difference spectrum (a) − (b). (d) The first-derivative ESR spectrum of R_I. (e) Difference spectrum (c) − (d). (f) Simulated spectrum of the vinyl-type radical, $CH_2=C-C_9H_{19}$, using the ESR parameters $a(H_2C=C-)$ = 3.0 and 5.8 mT and $a(=C-CH_2-)$ = 1.1 and 3.0 mT. (g)−(l) Integrated spectra of (a)−(f), respectively.

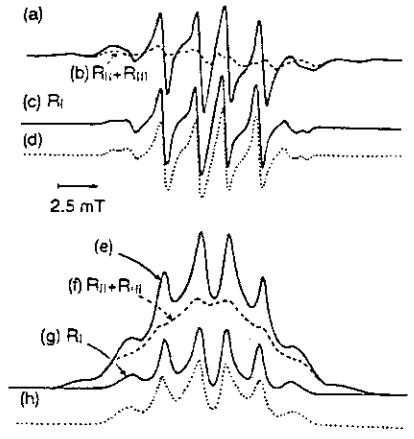

Fig.9 First-derivative ESR spectra observed for (a) n-$C_{11}H_{24}$ and (b) n-$C_{13}H_{28}$(5.0 mol %)/n-$C_{11}H_{24}$ mixed crystals irradiated at 77 K. The spectrum of (a) is composed of three kinds of alkyl radicals, $CH_2-CH_2-C_9H_{19}$ (R_I), $CH_3-CH-CH_2-C_8H_{17}$ (R_{II}), and $CH_3-CH_2-CH-CH_2-C_7H_{15}$ (R_{III}), while that of (b) is mainly composed of R_{II} and R_{III}. (c) Difference spectrum (a) − (b). (d) Simulated spectrum of R_I using the ESR parameters reported. (e) − (h) Integrated spectra of (a)−(d).

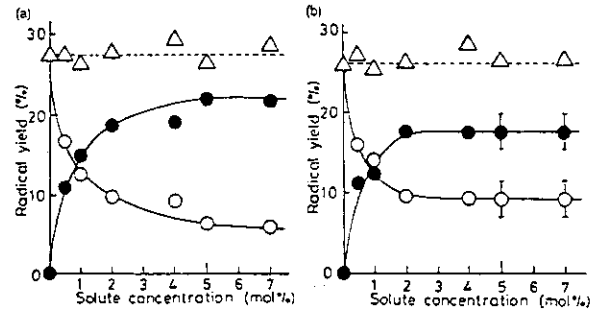

Fig.10 Dependence of the yield of the terminal type of radical R_I (○) and the vinyl-type radical, $CH_2=C-C_9H_{19}$, (●) and the sum of them (△) on the solute concentration in (a) 1-undecyn/n-$C_{11}H_{24}$ and (b) 1-tridecyne/n-$C_{13}H_{28}$ mixed crystals.

in the same way as the above radiolysis of $C_mH_{2m+2}/C_{10}D_{22}$ mixed crystals. Namely, some of the radiation-induced hydrogen atoms can escape to the boundary regions in orthorhombic crystals having a wider boundary width than triclinic crystals, and selectively form Rv radicals by addition to the chain-end carbon atom of $CH{\equiv}C\text{-}CH_2$- triple bond of 1-alkyne molecules, which are exposed to the regions. The possibility of ion molecular reaction mechanism was excluded from the ionization potential difference between the solute and the matrix molecules. These results provide conclusive evidence for H atom reaction mechanism in alkane radiolysis.[5]

The easy migration of H atoms in orthorhombic alkanes has theoretically discussed by molecular orbital calculations.[6]

B)Extremely unstable ions:

From the finding of stable trapping of radiation-induced electrons,[3] we tried and succeeded for the first time to trap and detect ESR spectroscopically the extremely unstable anions of mono-unsaturated hydrocarbons using alkane mixed crystals with alkenes and alkynes.[7,8] The ESR spectra of the anions of hexene isomers(1-, 2-, and 3-hexenes) in n-hexane matrix are shown in Fig.11.[9] They were found to have a pyramidal radical structure of trans form with a slight σ-character. Butene-1 and -2 anions have the same structure.[9] The hexene cations were also trapped and found to have a planer π radical structure.[7,9]

The anions of hexyne isomers(-1,-2, and -3) were trapped in hexyne/hexane mixed crystal as shown in Fig.12[8] Acetylene radical anion was also

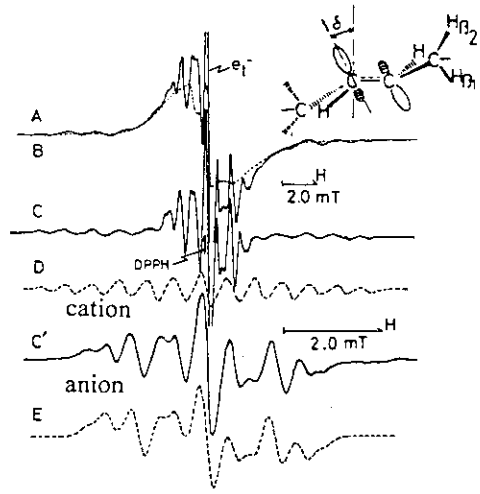

Fig.11 The first-derivative absorption ESR spectra observed for *trans*-3-hexene (4.0 mol %)/*n*-hexane-d_{14} mixed crystals (A) irradiated at 4.2 K and (B) after illuminated by visible light. (C) The difference spectrum obtained by subtracting spectrum B from spectrum A. (C') The expanded spectrum of the difference spectrum observed for the *trans*-3-hexene (8.0 mol %)/*n*-hexane-d_{14} mixed crystals. The ESR spectral simulations for the *trans*-3-hexene (D) cation and (E) anion radicals.

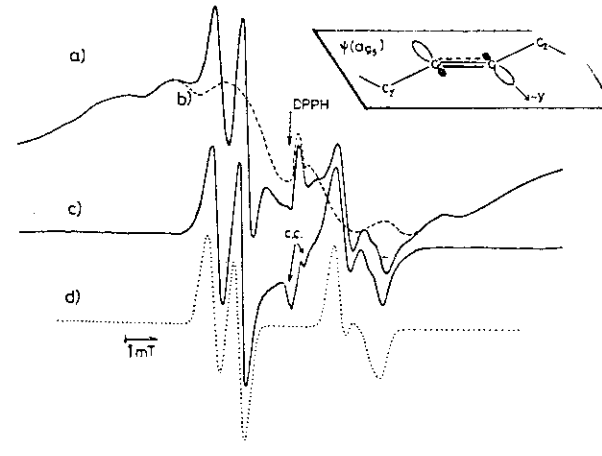

Fig.12 The first derivative absorption ESR spectra observed for 1-hexyne (2.0 mol %)/*n*-hexane mixed crystals: (a) irradiated at 4.2 K and (b) after illumination by visible light. (c) The difference spectrum obtained by subtracting *b* from *a*. c.c. indicates ESR signals of the color centers formed in the quartz sample tube. (d) The simulated spectrum of the 1-hexyne radical anion using the ESR parameters listed in Table I.

produced in ethane matrix crystals.[10] These alkyne anions were found to have a trans-bent form H-C(H)≡C-C in a plane and to have the unpaired electron orbital with a σ-character as shown in Fig.12. The geometrical and electronic structures of these mono-unsaturated anions and cations were discussed in detail.[7-10]

One of the authors(H.M.) had studied the radiolysis of various organic compounds using single crystal ESR and ENDOR spectroscopies.[11] The single crystals were useful to clarify the structure of radicals with complex nuclear spin systems composed of halogen and nitrogen atoms such as N-bromosuccinimide,[16,17] freon[11,18] and dibromomethane.[19] We have extended the study to the radiolysis of carbon tetrachloride, which radiolysis mechanism is not clarified yet in spite of a large number of optical and ESR studies. Figure 13 shows the angular dependence of the ESR spectrum of CCl_4^+ cation in an irradiated CCl_4 single crystal. The complex ESR pattern of the cation in the polycrystalline powder could be simulated by the aide of the analysis of the single crystal spectra(Fig.14). The cation in CCl_4 was found to have a complex structure of a dimer type as shown in Fig.14.[20]

The CCl_4^- anion was also studied and found to have a predissociating molecular structure $(CCl_3...Cl)^-$ and to be converted to CCl_3 radicals upon elevating temperature.[21]

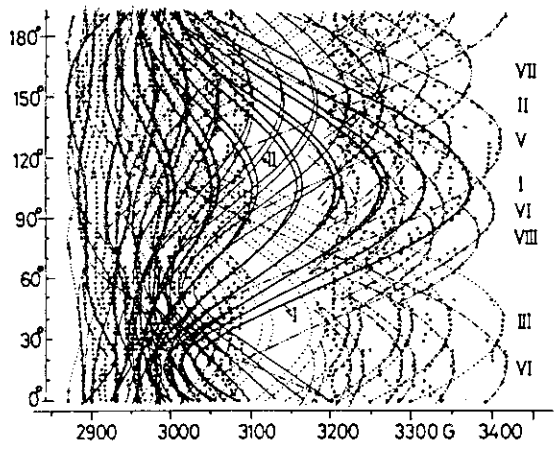

Fig. 13 The angular dependence of the ESR spectrum of the CCl_4^+ radical cation in the single crystal plane vertical to the ESR sample tube. I-VIII indicate the magnetically inequivalent sites whose spectral angular dependence could be measured.

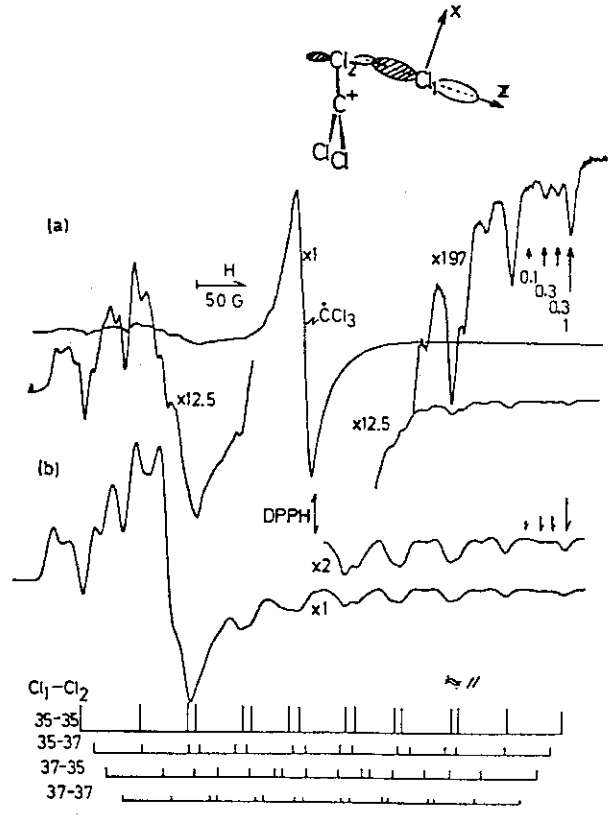

Fig.14 (a) Observed ESR spectrum of the CCl_4 powder sample irradiated at 77 K. (b) Simulated spectrum of the CCl_4^+ radical cation using the ESR parameters listed in Table I. (b) is the superposed spectrum of the four kinds of combinations of ^{35}Cl and ^{37}Cl isotopes (see the text). The arrows and the numbers indicate the resonance field lines at the highest magnetic field and their relative intensities for the four isotopic combinations, respectively.

C)Behavior of e-, holes, and H atoms, and isotope effects

The transfer and trapping of electrons, holes, and H atoms and their crystal structure dependencies in alkanes and a various mixed crystals were studied and briefly described in the above A) and B) sections[3-6,9] It should be noted that the trapping stability(decay rate) of electrons as well as the yield largely depends on the crystal structure of the binary n-alkane mixed crystals with different chain lengths. A higher stability and a higher yield were observed in triclinic crystals than in orthorhombic crystals and were understood by the effective size of the voids in the binary alkane crystals in addition to the width of the layer boundary regions.[3]

Another topics is a very large H/D isotope effect observed in H_2O/ D_2O mixed ice.[13] The radiolysis study of water is of fundamental importance to

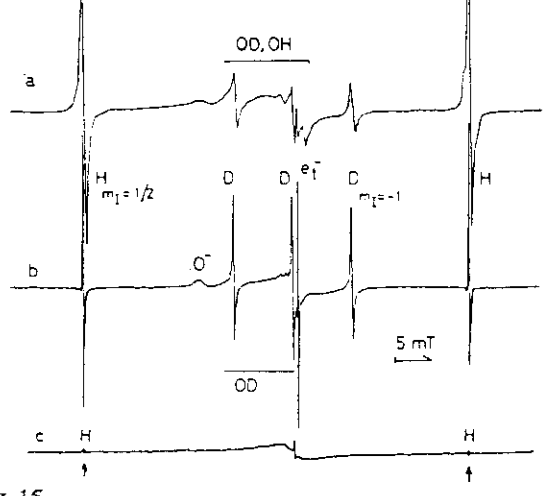

Fig. 15 First-derivative ESR spectra observed for X-irradiated H_2O/D_2O polycrystals containing H content (a) 50 and (b) 1.0 atomic %, and (c) for a blank sample tube without mixtures, respectively. X-ray irradiation (45 kV, 40 mA for 10 min) and ESR measurement was made at 4.2 K. Measurement conditions: microwave power = 0.13 μW, 100 kHz field modulation width = 0.76 G. (b) Observed after an hour from the end of irradiation and the amount of trapped electrons has decreased $\sim 1/10$ as much as the initial yield immediately after irradiation (see text).

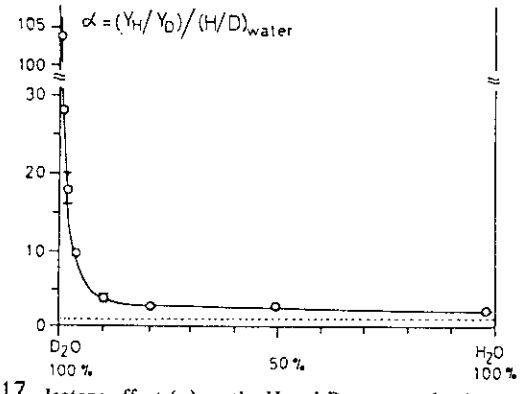

Fig. 17 Isotope effect (α) on the H and D atom production in X-irradiated H_2O/D_2O polycrystals at 4.2 K as a function of the H content of the mixtures.

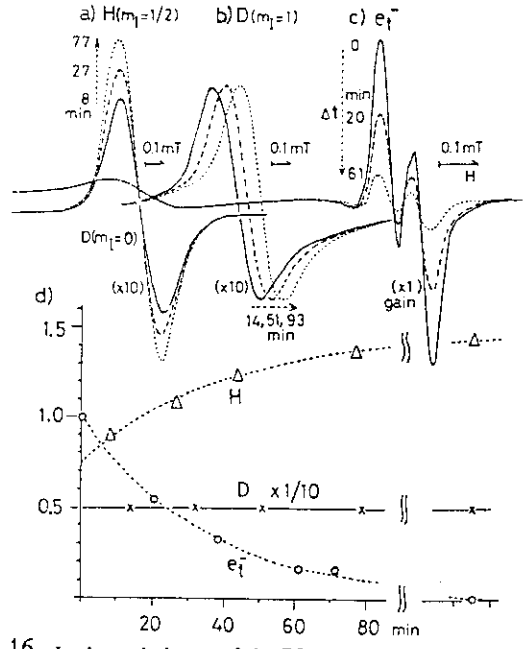

Fig. 16 Isothermal change of the ESR signal intensities for (a) H atoms, (b) D atoms, and (c) trapped electrons produced in H_2O (1.0 H atomic %)/D_2O polycrystals X-irradiated at 4.2 K. ESR measurement conditions: microwave power = 0.13 μW, field modulation width = 0.3 G. The numbers without parentheses associated with dotted arrows indicate the passed time (Δt) from the first ESR measurement immediately after irradiation. (d) Isothermal behavior of the relative amount of e_t (O), H (Δ), and D (×) at 4.2 K. Trapped electrons selectively converted to H atoms in the first order kinetics with a rate of $|k| = 0.029 \pm 0.002$ min^{-1}. The dotted curves represent the calculated values using the above rate.

living organisms and nuclear reactor technology. It has been acknowledged that hydrogen atoms(H) are produced in water radiolysis by two distinct mechanisms. One is direct dissociation of excited H_2O^* molecules and the other is the ionic reaction of electrons(e^-) and hydronium ions(H_3O^+). The H/D isotope effect in water radiolysis was studied at 4.2 K by ESR spectroscopy to elucidate the radiolysis mechanism. Radiation-induced electrons, which are trapped only in the H_2O/D_2O mixtures with H-contents lower than 3%(Fig.15), were selectively converted to isolated H atoms at 4.2K (Fig.16). A very large isotope effect was observed for the rate of the conversion of electrons to H and D atoms: $(k_H/k_D)/(H/D)_{ice} > 10^3$, presumably due to tunneling(Fig.16d). The net isotope effect for the atomic hydrogen yield(Y) including the initial production was $(Y_H/Y_D)/(H/D)_{ice} = 10\text{-}10^2$ and 3.5-2.5 for 3.0-0.25 and 10-90 % H-contents, respectively (Fig.17). The origin of the large isotope effect in the low H-content mixtures can be understood as follows. The deuteron D^+ produced by ion-molecular reaction(1) migrates in the form D_3O^+ during the thermalization of electrons. The charge + is stabilized in a form HD_2O^+ via a reaction (2) having the enthalpy change $\Delta H = -1.0$ kcal/mol.

$$D_2O^+ \text{---(+}D_2O\text{)-----> } OD' + D_3O^+ \qquad (1)$$

$$D_3O^+ + HDO\text{-------> } D_2O + HD_2O^+ \qquad (2)$$

$$e^-_{therm} + HD_2O^+ \text{---> } HD_2O\text{---> } \begin{matrix} H + D_2O \\ D + HDO \end{matrix} \quad \text{or} \qquad (3)$$

The large H/D effect is resulted via a tunneling effect in O-H, O-D bond dissociation reaction of HD_2O species produced by charge recombination (3). These findings gave unequivocal evidence for the suggested reaction of electrons and H_3O^+ in water radiolysis and implying a possibility of isotope separation.

The trapping and reactions of H atoms in N_2 and H_2O low temperature matrices have been studied on the idea of K. Hiraoka in order to simulate the molecular evolution in space.[14]

LITERATURES

1) M.Iwasaki, K.Toriyama, M.Fukaya, H.Muto, K.Nunome, J.Phys.Chem., 89, 5278 (1985); K.Toriyama, M.Iwasaki, M.Fukaya, J.Chem.Soc.,Chem. Commun.,1293 (1982); and references cited theirin.
2) H.Muto, K.Nunome, K.Toriyama, M.Iwasaki, Radiat.Phys.Chem. 23, 607 (1984), H.Muto, K.Toriyama, K.Nunome, M.Iwasaki, Radiat.Phys.Chem., 19, 201 (1982); and references cited theirin.
3) H.Muto, K.Nunome, K.Toriyama, M.Iwasaki, J.Phys.Chem., 93, 4898 (1989).
4) H.Muto, K.Nunome, M.Fukaya, J.Phys.Chem., 94, 418 (1990).

5) K.Matsuura, H.Muto, J.Phys.Chem., 98, 10112 (1994).
6) K.Matsuura, H.Muto, 35th Radiation Chemistry Symposium of Jpn., (1993); to be submitted for pubulication.
7) H..Muto, K.Nunome, K.Matsuura, J.Amer.Chem.Soc., 113,1840(1991).
8) K.Matsuura, H.Muto, J.Chem.Phys., 94, 4078 (1991).
9) K.Matsuura, H.Muto, K.Nunome, J.Phys.Chem., 95, 9481 (1991).
10)K.Matsuura, H.Muto, J.Phys.Chem., 97, 8842 (1993).
11)H.Muto, "Trapped anions in organic crystals" in Radical Ionic Systems, Eds.by A.Lund and M.Shiotani, pp337-359 (1991), Kluwer Academic Publishers(Neitherlands.
12)H.Muto, Radiation Chemistry(J.Radiat.Chem.Soc.Jpn),55, 2 (1993); Japanease.
13)H.Muto, K.Matsuura, K.Munome, J.Phys.Chem., 96, 5211 (1992).
14)K.Hiraoka, A.Yamasita, Y.Yachi, K.Aruga, T.Sato, H.Muto, Astrophys.J., 443, 363 (1995).
15)M.Iwasaki, H.Muto, K.Toriyama, J.Chem.Phys., 55, 1894 (1971).
16)H.Muto, L.D.Kispert, J.Chem.Phys., 72, 2300 (1980).
17)H.Muto, L.D.Kispert, J.Chem.Phys., 73, (1980).
18)M.C.R.Symons, B.W.Wren, H.Muto, K.Toriyama, M.Iwasaki, Chem.Phys. Letter 127, 424 (1986).
19)M.C.R.Symons, H.Muto, K.Toriyama, K.Nunome, M.Iwasaki, J.Chem.Soc. Perkin Trans. II, 2011 (1986).
20)H.Muto, K.Nunome, M.Iwasaki, J.Chem.Phys., 90,6827 (1989).
21)H.Muto, K.Nunome, J.Chem.Phys., 94, 4741 (1991).

3. Neutron Diffraction Studies on Proton Tunneling Dynamics

Yasusada Yamada (Waseda University)

(not yet arrived)

4. Experimental Investigation on the Formation of Interstellar Molecules from the Reactions of Hydrogen Atoms with Molecules Trapped in the Dust Grains

Kenzo Hiraoka
Faculty of Engineering, Yamanashi University,
Takeda-4, Kofu 400, Japan

Introduction

In interstellar clouds, ion/molecule reactions are the dominant processes for the formation of interstellar molecules. Because the temperature of molecular clouds and dark clouds is 10-20 K, all gases except for He, Ne and H_2 may be condensable on the surface of dust grains and form mantles on the dust. In order to elucidate the chemical evolution of dark clouds, it is important to investigate the chemical processes taking place on the surfaces of dust grains and in their mantles.

The high mobility of H atoms in solids suggets that hydrogen atoms play a major role in the solid state chemical evolution of dense clouds: i.e., they diffuse long distances on grain surfaces and in mantles and react with trapped and immobilized atoms(e.g., N, O, and C atoms) and molecules(e.g., CO) to form hydrogenated products in the mantles.

Reactions on the surfaces of dust grains may be critical, though studies of surface reactions are not yet as quantitative and precise as studies of gas-phase reactions. In this work, the reactions of hydrogen atoms with nitrogen atoms trapped in an N_2 matrix and CO molecules in the temperature range of 10-30 K have been studied in order to obtain information on the possibility for the formation of interstellar molecules (i.e., ammonia, formaldehyde, and methanol) in the grain mantles.

The experimental techniques developped in our laboratory are described in detail in the following section.

Experimental Method

The cryocooler(IWATANI PLANTECH, type D310) and a quadrupole mass spectrometer(ULVAC, MSQ-300) were housed in a high-vacuum chamber(ULVAC, EBD-50M). The vacuum chamber was evacuated by two turbomolecular pumps(ULVAC, UTM 300M, 300 L/s and SEIKO SEIKI,

H200C, 200 L/s) connected in tandem. The bake-out of the vacuum chamber could not be made because the temperature of the cryocooler used in the present experiment could not be raised above ~340 K. The base pressure of the vacuum system under the current experimental conditions was $\sim 1 \times 10^{-8}$ mmHg. The temperature of the cold head of the cryocooler was changed in the range of 340-10 K with a stability of ± 0.1 K. Temperature-programmed mass spectra of the reaction products were measured with a constant programming rate of 7 K/min using a computer-controlled temperature regulator.

The experimental setup used in the present work is shown in Fig.1. The sample gas was introduced into the vacuum chamber through a stainless steel capillary tube(1 m long with 1 μm inner diameter). The terminal end of the capillary ((3) or (4) in Fig.1) was connected to the quartz discharge tube ((1) or (2))(inner diameters of the discharge tube and the bottleneck are 8 mm and 0.25 mm, respectively). Pressure of the sample gas reservoir which was measured by a capacitance manometer(MKS Baratron, type 122A) was kept constant at 760 mmHg. The precise calibration of flow rates for sample gases through capillaries was made. The sample gas was passed through a liquid-N_2 cooled molecular sieve 5A trap in order to eliminate impurity gases and introduced into the reaction cell through the capillary. The base pressure in the vacuum chamber did not increase when N_2 or CO was sprayed over the surface of the cold head of the cryocooler at 10-20 K. This indicates that the accommodation coefficient of sample gases(N_2 or CO) on the cold surface is nearly unity and almost all gas molecules were condensed on the cold surface. In such experimental conditions, the thickness of the deposited gas could be estimated by the amount of introduced gas and the area for the deposition.

H_2 gas(99.99999 %) was passed through a trap filled with molecular sieve 5A at liquid-N_2 temperature and introduced into the reaction cell through the capillary(1). With high voltage applied to the capillary(± 3-± 10 kV), a stable glow plasma was generated in the bottleneck discharge tube(1). It is known that the plasma activated H_2 is mainly composed of ground state H atoms and vibronically ground state H_2 molecules. It is also known that the first order wall loss rate copnstant(2.1 s^{-1}) of atoms is small and thus the decrease in H atom concentration may

be small in the discharge tube shown in Fig.1. After the H_2 plasma spray over the deposited sample, the temperature-programmed mass spectra of the sample were measured.

The discharge tube(1) was in thermal contact with a base cold head through a 1 mm thick copper sheet. The discharge tube was firmly tightened with a copper sheet with indium foil between them in order to make the intimate thermal contact. It was found that the temperature of the discharge tube was 29 K when the cold head of the cryocooler was 13 K. When the discharge was started, a temperature rise of about 0.5 K was observed for the discharge tube(1). Because the temperature of the plasma-activated gas is known to be nearly equal to that of the wall of the discharge tube, the temperaturte of the sprayed H atoms over the solid surface may be about 17 K higher than that of the solid sample. During the H_2 plasma spray over the CO film, the temperature rise of the metal substrate was not observed within $\pm$0.1 K.

When a high voltage was applied to the capillary tube without using a quartz discharge tube, it was difficult to maintain a stable discharge. This is because the gas pressure in the reaction cell becomes too low due to the quick diffusion of gas molecules in the vacuum chamber. The experimental results obtained will be presented in the meeting.

References

(1)K.Hiraoka,N.Ohashi,Y.Kihara,K.Yamamoto,T.Sato, and A.Yamashita,Chem.Phys.Lett.,229(1994)408.

(2)K.Hiraoka,A.Yamashita,Y.Yachi,K.Aruga, and T.Sato, Astrophys.J.,443(1995)363.

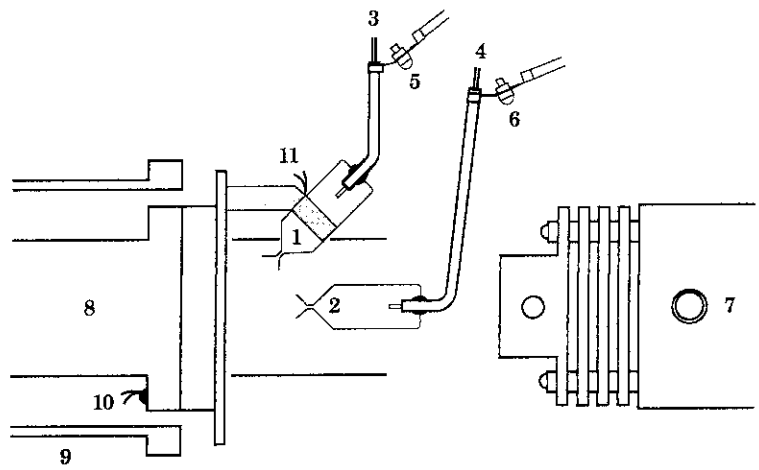

Fig. 1. Schematic diagram of the experimental apparatus. (1) Quartz bottleneck discharge tube for H_2 plasma spray. The discharge tube is connected with the cold head of the cryocooler with copper sheet. The discharge tube was tightened by the copper sheet firmly with indium foil between the mating surfaces in order to make good thermal contact. The temperature of the discharge tube is about 16 K higher than that of the cold head (10–20 K). (2) Quartz bottleneck discharge tube. (3) and (4) Stainless steel capillary tubes (1 m×1 μm ∅) for introduction of the sample gases. (5) and (6) Leads for the high voltage supply. (7) Quadrupole mass spectrometer (ULVAC, MSQ-300). (8) Cold head of the cryocooler (IWATANI PLANTECH, type D310). (9) Thermal shield for the cold head. (10) and (11) Au+0.07% Fe versus chrome thermocouples which are calibrated at liquid H_2, liquid N_2 and ice/water temperatures.

5. ESR Study on Hydrogen-Atom Abstraction in Cryogenic Organic Solids

Tsuneki Ichikawa

Graduate School of Engineering, Hokkaido University,
Sapporo, Japan

INTRODUCTION

The rate of chemical reaction is generally considered to be controlled by the frequency factor and the activation energy. The rate increases with decreasing the activation energy or the potential barrier for the reaction, if the other factor is unchanged. A typical example is the rate of hydrogen-atom abstraction from alkane molecules in liquid.[1] The rate of hydrogen-atom abstraction by hydrogen or deuterium atoms increases in the order of the primary, secondary and tertiary carbon atoms,[2] due to the decrease of the activation energy. However the rate of the hydrogen-atom abstraction in cryogenic solids does not follow this rule.[3,4] Although the tertiary C-H bond is the weakest, no tertiary alkyl radical is formed in the glassy matrices. However, no reason has been given for the preferential formation of the radicals. It is therefore worthwhile to carry out the detailed study on the hydrogen-atom abstraction and to find out a controlling factor of hydrogen-atom abstraction in cryogenic organic solids.

The present paper summarizes our recent results on the hydrogen-atom abstraction from protiated alkane molecule by deuterium atoms in cryogenic deuterated organic solids, obtained by the X-band ESR and electron spin-echo measurements of the product alkyl radicals at cryogenic temperatures.

EXPERIMENTAL

Samples used for the experiments were perdeuterated alcohols or alkanes containing 2 vol. % of protiated solute alkanes (RH). Deuterium atoms were generated below 77 K either by γ-radiolysis

of the deuterated matrix molecules (MD),

$$MD + \gamma \longrightarrow M\cdot + D,$$

or by photo-ionization of triphenylamine (TPA) followed by photo-electron capture by deuterium chloride (DCl),

$$TPA + 2h\nu \longrightarrow TPA^{+\cdot} + e^{-}, \qquad e^{-} + DCl \longrightarrow D + Cl^{-}.$$

Alkyl radicals generated by reaction

$$RH + D \longrightarrow R\cdot + DH$$

were detected by ESR or electron spin-echo spectroscopy, using insertion-type ESR cryostats.

Fig.1 shows an insertion-type cryostat invented by us for 4.2 K ESR measurements.[5] The cryostat consists of inner and outer Dewar vessels. The inner vessel consists of liquid helium and liquid nitrogen containers. The outer vessel has an opening not at the top but at the bottom. These vessels are made with Vycor glass except for the tip portions and have narrow unsilvered slits. The tip potions are made with high-purity quartz glass. The vessels are connected with each other at the upper part of the cryostat. The cold nitrogen gas from the nitrogen container passes through the thin gap between the inner and the outer vessels and goes out through the bottom of the cryostat. The rate of the gas flow is controlled by changing the diameter of a heat-conducting copper wire which is partially immersed in the liquid nitrogen. For preventing the bumping of the liquid nitrogen, a few peaces of porcelain or zeolite pellets are attached at the immersed part of the wire. Since the nitrogen gas is continuously cooled down by the liquid nitrogen until enterring into the tip portion, the temperature at the outer wall of the inner potion is kept constant as long as the evaporation rate of the nitrogen is unchanged. The temperature at the bottom of the inner vessel is approximately 100 K when a copper wire of 1.5 mm diam (a conventional wire for electricity) is used. The capacity for helium is about 400 cm^3 but only 200 cm^3 of liquid helium keeps a sample of 3 mm diam at 4.2 K for 9 h when liquid nitrogen is added every 1h. No ESR signal noise is induced by the addition of liquid nitrogen.

The characteristic feature of this cryostat is the induction of

no ESR noise by the boiling of liquid nitrogen. The inner vessel of a conventional cryostat for liquid helium is usually immersed in liquid nitrogen. Since the dielectric constants of liquid and

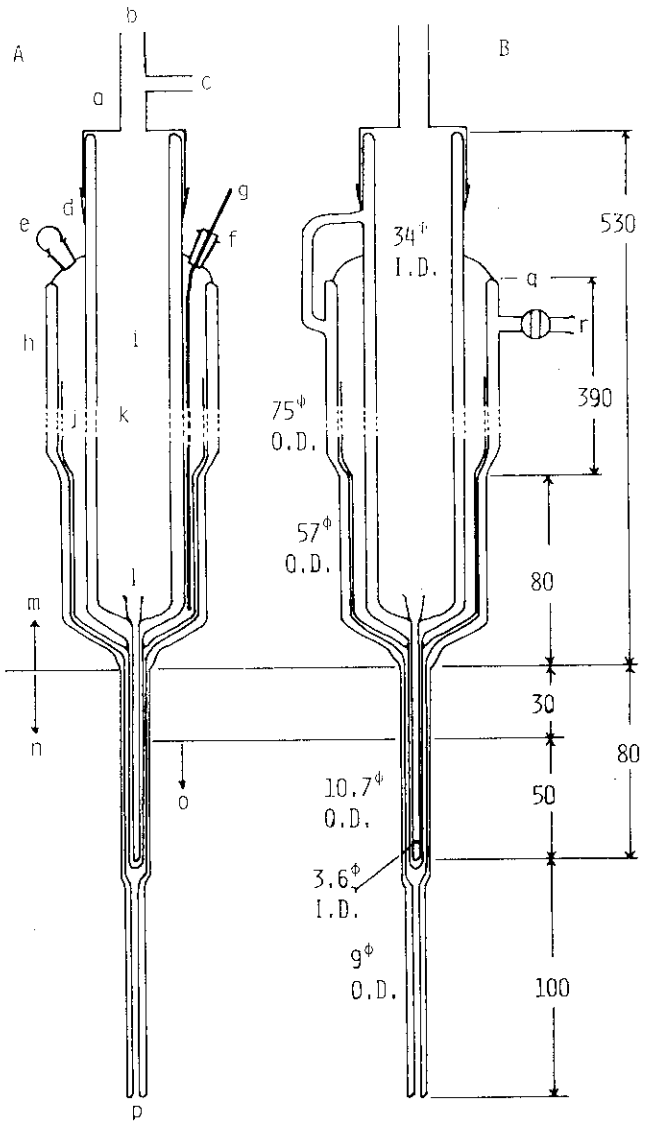

Fig. 1. Cross sections of the cryostat for ESR measurements at 4.2 K. Cross section B is perpendicular to cross section A.
(a) Polyethylene cap, (b) He inlet (c) He outlet, (d) rubber band, (e) N_2 inlet, (f) rubber stopper, (g) heat conductor. (h) outer Dewar vessel, (i) inner Dewar vessel, (j) nitrogen container, (k) He container, (l) funnel for preventing the presipitation of solidified air in the tip portion, (m) Vicor glass, (n) high-purity quartz glass, (o) unsilvered tip portion, (p) N_2 outlet, (q) stop cock, (r) to vacuum.

gaseous helium at 4.2 K are almost the same, the boiling of the liquid helium in a ESR cavity does not cause the ESR noise. However, since the dielectric constants are much different between liquid and gaseous nitrogen, boiling of the liquid nitrogen causes abrupt change of the microwave resonance frequency of the cavity and disturbs ESR measurements. The simplest way of eliminating the boiling noise is to use a cryostat without outer vessel in the cavity. However this causes direct exposure of the helium vessel to the ambient temperature through vacuum, and thereby increases the rate of liquid helium consumption by a factor of 20. On the other hand, the keeping time of the liquid helium is unchanged even if the tip portion of our cryostat is immersed in liquid nitrogen. Therefore the structure shown in Fig. 1 is quite effective both for reducing the evaporation rate of liquid helium and eliminating the boiling noise.

Although the cryostat in Fig. 1 has excellent ability of keeping liquid nitrogen for long time without giving ESR noise, it can be used only for 4.2 K measurements. Commercially-available variable-temperature cryostats generally uses cold He gas as a refrigerant below 77 K. The cold He gas is supplied from a liquid He container through a transfer tube. One drawback of these cryostats is the fast consumption of liquid He. For reducing the running cost, it is therefore necessary to have a He recovery system composed of a He gas reservoir and a He gas compressor. However the recovery system is also expensive. The best way is therefore not to introduce a He recovery system but to invent a cryostat with slow consumption of liquid He.

Fig. 2 shows two types of variable-temperature cryostats[6] which were intended to minimize the loss of liquid He. Although cold He gas is used as a refrigerant, it is supplied not through a transfer tube but directly from the liquid He reservoir. For type-A cryostat, the He gas passes through the bottom tip by plugging the He gas outlet at the upper part of the He container, and then released from the outer wall of the He Dewar. Although this cryostat could keep 25 K for 1 h with 850 cm^3 of liquid He, the rate of He consumption was not so low as expected. The heat from the top of the He container is used completely for boiling the liquid He, once the He gas outlet of the He container is plugged.

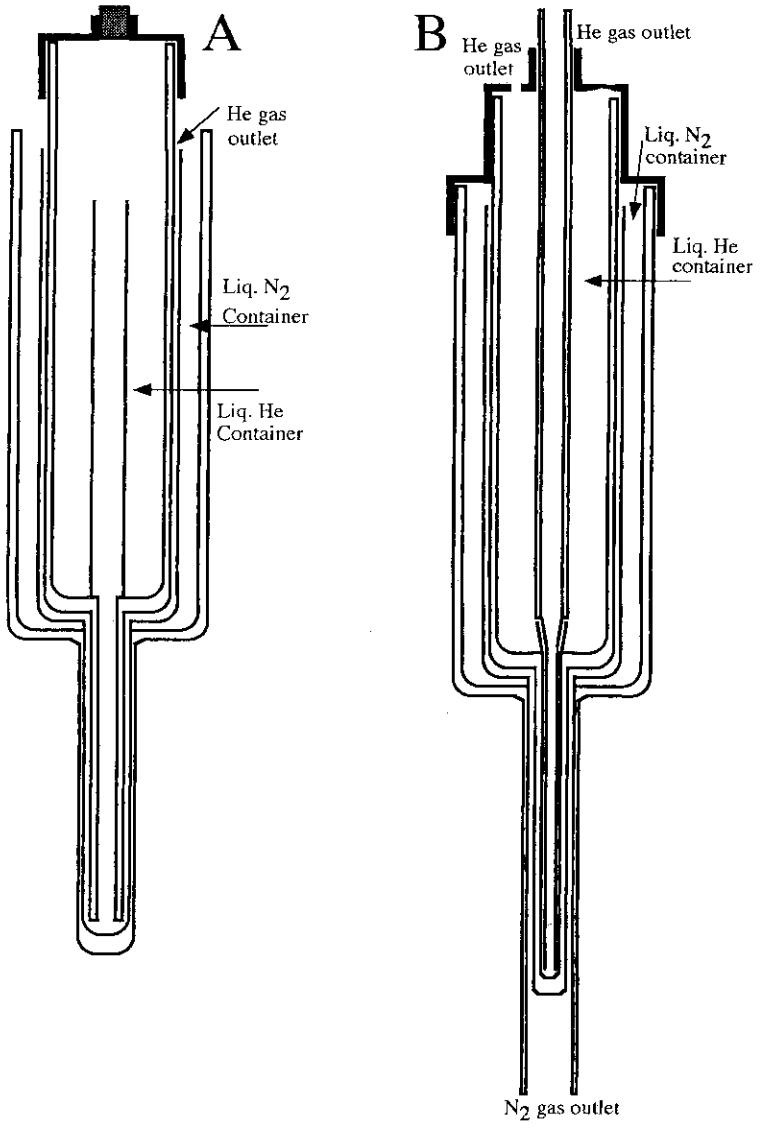

Fig. 2. Cross sections of two types of variable temperature cryostat.

The characteristic feature of type-B cryostat is that the leakage of liquid He from the He container to the bottom tip is used instead of the pressurized gas flow from the upper part of the container. The evaporated He removes the heat penetrated from the upper part of the cryostat, so that the evaporation rate is less than 1/20 of type-A cryostat. However, because of periodic penetration of liquid He, the stability of the temperature is not so good as type-A cryostat.

RESULTS AND DISCUSSION

Table 1 summarizes our resent results[7] on the selectivity of hydrogen abstraction at 77 K from 2 vol. % protiated solute alkanes (RH) in deuterated matrices by deuterium atoms. The hydrogen abstraction proceeds through quantum-mechanical tunneling of alkane C-H hydrogen, since the deuterium atoms selectively abstract the hydrogen atoms of solute molecules. Although the tertiary C-H hydrogen is preferentially abstracted from branched alkanes in liquid, only the penultimate secondary hydrogen is abstracted in amorphous solids.

The selectivity is much peculiar for n-alkanes. In crystalline n-alkanes deuterium atoms are known to migrate through channels composed of the arrays of head and tail methyl groups of alkane molecules,[8] so that the probability that the C-H hydrogen encounters a deuterium atom is much lower for the internal secondary hydrogen than the penultimate one. However a considerable amount of the internal hydrogens were abstracted. On the other hand, although n-alkane molecules in amorphous solids have random structures and the encounterring probability is about the same for the penultimate and the internal hydrogen atoms, highly selective abstraction of the penultimate secondary C-H hydrogen took place only in amorphous solids.

These peculiar features have been explained consistently by introducing the phenomenalistic concept of *pin-down effect*[7] which implies that alkyl arms bonded to a C-H carbon atom of an alkane molecule and piled into an amorphous solid "*pin down*" the C-C-C bond to prevent the deformation of the bond from the original alkane sp^3 state to the final radical sp^2+p state. The intramolecular location of the carbon atom to be hydrogen-abstracted is determined by the pin-down effect and the activation energy for the hydrogen abstraction.

In amorphous solids, the pin-down effect increases with increasing number and length of alkyl chains bonded to a carbon atom, so that the tertiary carbon atom with three alkyl chains is difficult to be hydrogen-abstracted even the activation energy is the lowest. Although the pin-down effect is the smallest for the primary C-H carbon atoms, the primary carbon atom is not hydrogen-abstracted due to the highest activation energy. The pin-down

Table 1. Selectivity of hydrogen abstraction at 77K in solids.

Alkane	Deuterated Matrix	Location of hydrogen abstraction			
		$R-CH_3$[a]	$R-CH_2-Me$[b]	$R-CH_2-R$	$R_3{\equiv}CH$
2-methylpentane	methanol(A)[c]	0	~100%	trace	0
3-methylpentane	methanol(A)	0	~100%	0	0
2-methylhexane	2-propanol(A)	0	~100%	trace	0
3-methylhexane	2-propanol(A)	0	~100%	0	0
n-hexane	methanol(A)	0	~100%	trace	/
	n-hexane(C)[d]	0	~80%	~20%	/
n-octane	2-propanol(A)	0	~100%	trace	/
	n-octane(C)	0	~80%	~20%	/

a) R=alkyl group other than methyl group, b) Me=methyl group, c) (A)=amorphous, d) (C)=crystal. The relative reactivity of hydrogen abstraction in liquid alkane at room temperature is about 1:5:5:40 for $R-CH_3$, $R-CH_2-Me$, $R-CH_2-R$ and $R_3{\equiv}CH$.[2)]

effect for the penultimate carbon atom is the lowest within secondary carbon atoms, so that the penultimate secondary radicals are selectively generated in amorphous solids. The experimental fact that the paramagnetic relaxation of the alkyl radicals generated in amorphous solid increases with increasing length of alkyl chains bonded to the radical carbon supports the validity of the above assumption, since the relaxation is induced by the motion of the chains.

In crystalline n-alkanes, all the carbon atoms in a molecule are in the molecular plane. The in-plane accordion motion of a flat carbon skeleton is easy to take place without exerting much strain to the surrounding. The accordion motion causes the simultaneous bending of all the C-C-C bonds in a molecule, so that both the penultimate and the internal secondary carbon atoms are hydrogen-abstracted.

Because of low viscosity of liquid, the pin-down effect is not important for the reaction in liquid.

The concept of the pin-down effect is very powerful for

predicting the intramolecular location of hydrogen abstraction. However, it is phenomenalistic and needs a theoretical foundation. The simplest possible explanation is that the deformation of the C-C-C bond is necessary for attaining minimum potential barrier for the hydrogen abstraction. However this is not plausible. As pointed out by Polanyi et al., the configration of carbon atoms at the transition state of hydrogen abstraction is the same as the initial alkane state. The molecular-orbital calculation of the potential surface for the hydrogen abstraction also showed that the potential surface is scarcely changed by the continuous optimization of the bond angle during the reaction. We therefore need to find another factor cntrolling the chemical reaction in solid.

We believe that the dissipation of the heat of hydrogen abstraction to vibration motions around the hydrogen-abstracted carbon atom affects the rate of hydrogen abstraction in solid. Since the total energy of the reaction system is conserved before and after the reaction, the heat of hydrogen abstraction (ca. 3500 cm^{-1}) must be transferred as translational, vibrational and rotational energies of product molecules. In gasous and probably in liquid states, most of the heat can be transferred efficientry as translational energy of the product DH molecule. The translational motion of the product molecules is highly restricted in solid, so that the transfer of the heat of reaction to the vibrational energy becomes a rate-determinant process in the reaction.

The chemical reacton causes sudden change of the location of nuclei in a reactant molecule from the initial equilium (ground) state to the final non-equilibrium (excited) state. The heat of reaction is therby transferred to the vibrational energy of the product molecules. The rate of heat transfer is expressed quantum-mechanically as a Frank-Condon factor or the overlapping of vibrationalwave functions between the initial reactant state and the final vibrationally-excited product state.

The hydrogen abstraction causes change of the σ orbitals about the carbon atom from sp^3-like to sp^2-like. For the C-C-C bond, it is the change of the equilibrium bond angle form 115° to 120° for secondary carbon, and 110° to 115° for tertiary carbon. The rate

of heat transfer decreases with decreasing difference of the equilibrium angles. The difference can be decreased by increasing the steric hindrance to the bending motion, because the steric hindrance push the equilibrium angle of the product radical closer to the initial state. The rate of heat transfer therefore decreases with increasing number and length of alkyl chains bonded to a hydrogen-abstracted carbon atom. The pin down effect thus plays an significant role in the hydrogen abstraction from alkane molecules in solid.

The validity of the above explanation can be confirmed more regolously by examining the effect of the rigidity and the tmperature of organic matrices on the selectivity of the hydrogen abstraction.

EXPERIMENTAL

References

1) W. Siebrand, T.A. Wildman, and M.Z. Zgierski, J. Am. Chem. Soc., 106, 4083, 4089 (1984).

2) W. A. Pryor and J. P. Stanley, J. Amer. Chem. Soc., 93, 1412 (1971)

3) Henderson, D. J.; Willard, J. E. *J. Amer. Chem. Soc.* 1969, 91, 3014

4) Ichikawa, T.; Ohta, N. *Radiat. Phys. Chem.* 1987, 29, 429

5) Ichikawa, T.; Yoshida, H.; Yamada, H.; Tokairin, S.; Ikegami, Y. J. Magn. Reson., 1985, 64, 518

6) 山田 宏、菊地 毅光、市川 恒樹、東海林 正一、小野寺 信治 東北大学非水溶液化学研究所報告、第39巻1頁 (1989)

7) T. Ichikawa and H. Yoshida, J. Phys. Chem., 96, 7656, 7661 (1992).

8) Muto, H.; Nunome, K.; Fukaya, M. *J. Phys. Chem.* 1990, 94, 418.

6. H Atom Quantum Mechanical Tunneling in Reactions of Carbenes with Solidified Organic Molecules at Low Temperature

Hideo TOMIOKA

Chemistry Department for Materials, Faculty of Engineering
Mie University, Tsu, Mie 514 JAPAN

Studies on reactions of carbenes in reactive organic glasses at low temperatures clearly reveal that solution results and liquid phase mechanistic rules cannot be readily extrapolated to matrix conditions. Thus, the usual course of reaction of carbene with an alkene in solution results in the formation of a cyclopropane for both the singlet and triplet states although a one-step addition possible for singlet carbene produces the cyclopropane stereospecifically and a stepwise pathway with the triplet state affords two possible stereoisomers of the cyclopropane. In a sharp contrast, the formal insertion products into the allylic C-H bonds of alkenes are produced at the expense of the cyclopropane when carbene is generated in alkene matrix at low temperature(eq 1).

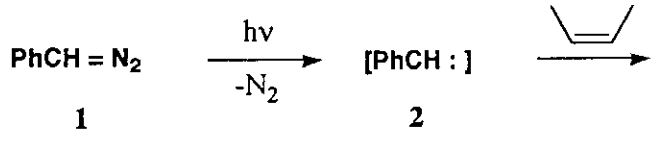

1 2

(1)

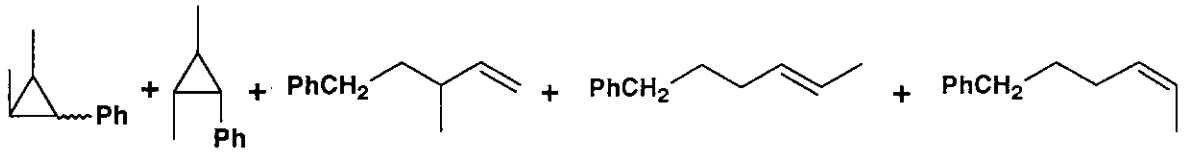

	3	4	5	6	7
0°C	92.7 %	2.1 %	1.4 %	0.4 %	3.5 %
-196°C	43.9	3.2	18.5	4.9	29.0

Similar results are obtained in the reaction with alcohols, where the C-H insertion products are formed in low temperature alcoholic matrices at the expense of the O-H insertion products which are predominant products in the reaction with alcoholic solution at ambient temperature(eq 2). The ^{13}C labelling experiments as well as deuterium kinetic isotope effects suggest that these C-H insertion products are most probably produced from the triplet carbene, not from the singlet, by abstraction of H atom from the matrix followed by the recombination of the resulting radical pairs.

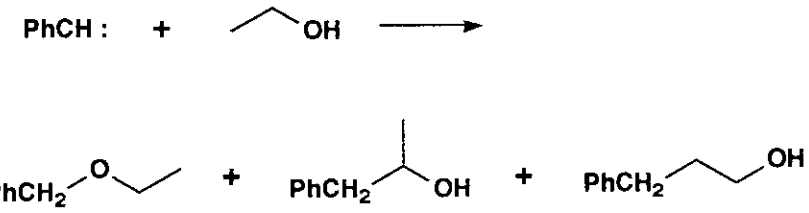

(2)

	12	13	14
0°C	83.5 %	0 %	0 %
-196°C	20.8	64.2	4.8

Kinetic studies using ESR and laser flash photolysis techniques demonstrate that the mechanism of a H-atom transfer reaction changes from a completely classical process in a soft warm glass to a completely quantum mechanical tunneling process in a cold hard glass. Thus, as the reaction temperature is lowered, the classical reaction rate decreases, and eventually becomes much slower than decay by hydrogen atom tunneling. The members of the radical pairs which usually diffuse apart in a fluid solution are not able to diffuse apart owing to the limited diffusibility within a rigid matrix and therefore recombine with high efficiency to give the CH "insertion" products(eq 3).

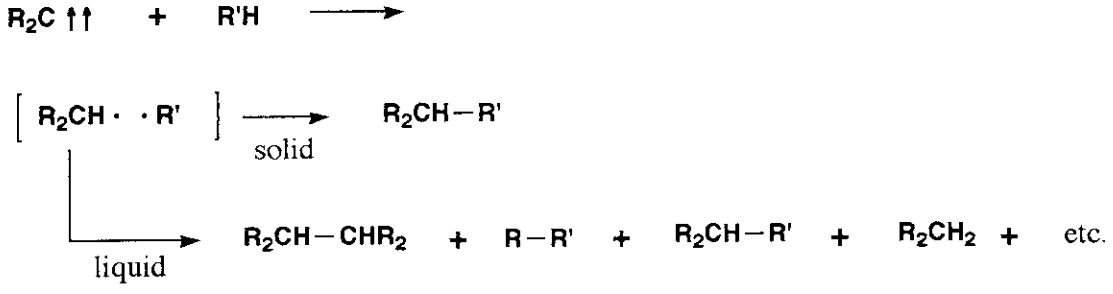

(3)

A rather surprising and intriguing difference between the C-H insertion undergone by singlet carbenes in fluid solution at ambient temperatures and one by triplet carbenes in matrix at low temperature is noted. Thus, a marked increase in the primary and secondary C-H insertion over the tertiary is observed in the matrix reaction indicating that triplet carbenes tend to abstract H from less crowded C-H bonds(eq 4). This is interpreted to indicate that the distance between carbenic center and tunneling H becomes important in H atom tunneling process. More surprisingly, the C-H insertion by triplet carbene by the abstraction-recombination mechanism in a rigid matrix proceeds with retention of the configuration, suggesting that the solid state prevents motion of the radicals to the extents that do not allow for racemization to occur(eq 5).

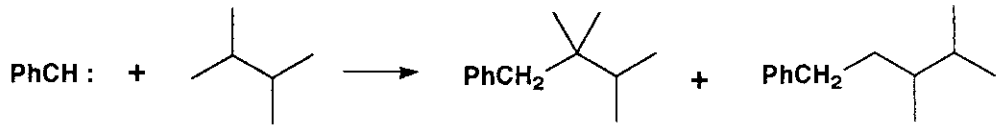

(4)

16 **17**

0 °C	92 %	5.2 %
-196 °C	52 %	48%

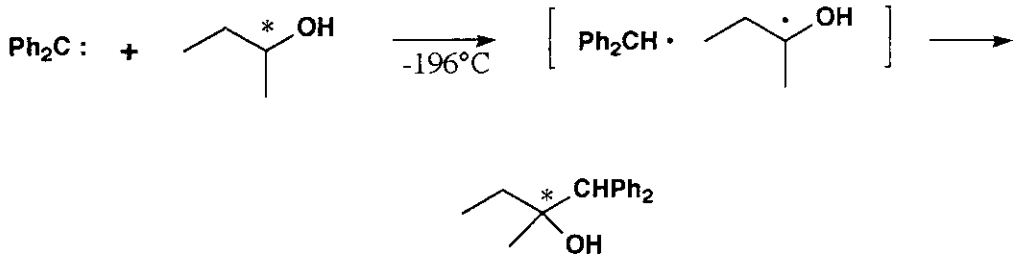

(5)

22

Reactions with heteroatom substrates such as ethers, amines, alkyl halides and ketones are also subject to the matrix effects and the C-H insertion products increase at the expense of singlet carbene reaction products resulting from the interaction with the heteroatoms. Stereoselectivities of cyclopropanation to styrenes are also shown to be affected by the matrix effects. tert-Butyl alcohol matrix is shown to be unreactive toward carbenes and thus can be used as a "solvent" in matrix carbene reactions presumably due to a large inert guest cavity provided by bulky tertiary alcohol which binds a molecular aggregate inside it. H atom tunneling in the matrix is also shown to compete with very efficient intramolecular migration of hydrogen to the carbenic center. Migration aptitude as well as stereochemistry are also found to be subject to the matrix effects.

H. Tomioka, *Res. Chem. Intermed.*, **20**, 605 (1994).
M. S. Platz, *Acc. Chem. Res.*, **21**, 236 (1988).
B. B. Wright, *Tetrahedron*, **41**, 1517 (1985).

7. An ESR Study on Trimethylenemethane Radical Cation

M. Shiotani and K. Komaguchi
Faculty of Engineering, Hiroshima University,
Higashi-Hiroshima, 739, Japan.
A. Lund
Department of Physics and Measurement Technology,
Linköping University of Technology, S-581 83 Linköping, Sweden.

The electronic structure of trimethylenemetane (TMM) radical cation was studied by ESR spectroscopy and *ab-initio* MO calculations. The 4.2 K ESR spectrum of TMM^+ consists of a septet with isotropic ^1H *hf* splitting of 0.93 mT (6 H) in a halocarbon matrix. No appreciable ESR line-shape change was observed between 4 K and 125 K. The *ab-initio* MO calculations resulted in the TMM^+ with a $^2A_2$ state in distorted C_{2v} structure, in which the unpaired electron mainly resides in the p_z orbitals of the two equivalent terminal carbons. The spectra were explained by an intramolecular dynamics among three energetically equivalent C_{2v} structures to average the structural distortion out giving an apparent D_{3h} structure even at a low temperature of 4.2 K.

Since the low temperature matrix isolation technique combined to ionizing radiation was applied to ESR spectroscopy in order to study organic radical cations in the late 1970s, a large number of studies have been made on the electronic structure, dynamics, and reactions of the radical cations [1,2]. The electronic structure of radical cations whose parent molecules have a degenerate or near-degenerate highest occupied molecular orbital (HOMO) has been especially interested with the aim of observing a structural distortion expected due to Jahn-Teller or pseudo Jahn-Teller effect [1-13]. Here we wish to report an ESR study on the structure of trimethylenemethane (TMM) radical cation. TMM is one of the most attractive organic molecules to investigate the electronic

structure because of a rather small fundamental molecule with a high symmetry and a triplet state with a doubly degenerate HOMO in the ground state [14].

The experimental ESR spectra are shown in Figure 1. The spectra were observed for trimethylenemethane (TMM) radical cation generated by γ-ray irradiation of the solid solutions containing ca. 0.2 mol % of methylenecyclopropane (MCP) in CF_2ClCF_2Cl matrix at 4.2K. The spectral line shape is almost independent of temperatures from 4.2K to 125K except for slightly decreasing in the line width with increasing temperature (spectrum *1b*). Relative intensities of the septet are close to a binomial one, 1:6:15:20:15:6:1, and the line shape is successfully reproduced by employing magnetically equivalent six protons with 0.93 mT *hf* splitting and a line width (ΔH_{msl}) of 0.6 mT as shown with the dotted lines. The magnetically equivalent six protons can not be attributed to any radicals with the original ring-closed MCP geometrical structure, but with ring-opened TMM radical cation.

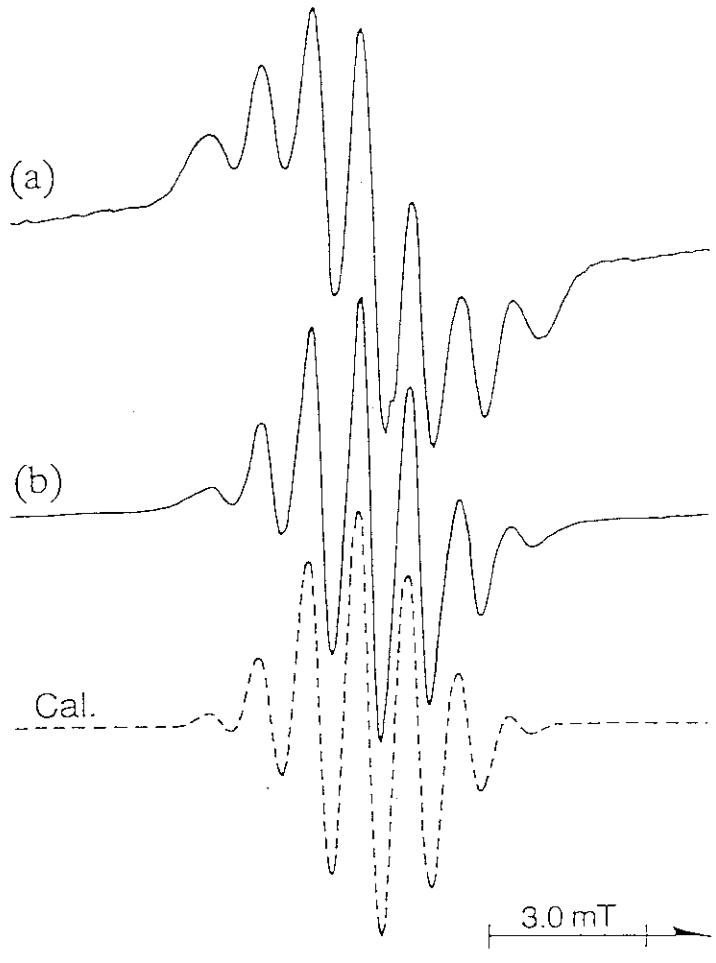

Fig. 1. ESR spectra of trimethylenemethane radical cation (TMM^+) observed (a) at 4.2K and (b) at 77K. The dotted lines are a spectrum simulated to the 77K. The TMM^+ was generated by γ-ray irradiation of the solid solution of *ca.* 0.2 mol % methylenecyclopropane (MCP) in $CF_2ClCFCl_2$ at 4.2K.

The TMM has a triplet state with doubly degenerate highest occupied molecular orbital (HOMO), e'', in the ground state. The TMM^+ has a doublet state with one unpaired electron. However, the original D_{3h} symmetry of TMM may be reduced to a lower one, probably C_{2v}, due to a Jahn-Teller effect. Then,

the degenerate SOMO, e'', in D_{3h} should be split into a_2 and b_1 orbitals in the C_{2v} symmetrical structure through a structural distortion *via* e' vibration (see the following Insert).

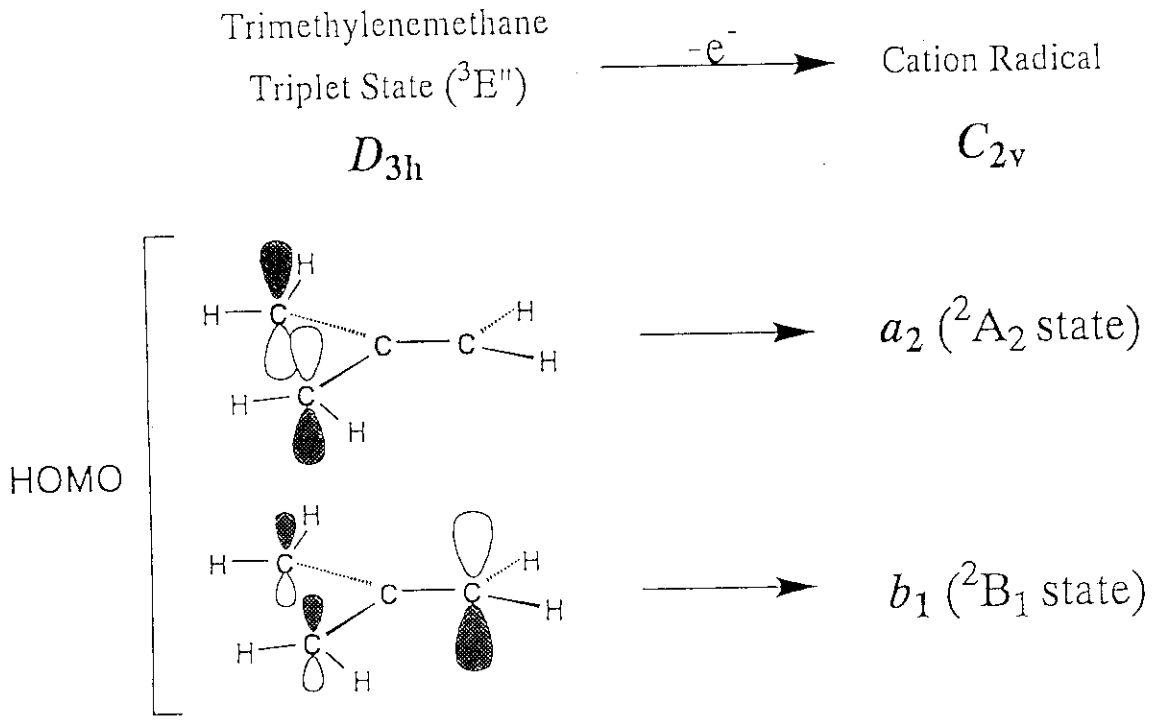

In order to see which state of $^2A_2$ and $^2B_1$ is responsible for the observed TMM^+ the *ab-initio* MO calculations were performed. Figure 2 shows two states, $^2A_2$ and $^2B_1$ of the C_{2v} geometrical structure of TMM^+, which were optimized by the *ab-initio* MO calculations at UHF/6-31G** level on Gaussian 90 program. The $^2A_2$ structure has one shorter C-C bond of 1.397 Å along the C_2 axis, the other two C-C bonds having a longer bond length of 1.412 Å. On the other hand, in the $^2B_1$ structure the unique C-C bond becomes longer (1.452 Å) than the other two C-C bonds (1.385 Å). The ^1H *hf* splittings were evaluated for the two optimized structures by means of the INDO MO method (values in parentheses). The total *hf* splittings of 5.26 mT and 5.22 mT calculated for both structures are in fairly good agreement with the experimental value of 5.58 mT. The MO calculations resulted in that the $^2A_2$ structure is more stable by *ca.*0.3 eV in the total energy than the $^2B_1$ structure. Thus, the former structure seems preferable as the ground state of TMM^+ with a distorted C_{2v} structure, though the energy

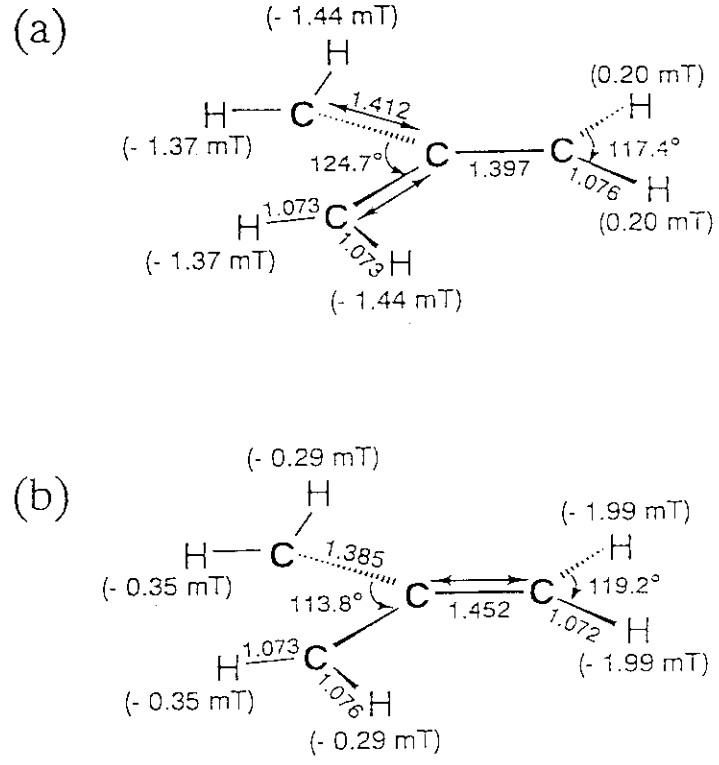

Fig. 2. The optimized geometrical structures of TMM^{+} with C_{2v} symmetry by using the *ab-initio* MO calculations at 6-31G** level. The bond lengths in Å. The isotropic ^{1}H *hf* splittings were evaluated for two states, (a) $^{2}A_2$ and (b) $^{2}B_1$, with C_{2v} by the INDO MO method (in parentheses).

difference is not so large. In the $^{2}A_2$ structure the unpaired electron mainly resides in the $2p_z$ orbitals of two equivalent terminal carbons, similar to the case of allyl radical. To be consistent with the experimental results we propose that an intramolecular dynamics takes place between the three magnetically equivalent C_{2v} structures so as to give an apparent D_{3h} structure with six equivalent hydrogens even at a low temperature of 4.2K.

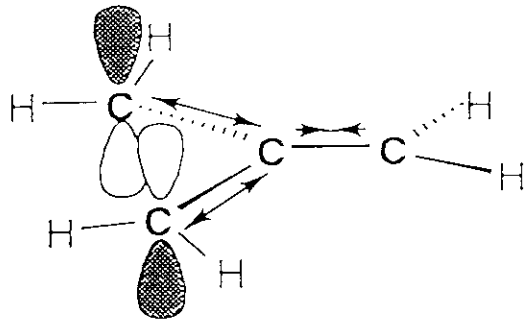

a_2 in C_{2v}

SOMO

Acknowledgment: K. K. and A. L. thank the JSPS Fellowships for Japanese Junior Scientists and for research in Japan, respectively.

References :

[1] M. Shiotani, *Magn. Reson. Rev.*, **1987**, 12, 333
[2] A. Lund and M. Shiotani, Eds.; *"Radical Ionic Systems"*, Kluwer Academic Publishers, Dordrecht, The Netherlands, **1991**.
[3] M. Shiotani, M. Lindgren, and T. Ichikawa, *J. Am. Chem. Soc.*, **112**, 967- 73 (1990).
[4] M. Shiotani, L. Sjöqvist, A. Lund, S. Lunell, L. Eriksson, and M. B. Huang, *J. Phys. Chem.*, **94**, 8081 (1990).
[5] L. Sjöqvist, M. Lindgren, A. Lund, and M. Shiotani, *J. Chem. Soc. Faraday Trans.*, **86**, 3377-82 (1990).
[6] M. Shiotani, M. Lindgren, N. Ohta, and T. Ichikawa, *J. Chem. Soc. Perkin Trans. 2*, 711- 19 (1991).
[7] M. Shiotani, K. Komaguchi, J. Ohshita, M. Ishikawa, and L. Sjöqvist, *Chem. Phys. Lett.*, **188**, 93 - 99 (1992).
[8] M. Lindgren, M. Matsumoto, and M. Shiotani, *J. Chem. Soc. Perkin Trans. 2*, 1397 - 1402 (1992).
[9] K. Komaguchi, M. Shiotani, M. Ishikawa, and K. Sasaki, *Chem. Phys. Lett.*, **200**, 580 - 86 (1992).
[10] L. A. Eriksson, L. Söqjvist, S. Lunell, M. Shiotani, M. Usui, and A. Lund, *J. Amer. Chem. Soc.*, **115**, 3244- 49 (1993).
[11] M. Shiotani, M. Matsumoto, and M. Lindgren, *J. Chem. Soc. Perkin Trans. 2*, 1995 - 2002 (1993).
[12] A. Hasegawa, M. Shiotani, and Y. Hama, *J. Phys. Chem.*, **98**, 1834 -39 (1994).
[13] M. Lindgren, K. Komaguchi, and M. Shiotani, *J. Phys. Chem.*, **98**, 8331- 38 (1994).
[14] O. Claesson, A. Lund, T. Gillbro, T. Ichikawa, O. Edlund, and H. Yoshida, *J. Chem. Phys.*, **1980**, 72(3), 1463-1470.

8. Tunneling Reaction of Recoil Tritium Atom with H_2 at Very Low Temperature
-Low Temperature Tritium Chemistry Using Nuclear Reactor-

Yasuyuki Aratono

Advanced Science Research Center, Japan Atomic Energy Research Institute, Tokai-mura, Ibaraki-ken 319-11, Japan

The study of recoil tritium reaction with hydrogen (n-H_2, p-H_2 and D_2) at 4.2 and 77K was carried out using low temperature neutron irradiation facility of JRR-4 at Japan Atomic Energy Research Institute(JAERI). In n-H_2 - D_2 mixture diluted with large amount of Xe moderator(99.0 and 99.8 mol%) at 77K, the isotope effect for H and D abstraction by recoil tritium, k_H/k_D, was 7, suggesting the contribution of tunneling abstraction by thermalized tritium. The effect of rotational quantum state(J=0,1) of H_2 on the tunneling abstraction reaction was also investigated. The ratio of rate constant of p-H_2(J=0) +T$\rightarrow$ HT + H to o-H_2(J=1) + T $\rightarrow$ HT + H was 4$\pm$2.

1. Introduction

The tunneling abstraction reaction caused by H and D atoms produced by γ-radiolysis of H_2 or D_2 and photolysis of HI or DI has been studied by Miyazaki et al. and very large isotope effect has been reported[1]. Tritium(^{3}H,T) is one of the hydrogen isotopes and thus is expected to abstract hydrogen in a similar manner as H and D atoms do. As T atom is formed through ^{6}Li(n, α)^{3}H nuclear reaction, the initial(recoil) kinetic energy is 2.74MeV. It is very large compared to that for H and D atoms produced by γ-radiolysis or photolysis(few eV). In addition, T atom is formed under very large γ-ray dose rate. In the present paper, some works on the tunneling abstraction by the thermalized T in the mixture of n- or p-H_2-D_2-Xe-^{6}LiF are introduced and characteristics of recoil T reaction compared to H and D reactions are discussed.

2. Experimental

2.1 Facilities for low temperature neutron irradiation at JAERI

Table 1 shows the facilities for the low temperature neutron irradiation at Japan Research Reactors 2, 3 and 4 at JAERI. .

Table 1 Facilities for low temperature neutron irradiation at JRR-4

Reactor	irradiation port	thermal neutron flux ($n/m^2/sec$)	γ-ray dose rate (Sv/h)	irradiation temperature (K)	maximum irradiation period
JRR-2[1]	DMNS	10^{11}	~0	<4.2	50hrs
JRR-3	neutron beam experimental facility	10^{12}	~0	<4.2	26days
JRR-4	pneumatic tube	$4.0x10^{17}$	$2x10^6$	77	15sec
JRR-4[2]	lid tank irradiation facility	$5.5x10^{13}$	50	4.2	6hrs

1)Japan Research Reactor-2, The reactor will be operated till March of 1997.

2)The facility is going to be reconstructed to reduce the γ-ray dose rate by about two orders of magnitude without reduction of thermal neutron flux.

Among the irradiation ports described in Table 1, the lid tank irradiation facility at JRR-4 , which is shown in Fig. 1, was mainly used in order to minimize the radiation effect and to produce necessary amount of tritium activity.

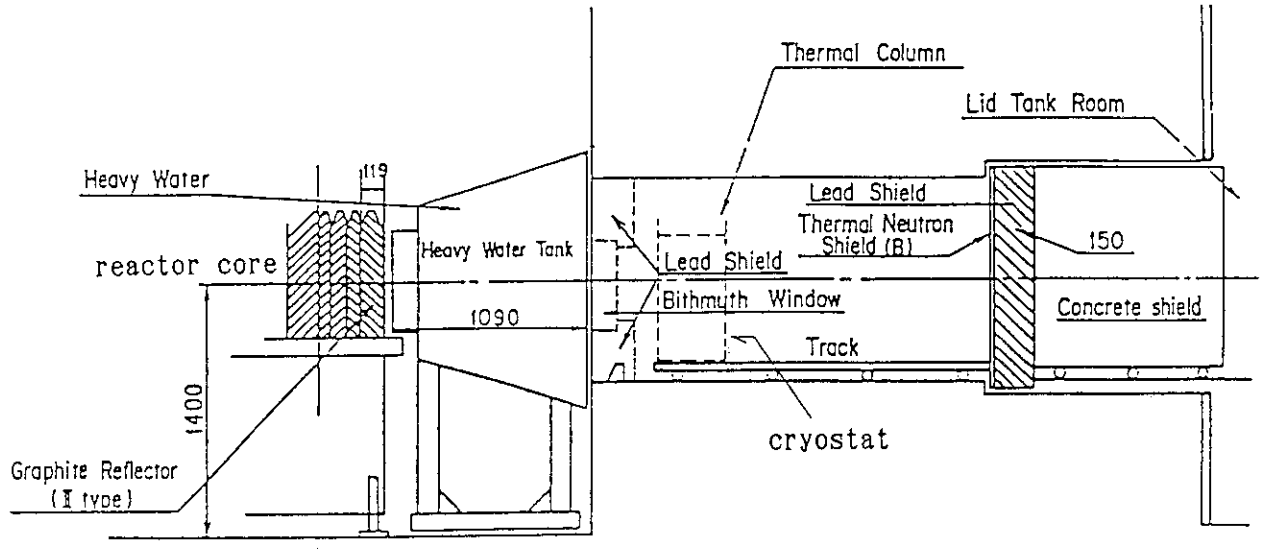

Fig. 1 Lid tank neutron irradiation facility at JRR-4

2.2 Cryostat

Fig. 2 shows the cryostat used for the lid tank irradiation facility at JRR-4. It is made of stainless-steel. As the whole body is exposed to in-pile radiations(neutron and γ-ray), plastics and materials which cause high induced radioactivity were not used.

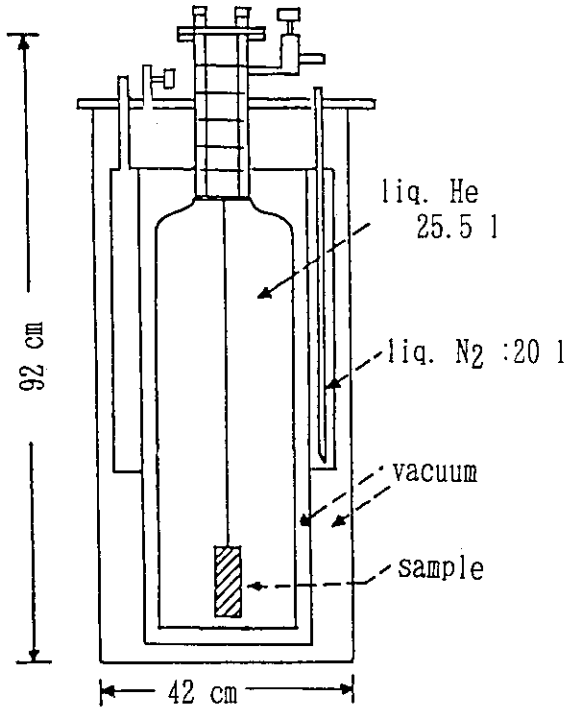

Fig. 2 Stainless-steel cryostat for low temperature irradiation

2.3 Neutron irradiation

The mixture of n- or p-H_2-D_2-Xe-^{6}LiF was sealed into the quartz cell, put into the cryostat and irradiated at 4.2 or 77K for 6 hours. The separation procedure of p-H_2 from n-H_2 was described elesewhere[2]. In order to prevent p-H_2 from changing into o-H_2, the samples of p-H_2 sealed into quartz cells were stored at 4.2K before neutron irradiation. The conversion of p-H_2(or o-H_2) into o-H_2(or p-H_2) during the neutron irradiation can be neglected.

2.4 Analysis of reaction products

After the neutron irradiation, the samples were warmed to room temperature for analysis of HT and DT. The separation of HT and DT was carried out with radio-gas chromatograph(1.2m long activated alumina column containing 10 wt% manganese chloride) at 77K. The typical radio-gas chromatogram of HT and DT is shown in Fig. 3.

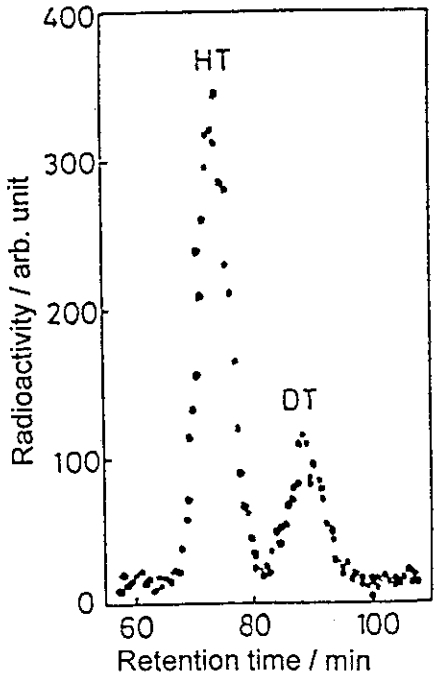

Fig. 3 Radio-gaschromatogram of HT and DT

3. Results and discussion

3.1 Tunneling abstraction by recoil tritium atom in solid n-H_2-D_2-Xe-^{6}LiF mixture at 77K[3]

The fractions of HT yields produced by recoil T in n-H_2-D_2-^{6}LiF mixture(●)

and n-H_2-D_2-Xe-^{6}LiF mixture(○:99.0 mol % Xe, △ : 99.8 mol % Xe) are shown in Fig. 4. In the former, the isotope effect(k_H/k_D) was close to the calculated value of 1(dotted line). However, when 99.0 and 99.8 mol% of Xe was added in the mixture as a moderator for the energetic T atom, the isotope effect increased and agreed with the calculated value of k_H/k_D=7(solid line). From the results, it was concluded that the recoil T atom is thermalized by the sequential collision with Xe, diffuses into the solid matrix and reacts with H_2 and D_2 by the quantum mechanical tunneling reaction.

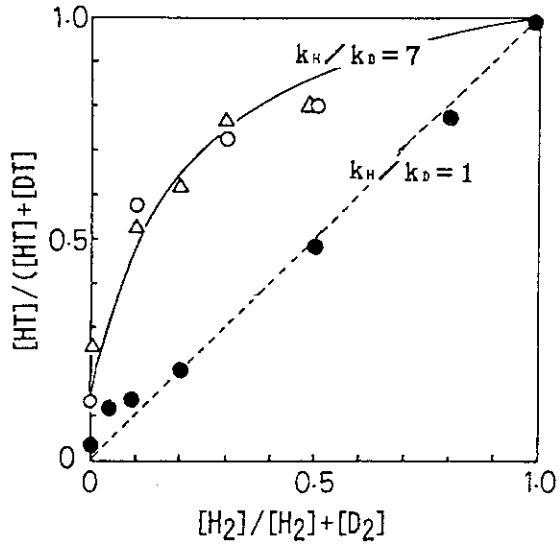

Fig. 4 Fraction of HT yield produced by recoil T atom reaction
(●) n-H_2-D_2
(△) n-H_2-D_2-Xe(99.8 mol%)
(○) n-H_2-D_2-Xe(99.0 mol%)

3.2 Effect of Rotational Quantum State(J=0,1) on the Tunneling Reaction of $H_2 + T \rightarrow H + HT$ in Xenon-Hydrogen Mixtures at 77K[4)]

Fig. 5 shows the ratio of HT yields to DT yields, [HT]/[DT], produced by a recoil T reaction in solid n- or p-H_2-D_2-Xe-^{6}LiF mixtures at 77K, against the hydrogen isotope ratio, $[H_2]/[D_2]$. The total concentration of H_2 and D_2 is fixed at 1 mol%(99 mol% of Xe) . Closed circles and open circles represent the results for p-H_2 and n-H_2, respectively. The dotted line shows the results in solid hydrogen of the H_2-D_2 mixtures without xenon at 4.2K[5)]. The HT/DT ratio increases roughly linearly with an increase in the H_2/D_2 ratio. However, it does not extend to zero when the ratio is extrapolated to a zero concentration of H_2. Some HT may be produced by wall reactions or some un-identified reactions. Thus, the isotope effect on the tritium reaction was estimated from the slope of the linear relationship between the [HT]/[DT] and $[H_2]/[D_2]$ ratios.

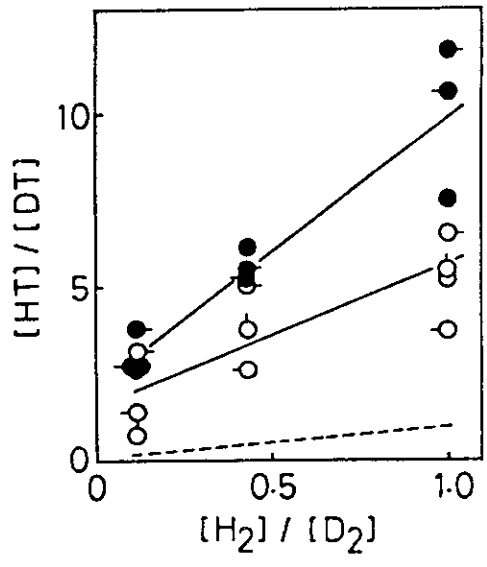

Fig. 5 The ratio of HT yields to DT yields, [HT]/[DT], against the hydrogen isotope ratio of H_2 to D_2, $[H_2]/[D_2]$.
(●, ●, ●) : [HT]/[DT] in p-H_2-D_2-Xe
(○, ○, ○, ○) : [HT]/[DT] in Xe-n-H_2-D_2
The dotted line shows the result of H_2-D_2 mixtures at 4.2K without xenon, quated from 5).

The large isotope effect shown in Fig. 5 suggests that most of the HT and DT are not formed by reactions of hot T atom, but by the tunneling reaction of thermalized T atom because the isotope effect through hot atom reaction has been reported to be about 1.

By taking into consideration of nuclear spin isomer composition in n-H_2(75% o-H_2 and 25% p-H_2), k_H(p-H_2)/k_H(o-H_2) is estimated as 4 ± 2. The effect of rotational quantum states on a tunneling reaction H + H_2 at 4.2K was reported to be 3.6[2]. Therefore it is concluded that both T and H atoms react more effectively with H_2 molecules at J=0 than those at J=1 and that the ratio of rate constants, k(J=0)/k(J=1), for the H(T) + H_2 tunneling reaction is about 4.

4. Conclusion

The tunneling abstraction from H_2 and D_2 by thermalized T atom was experimentally shown in the thermal neutron irradiation at the lid tank irradiation facility of JRR-4 at 77K. The isotope effect for T atom obtained by the present experiment is much smaller than those for H and D atoms. The similar tendency in the isotope effect was observed in the reaction of recoil T atom with alkane mixtures[6]. As was described previously, T atom is produced with a very large recoil energy under the high γ-ray dose rate. These two factors are considered to reduce the isotope effect for T. In order to clarify the different behavior among hydrogen isotopes, the experiment applying photolysis of TI or TBr and γ-radiolysis of T_2 is now under consideration.

References

1) T. Miyazaki, N. Iwata, K. Lee, and K. Fueki, J. Phys. Chem., **93**(1983)3352.
2) T. Miyazaki, T. Hiraku, K. Fueki, and Y. Tsuchihashi, J. Phys. Chem, **95**(1991)26.
3) H. Hase, K. Ishioka, and M. Miyatake, Bull. Chem. Soc. Japan, **65**(1992)2526.
4) Y. Fujitani, T. Miyazaki, N. M. Masaki, Y. Aratono, and E. Tachikawa, Chem. Phys. Letters, **214**(1993)301.
5) Y. Fujitani, T. Miyazaki, K. Fueki, N. M. Masaki, Y. Aratono, M. Saeki, and E. Tachikawa, J. Phys. Chem., **95**(1991)1651.
6) Y. Aratono, E. Tachikawa, T. Miyazaki, Y. Kawai, and K. Fueki, J. Phys. Chem, **86**(1982)248.

9. Low-Temperature Irradiation Cryostats for Fundamental Research on Radiation Damage

Akihiro Iwase

Advanced Science Research Center, Japan Atomic Energy research Institute

Tokai-mura, Naka-gun, 319-11, Ibaraki, Japan

Low temperature irradiation is one of the most important experimental methods for fundamental research on radiation damage because the thermal motion of irradiation-produced defects is frozen during irradiation and we can see the primary state of damage. For a last decade, our research group has been involved in the study of irradiation damage in metals by low-temperature irradiation. In this report, I show two low-temperature irradiation cryostats used for our experiments and some results.

We have used two cryostats which are connected to a 2MV VdG accelerator and tandem accelerator, respectively. Figure 1 shows the cryostat interfaced to the center duct of a 2MV VdG accelerator. Ion beam comes from the left side of the figure. The ion species are H, He, C, N, O, Ne and Ar, and ion energies are 0.5-2.0 MeV. To avoid the contamination of specimen, a liquid nitrogen trap is used. A homogeneity of defocused beam is confirmed using a beam viewer(quartz plate) and the beam shape is defined by 3mm x 6mm aperture. The specimen is attached to the specimen holder which is surrounded by 77K and 4K thermal shields. To measure an ion beam current accurately, a secondary-electron suppressor is used. The voltage between the suppressor and the ground is about -300V. The chromel/Au-Fe thermocouple at the rear side of the specimen holder is used for the measurement of specimen temperature. During irradiation, the temperature is held below 6K. Constantan heater is used for the warm up of the specimen temperature to 300K. A similar cryostat for low-temperature irradiation is interfaced to tandem accelerator (Fig. 2). Ion species are C, F, Si, Cl,Br, I and Au. Ion energies are 84-200MeV.

Specimens used in the present experiment are thin foils of typical FCC metals(Al, Cu, Ag, Ni and Pt). As the thickness of the specimen is much smaller than the ion range, irradiating ions pass through the specimen completely and the defect distribution in the specimen is almost homogeneous.

The experimental procedure is as follows; first, the electrical resistivity of the specimen is measured every 1 minute during irradiation. Irradiation time can be controlled by a beam shutter(or Faraday cup) in front of the specimen. Since the resistivity change by irradiation is nearly

proportional to the concentration of defects in metals, we can get the defect production rate through this experiment. When the defect concentration in the specimen reaches 1000-1500ppm, the irradiation ceases and the specimen is warmed up to 300K at a constant rate to get defect recovery spectra as a function of annealing temperature. An example of the experimental results is shown in Fig. 3. With increasing ion-fluence, the defect concentration increases and tends to be saturated . The saturation is caused by the annihilation of irradiation-produced defects during irradiation through the interaction between already existing defects and subsequently irradiating ion. This phenomenon is called "irradiation annealing". Defect recovery spectra for ion-irradiated Ni are shown in Fig. 4. A large recovery peaks are found around 60K . These recovery stages are called "stage I". Around the temperature of stage-I, only interstitials which are isolated and not clustered can thermally diffuse. Therefore, the stage-I recovery is caused by the recombination of such interstitials with immobile vacancies. As can be seen in Fig. 4, for high energy(84-120MeV) ion irradiations, the recovery of stage-I dramatically decreases with increasing ion mass and for 100MeV Br and I irradiation, it nearly completely disappears[1]. Such an anomalous behavior of stage-I recovery has never been observed for electron, neutron or low energy(several hundred keV)-ion irradiation. Figure 5 shows the amount of the defect recovery in stage-I as a function of electronic stopping power Se. The stage-I recovery decreases monotonically with increasing Se. This means that the electron excitation by ion plays an important role in the radiation annealing during high energy irradiation to Ni[1,2]. The effect of electron excitation on radiation annealing cannot be found in metals with weak electron-phonon interaction(Cu and Ag), and the effect remarkably appears in metals with strong electron-phonon interaction(Ni and Pt)[3]. From the experimental results, we concluded that in Ni and Pt, the energy of excited electrons is transferred to lattice through strong electron-phonon interaction and the lattice agitation is induced, resulting in the annihilation of stage-I defects. We also have found the possibility of defect production by electron excitation in some metals[4]. Concerning the details of the electron excitation effect on the radiation damage in metals, see review papers[5,6].

Recently, we have assembled two new low temperature irradiation chambers; one is connected to a 3MV single-end accelerator at Takasaki establishment and the other to a 20MV tandem accelerator at Tokai establishment. Both chambers have superconducting magnets and *in-situ* measurements of Hall voltage and magneto-resistance can be performed for ion or electron-irradiated specimens. Moreover, the specimen temperature can be held at 2-4K even during irradiation. Using these facilities, we will be engaged in the study of irradiation effect in not only metals but also semi-metals(graphite), semi conductors and high-Tc superconductors.

References

[1] A. Iwase, S. Sasaki, T. Iwata and T. Nihira; Phys. Rev. Lett. **58** (1987) 2450.

[2] A. Iwase, T. Iwata, S. Sasaki and T. Nihira; J. Phys. Soc. Jpn. **59** (1990)1451.

[3] A. Iwase, T. Iwata, T. Nihira and S. Sasaki; Mater. Sci. Forum **97-99** (1992) 605.

[4] A. Iwase, T. Iwata and T. Nihira; J. Phys. Soc. Jpn. **61** (1992) 3878.

[5] A. Iwase, T. Iwata and T. Nihira; Nihon Buturi Gakkaisi **48** (1993) 274.(in Japanese)

[6] A. Iwase and T. Iwata; Nucl. Instrum. Methods **B90** (1994) 322.

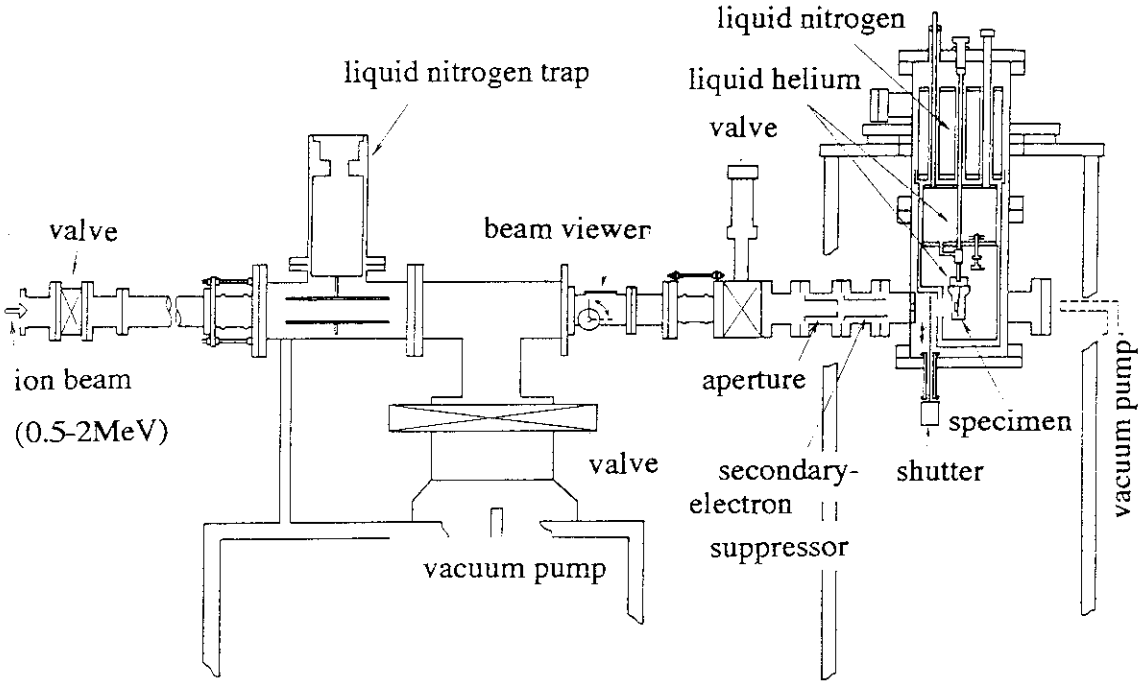

Fig. 1 Low temperature irradiation cryostat connected to a 2MV VdG accelerator

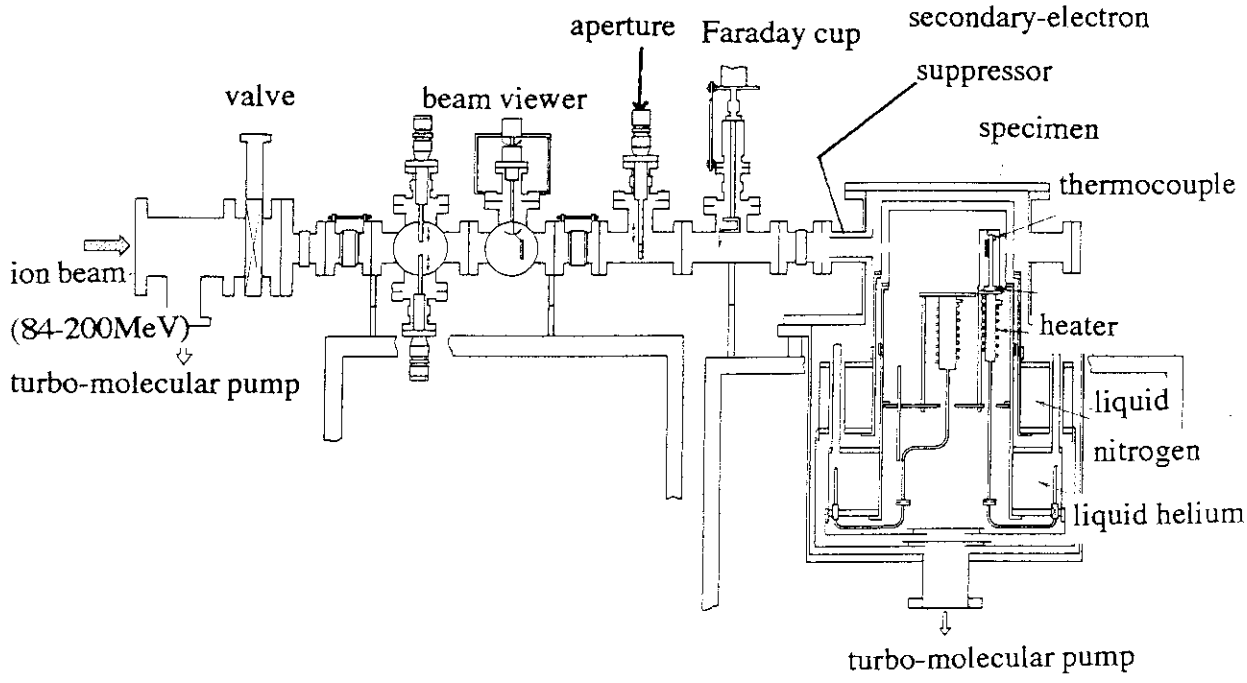

Fig. 2 Low temperature irradiation cryostat connected to a tandem accelerator

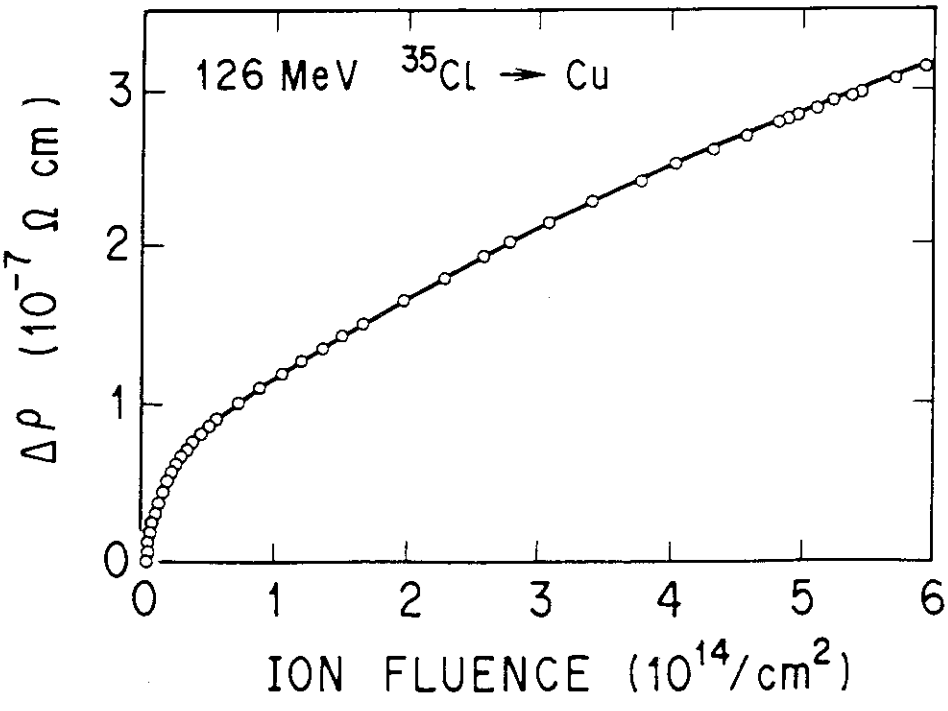

Fig. 3 Electrical resistivity change as a function of ion-fluence

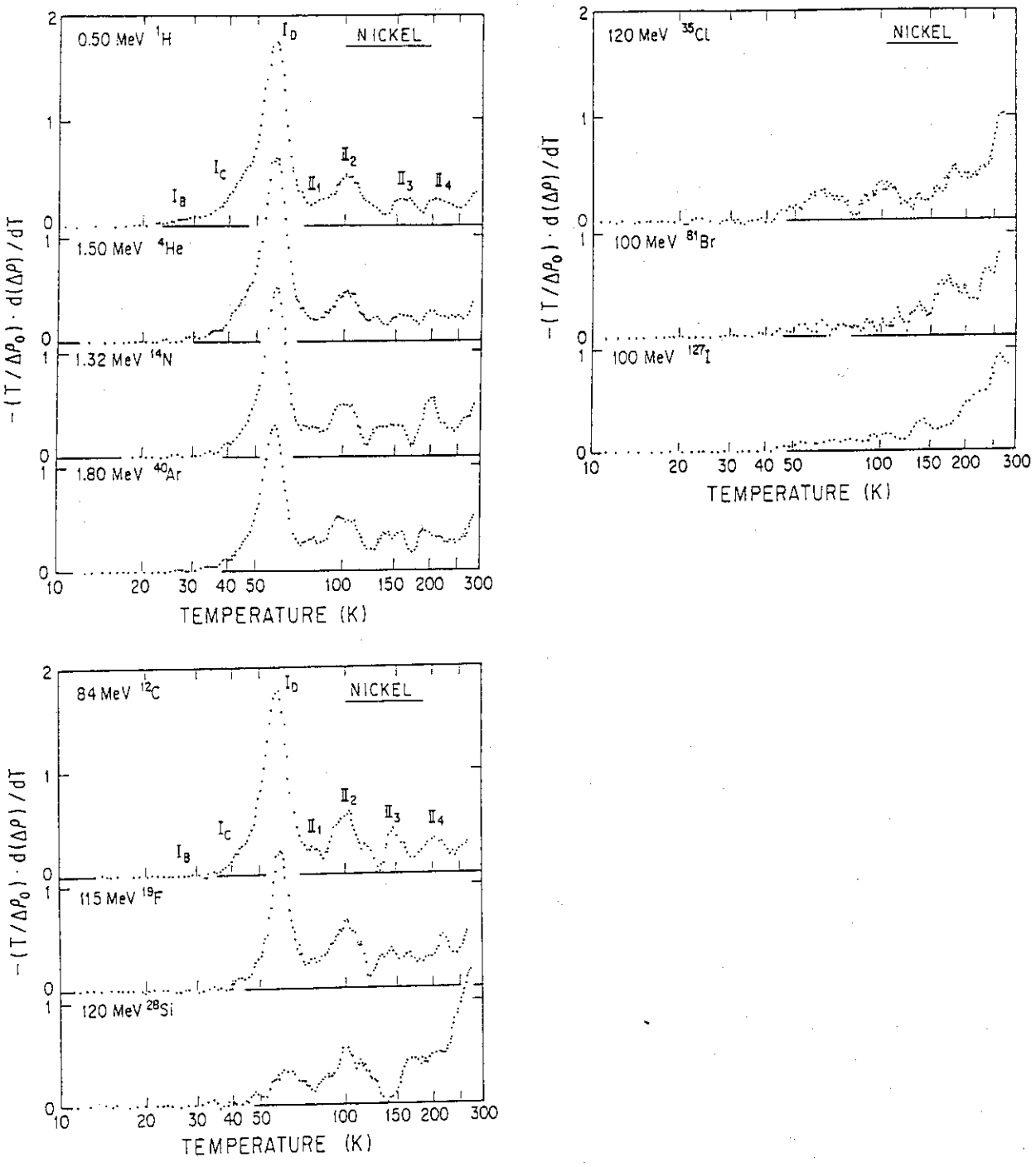

Fig. 4 Defect recovery spectra for ion-irradiated Ni

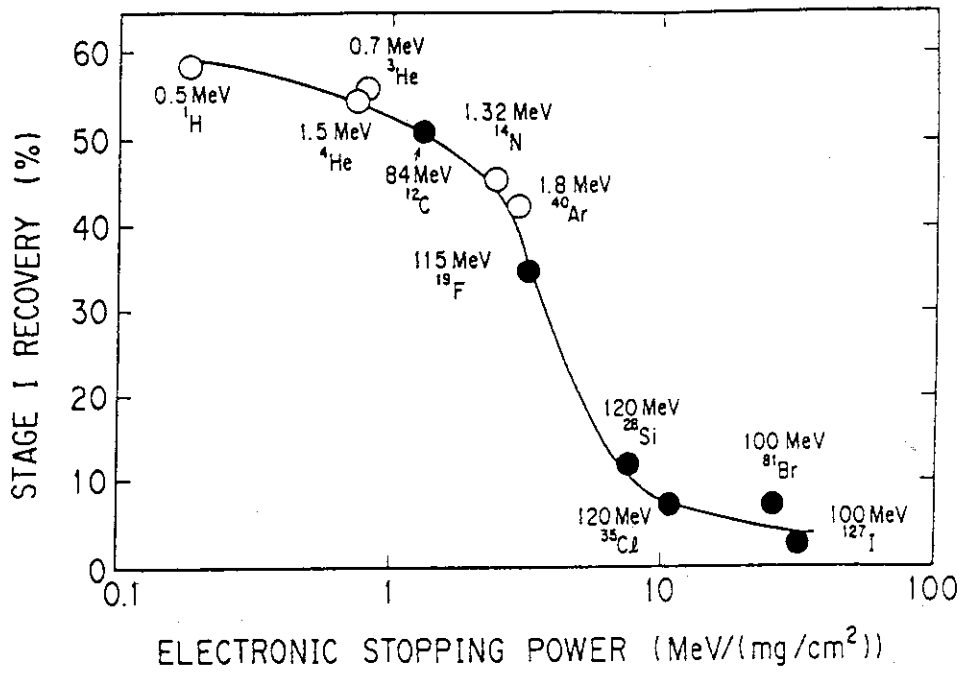

Fig.5 Amount of stage-I defect recovery for ion irradiated Ni as a function of Se

10. Pulsed High Magnetic Field ESR at Low Temperature

Koichi KINDO

Research Center for Extreme Materials, Osaka University, Machikaneyamacho 1-3, Toyonaka, Osaka 560, Japan
e-mail:kindo@rcem.osaka-u.ac.jp

Magnetic measurements have been carried out in High Magnetic Field Laboratory of the Research Center for Extreme Materials, Osaka University. In the field of ESR, much work has been done and covered the microwave frequency and the magnetic field as shown in Fig. 1. The microwave in the low frequencies are generated by Klystron and laser systems make the sub-millimeter waves available. High magnetic field up to 40 Tesla(T) is applied by means of pulsed method. Pulse duration is about 40 msec, which is long enough for ESR measurement. Different type of magnet system which produces the field up to 60 T in the duration of 0.4 msec is used for the submillimeter ESR.

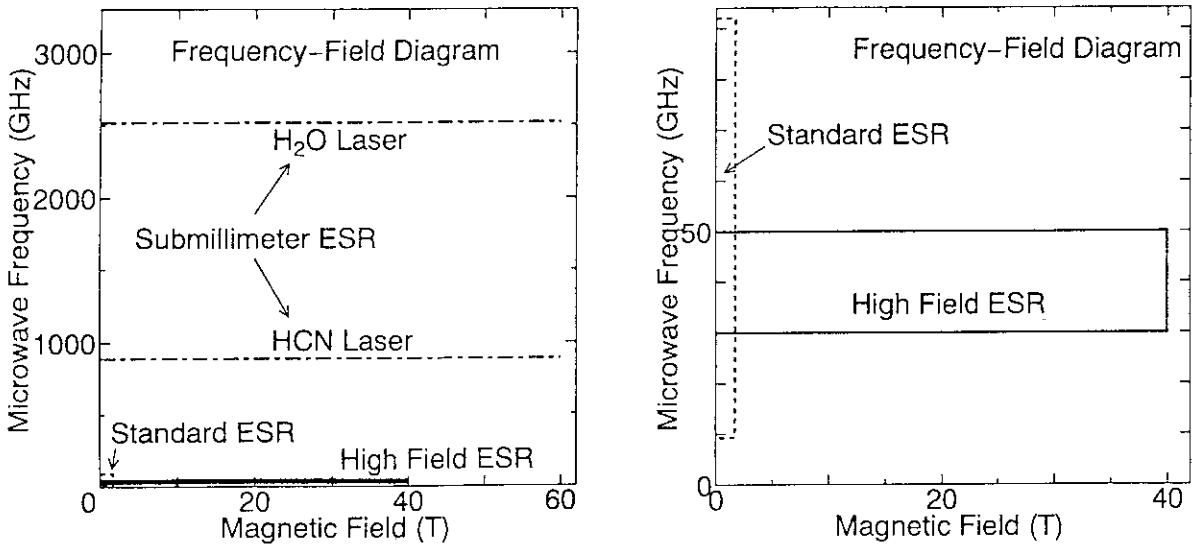

Fig. 1 Microwave frequency and magnetic field region covered by high field ESR.

Block diagram of high field ESR measurement is shown in Fig. 2. Standard reflection type of cavity and microwave frequency of 50 GHz are adopted for the system because the inner diameter of liquid helium Dewar is limited. Glass Dewar and cryostat is shown in Fig. 3. The wave guide of copper-nickel is used to avoid heat transfer.

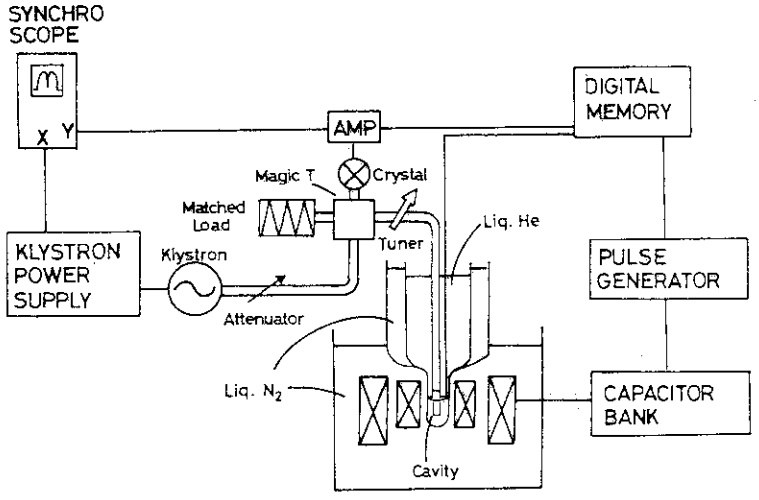

Fig. 2 Block diagram of high field ESR.

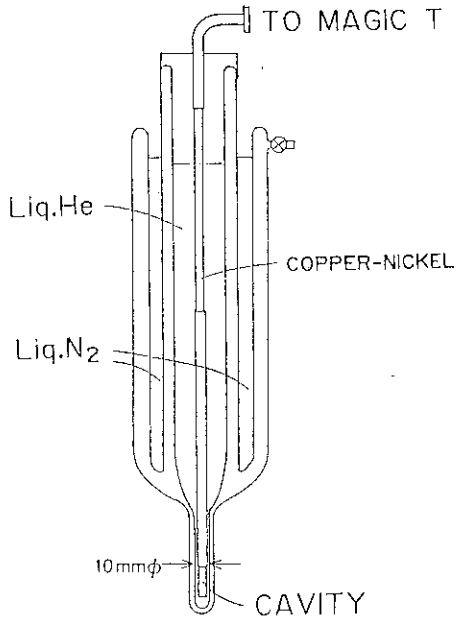

Fig. 3 Glass Dewar and cryostat for high field ESR.

Much work has been done by using the system and a few example are exhibited to show the effects. One dimensional antiferromagnet cupric oxide, CuO, related with the high T_c superconductor was studied[1] and very broad absorption which has a line width of more than 1 T, as shown in Fig. 4, was observed for the first time. Large line width could not have been observed by the standard technique and the pulsed field is effective to detect.

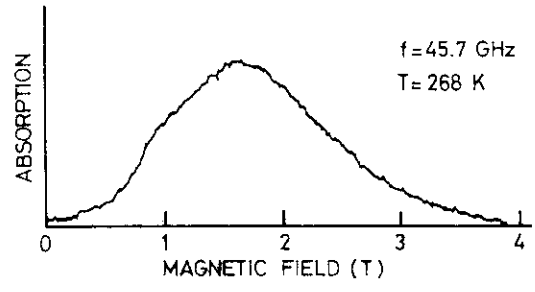

Fig. 4 Paramagnetic resonance of powdered CuO.

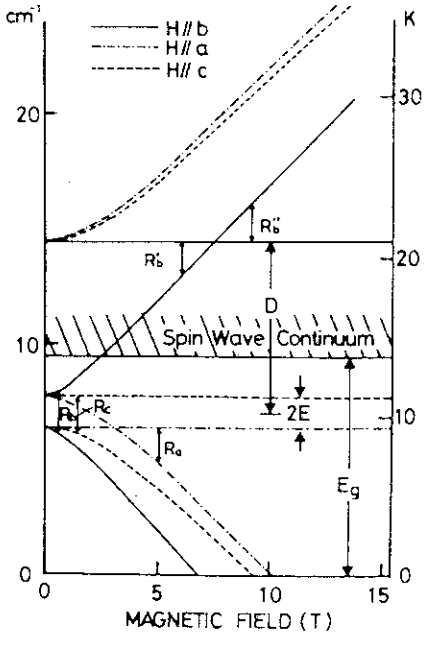

Fig. 5 Energy level diagram of NENP under a magnetic field.

Next example is also one dimensional antiferromagnet of S=1 system, which is called as Haldane material since Haldane conjectured energy spectrum of the system has different nature depending on wheter the spin is half-integer or integer. NENP is one of the best candidates for testing the conjecture and was investigated by high field ESR.[2] Elementary excitation of the Haldane system was cleared as Fig. 5 and the conjecture was proven. Last example is the study of URu_2Si_2,[3] which is a intermetallic compound and called as heavy fermion systems. Absorption is observed at very high field around 20 T as shown in Fig. 6. Effective g-value is obtained to be 0.15, which is small compared to the standard g-value and understood well by considering a combination of localized uranium moment and conduction electron spin.

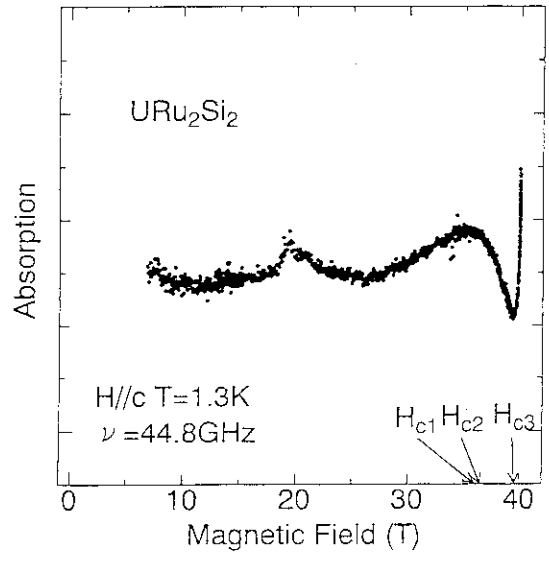

Fig. 6 ESR signal of URu_2Si_2 at 1.3 K.

As a conclusion, it is noted that high field ESR is very effective to tha case that the line width is broader than 1 T and/or the resonance field is extremely high.

1) K. Kindo, M. Honda, T. Kôhashi and M. Date; J. Phys. Soc. Jpn. **59** (1990) 2332-2335.
2) M. Date and K. Kindo; Phys. Rev. Lett. **65** (1990) 1659-1662.
3) M. Date and K. Kindo; J. Phys. Soc. Jpn. **62** (1993) 1482-1485.

11. Creep Behavior of an Epoxy Resin and an Epoxy-Based FRP in Condition of Simultaneous Supply of Radiation and Stress at Cryogenic Temperatures

Tetsuya Nishiura, Shigehiro Nishijima, and Toichi Okada

ISIR
Osaka University
Ibaraki, Osaka 567, Japan

ABSTRACT

Creep tests of an epoxy resin and an epoxy-based FRP in bending under irradiation condition have been carried out, to investigate the synergistic effects of radiation and stress on mechanical properties of FRP. Simultaneous supply of stress and irradiation on the epoxy resin and the FRP enhanced creep rates in comparison with that supply of the stress on a post-irradiated one did. ESR spectra measurement was also carried out to study the change of molecule of the resin irradiated. Increase of molecular weight between crosslinks was found out to be enhanced by the synergistic effect of radiation and stress. The mechanism of increased damage of FRP induced by the effects of simultaneous stress and irradiation is discussed.

INTRODUCTION

Materials used to construct a superconducting magnet for a fusion reactor will be subjected to radiation and stress. The mechanical properties of organic materials and organic composite materials (FRP) used as insulators and structural materials are more sensitive to radiation than the other magnet components. To build a successful fusion reactor, the FRP with superior resistance to radiation damage must be developed. There are many reports concerning degradation of the mechanical properties of FRP and polymers due to irradiation[1,2]. Most of the reports, describe test results in which the radiation damage was measured by using the "postirradiated" specimens. In the reactor, however, the resin and the FRP will be stressed during irradiation. To simulated fusion magnet conditions, therefore, the specimen has to be simultaneously subjected to radiation and stress at cryogenic temperature. Studies of the simultaneous effect of stress (or strain) and irradiation on the resin and the FRP are very few[3~10].

Creep tests of nylon fiber in the radiation field were made by Mokulskii et al[3], Regel et al[5], and Stepanov et al[4]. Creep tests of PSF film were conducted by Hill et al[6]. They observed the lifetime to be reduced and the creep rate to be enhanced in such simultaneous condition of stress and radiation. Tensile tests by Dickinson et al[7] were structured to evaluate the mechanical properties of rubber films, and much greater development of crack length was observed.

On bulky specimens of polymer, much greater creep rates during irradiation than before and after were reported by Bell et al[8~10].

Various mechanism on the simultaneous effect of stress and irradiation on the mechanical properties of polymers were proposed. However, the mechanism has not yet been proved, because of the lack of evidence on molecular structure. It is also difficult to apply their results to composites with commercial size.

The degradatiion of macroscopic properties must originate from the radiation induced structural changes at the molecular level. Eda and Iwasaki have investigated the structural change of epoxy resins by means of ESR spectroscopy and found that the cyclohexadienyl-

type radical is produced by hydrogene addition to the benzene ring and these reactions result in the radiation resitivity[11].

In the present work, a creep test under irradiation was performed to investigate the effect of simultaneous stress and irradiation on an epoxy resin and an epoxy-based composite.

The purpose of this study was to examine the deformation velocity of materials before, during, and after irradiation, to examine the dependence of the velocity on temperature, and also to examine the radiation induced structural change of epoxy resins by ESR method. The mechanisms of deformation during irradiation are discssed mainly on the basis of their temperature dependence.

EXPERIMENTAL PROCEDURES

Sample and Radiations

The materials were consisted of epoxy resin (Epicote 828-aliphatic amine) and an epoxy-based glass-cloth laminates (FRP from Lamivelle A, Nittoh Electron and Industry Co. Ltd.). Specimens for the test of creep and relaxation were cut to the shape shown in Fig.1 from plates of epoxy resin (5 mm thick) and FRP (2 mm thick); the figure shows the FRP specimens.

These specimens were irradiated with electron beams (20 MeV, 240 mA, 60-120 pps; dose rate of 0.6-2.0 MGy/h) in LINAC at ISIR, Osaka University.

Creep Test

The creep test apparatus and the specimen are shown in Fig. 1. Creep test was performed by measuring the deflection of the specimen which was loaded with a dead weight through lever in the three point bending test with 45 mm span length. Whole of the apparatus was held in the radiation field for the simultaneous effect tests. Creep test for postirradiated specimens was also performed.

The test temperature in creep tests was regulated by changing the flow volume of liquid nitrogen with an electromagnetic valve. The maximum fluctuation from the preset temperature value was ±10 K.

ESR Spectra

After irradiation ESR spectra were measured using a Bruker ESP 300(Germany) X-band spectrometer.

The temperature of sample for ESR was raised by lifting the specimen from the suface of liquid nitrogene and was controled by changing the distance lifted.The measurements were made at 77 K(ESR glass tube was dipped in liquid nitrogen).

RESULTS

Creep

Creep results at LNT are shown in Fig. 2 through 7. In the case of the epoxy resin, creep curves under non-irradiated condition reveal almost no increase of deflection except the region just after loading in such loads of 57.9 MPa ando 84.8 MPa (Fig. 2). For 8 MGy irradiated specimens which were irradiated at LNT and raised up to RT before test, as shown in Fig. 3, the creep curves show a similar trend like those of the non-irradiated specimens. When the irradiated specimens at LNT was tested without the warm up to RT, the creep curve shows larger increase in the steady state region than that with warm up does(Fig. 4). In the condition of the creep durig irradiation, creep curves reveal clearly much higher increase of deflection in the steady region than those of the specimens after irradiation(Fig. 5). This deflection increases with loads.

In the case of the FRP, creep curves show almost similar behavior like those in the case of the resin. The creep curves for the specimen during irradiation show higher increase

compared with those for the specimen after irradiation, although the increase is smaller than those of epoxy resin(Fig. 6 and 7).

The temperature dependence of creep rates are shown in Fig. 8 and 9. The lines for unirradiated epoxy resin have steeper slopes than the ones obtained during irradiation(Fig. 8). The respective activation energies calculated from these lines are 5.2 kcal/mole and 1.04 kcal/mole. The apparent activation energy of epoxy decreases by about 80% upon introduction into radiation field. Therefore, the mechnism of deformation for epoxy resin must be change involving a decrease in the activation energy.

The temperature dependence of the creep rated for FRP during irradiation is shown in Fig. 9. The rate did not vary with temperature, suggesting that the activation energy is negligible.

From these results, the creep rate under irradiation is confirmed to be accelerated than those for postirradiated specimens.

ESR Spectra

The behavior of ESR spectra with radiation dose is shown in Fig. 10. The intensity of the signal becomes larger with the dose and the shape of the signal does not change. The number of the unpaired electron (radicals) increases almost linearly with the dose (Fig.11).

The spectra behavior induced by raising the temperature of the sample are shown in Fig 12. The spectra become smaller with the temperature and the change of the signal shape is little. The number of the radicals decrease moderately untill 200 K and after that temperature decrease more rapidly (Fig. 13). The radicals are stable at lower temperatures and unstable at higher temperatures. This dependency of the stability on the temperature may be caused by the mobility of polymer segments. The radicals decrease by producing the electron pairs which induce the repairment of the molucule, the unsaturated bonds and the crosslinks. The unsaturated bonds formation among the reactions can make the degradation of polymer (scission of polymer).

DISCUSSION

In the steady state region of creep for the epxy resin after irradiation, the creep rate for the specimen without warm up is higher in comparison with the ones with warm up. This behvior would be understood, assuming that defects in the resin are proportional to the number of radicals, that is, the larger the number of radicals make the larger the nuber of defects. For the epoxy during irradiation, creep rates are much higher than those for the resin after irradiation without warm up. This behavior is not understood from the number of radicals because in situ number of radicals during irradiation must be smaller than those which irradiation is accomplished. Simultaneous effects of stress and radiation on the damage of the resin must be operated.

Stress should affect on the reaction process of scission and crosslink next to the excitation and ionization processes by irradiation. The situation of these processes are similar to the chemical reaction under stress. Three reactions must be considered.

1) In the case of scission reaction, molecular end groups made by scission are active and have probability of rebonding at the original chain site under no stress or strain. When the stress acts on the scission reaction, the active end groups are separated by the release of strain energy and the probability of rebonding thus decrease and scission of chemical bond is accomplished (diminish of cage effects).

2) In the case of crosslink reaction under stress, specific reaction like decrease of creep deformation may occur.

3) In the case where the reactions of scission and crosslink occur simultaneously under stress, scission releases the stress and the deformation increase and, thereafter, crosslink reaction fixes the deformation. Crosslink density is in this case not estimated to decrease drastically although the deformation increases.

Considering our results, the scission reaction under stress is assumed as the main mechanism of the acceleration of radiation damage.

CONCLUSIONS

Creep tests of an epoxy resin and an epoxy-based FRP during irradiation have been carried out, to investigate the effect of simultaneous stress and irradiation on the mechanical properties of the resin and the FRP. The study resulted in the following conclusions:
(1) The effect of simultaneous stress and irradiation results in more damage on the epoxy resin and the FRP than the effect of stress on a postirradiated one.
(2) ESR spectra is available to detect chemical change of materials at low temperature.
(3) The mechanism of increased deformation of polymers induced by such simultaneous effects has been proposed.
(4) Polymers and FRP in the circumstance of simultaneous existence of stress and irradiation have possibility of large deformation beyond the estimation based on the specimen after irradiation.

REFERENCES

1. D. Evans and J.T. Morgan, A review of the effects of ionizing radiation on plastic materials at low temperatures, Adv. Cryogenic Eng.(Materials)28:147(1982).
2. S. Egusa, Irradiation effects and degradation mechanism on the mechanical properties of polymer matrix composites at low temperatures, Adv. Cryogenic Eng. (Materials) 36: 861 (1990).
3. M.A. Mokul'skii, Kinetic process in irradiated substances, Vyskomol. soedin.2:No.1, 119 (1960) (Polymer Sci. USSR, 2:4, 211(1961)).
4. V.F. Stepanov, S.E. Vaisberg, and V.L. Karpov, Time-to-rupture and creep in radiation field, Fiziko-Khimicheskaya Mekhanika Materialov, 15, No.3: 306 (1969) (Soviet Mat. Sci.237).
5. M.P. Vershinina, V.R. Regel' and N.N. Chernyi, Effect of exposure to (Polymer Sci. USSR, 1606(1964)).
6. D.T. Hill, D.A. Lewis and J.H. O'donnel, Accelerated failure of bisphenol-a polysulfone during electron beam irradiation under an applied stress, J.Apll. Polymer Sci.44:115(1992).
7. J.T. Dickinson, M.L. Klakken, M.H. Miles and L.C. Jensen, Electron-beam-induced fracture of polymers J. Polymer Sci.(Polymer Phys. Ed.)23:2273 (1985).
8. J.P. Bell, A.S. Michaels, A.S. Hoffman and E.A. Mason, Transient acceleration of creep rates of polymers during high intensity irradiation, Adv.Chem. Soc.,66:79(1967).
9. T. Nishiura, S. Nishijima, K. Katagiri, T. Okada, J. Yasuda and T. Hirokawa, Radiation damage of composite materials - Creep and swelling -, Adv. Cryogenic Eng.(Materials) 36B: 855 (1990).
10. T. Nishiura, S. Nishijima, K. Katagiri, T. Okada, J. Yasuda and T. Hirokawa, Creep test of composite materials under irradiation condition, Proc. 11th Int. Conf. Magnet Tech. Eds. T. Sekiguchi and S. Shimamoto, Elsvier 708(1990).
11. B. Eda and M. Iwasaki, ESR study of radiation damage of bisphenol-A-based epoxy resin at low temperature: selective hydrogene addition to benzene-ring-forming cyclohexadienyl-type radical, J Polymer Sci.: Part A: Polymer Chem., 24: 2119(1986).

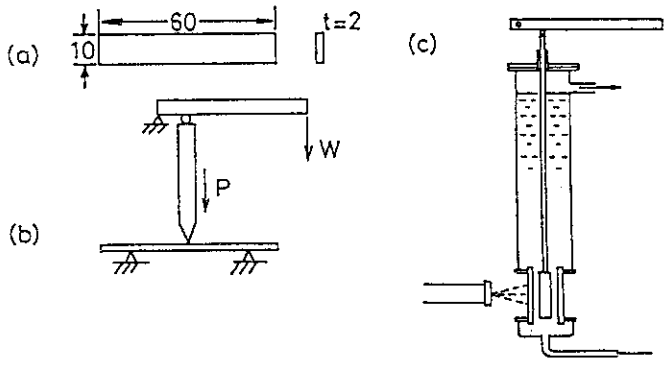

Fig. 1. The creep test specimen(a), the three point bending method(b) and the creep apparatus with e-irradiation source(c).

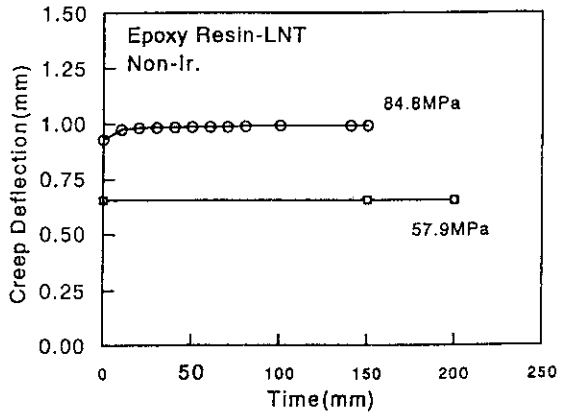

Fig. 2. Creep curves for non-irradiated epoxy-resin at LNT.

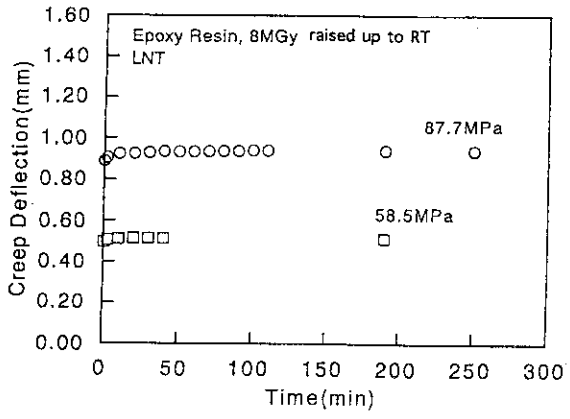

Fig. 3. Creep curves at LNT for irradiated epoxy-resin with raising to RT.

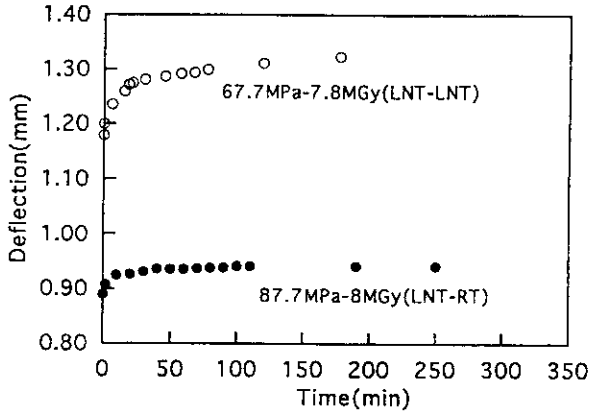

Fig. 4. Comparison of creep curves at LNT for irradiated epoxy resin between with and without raising to RT.

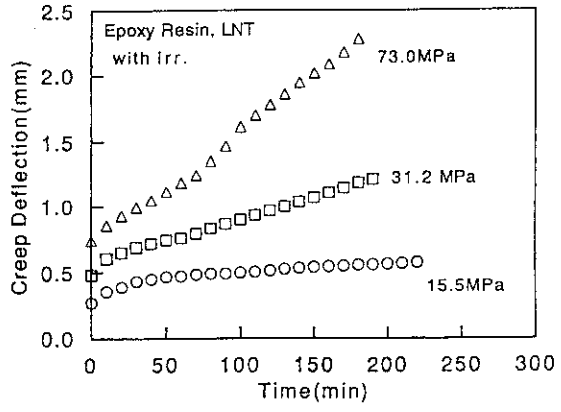

Fig. 5. Creep curves for epoxy-resin at LNT during irradiation.

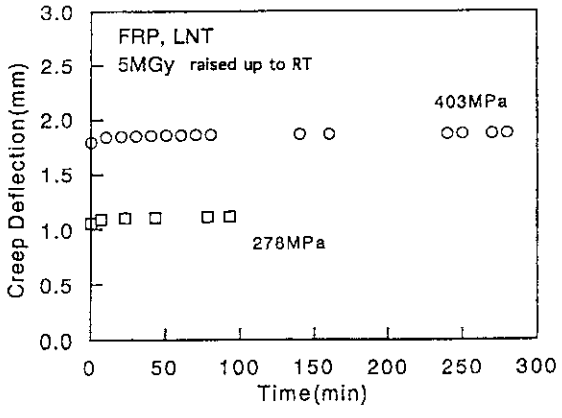

Fig. 6. Creep curves at LNT for irradiated FRP with rasing to RT.

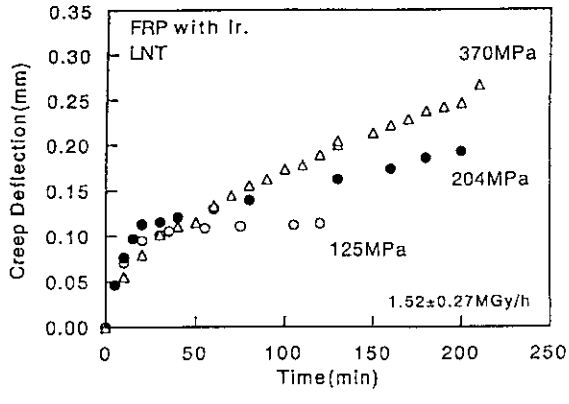

Fig. 7. Creep curves for FRP at LNT during irradiation.

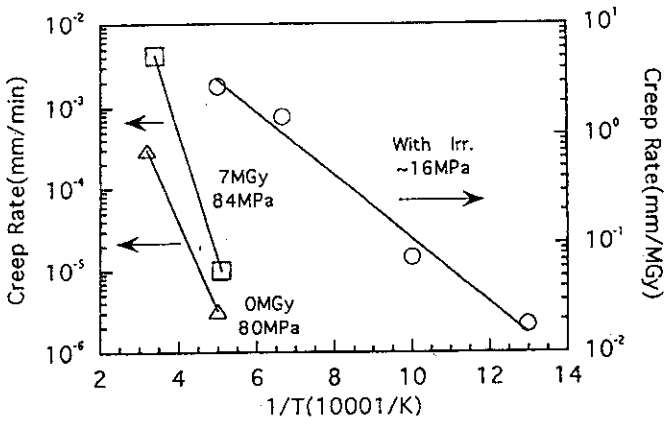

Fig. 8. The dependency of the creep rates of epoxy-resin on temperatures.

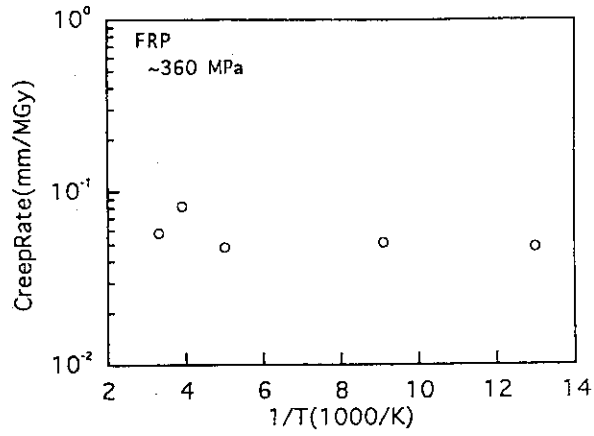

Fig. 9. The dependency of the creep rates of FRP on temperatures.

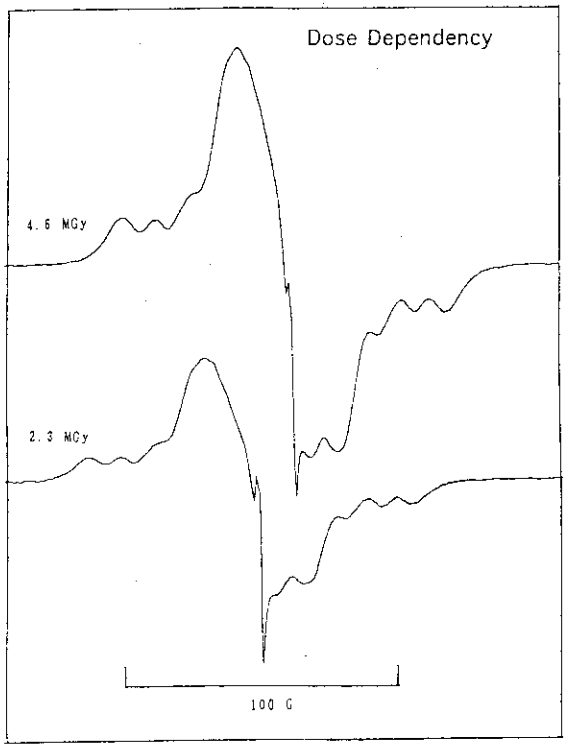

Fig. 10. Change of ESR signals with radiation dose.

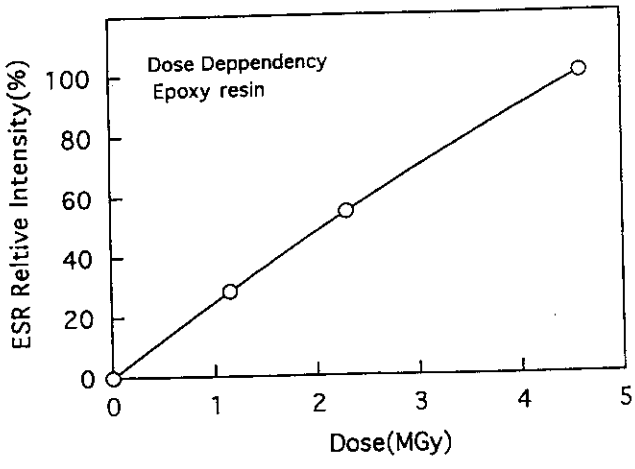

Fig. 11. The dependency of the number of radicals (ESR intensity) on radiation dose.

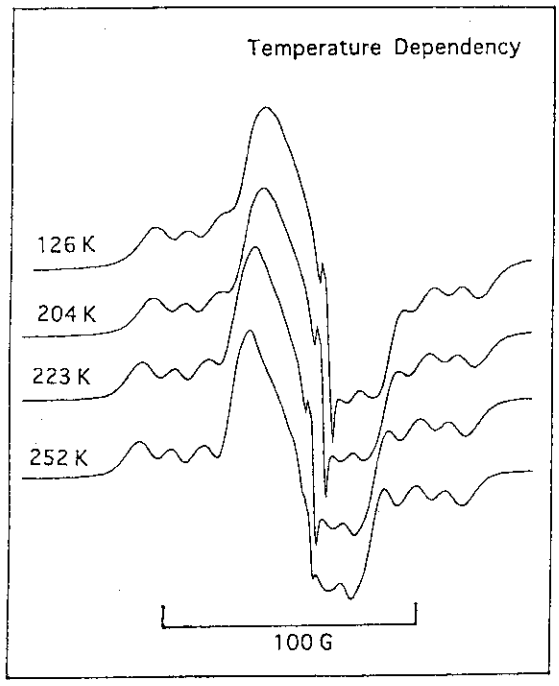

Fig. 12. Change of ESR signals with temperature.

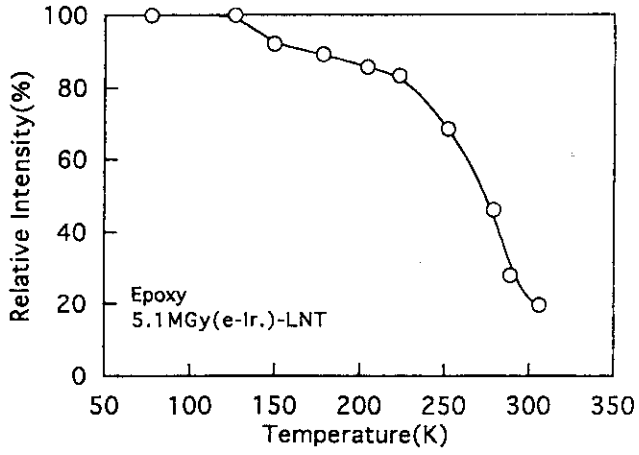

Fig. 13. The dependency of the number of radicals (ESR intensity) on temperatures.

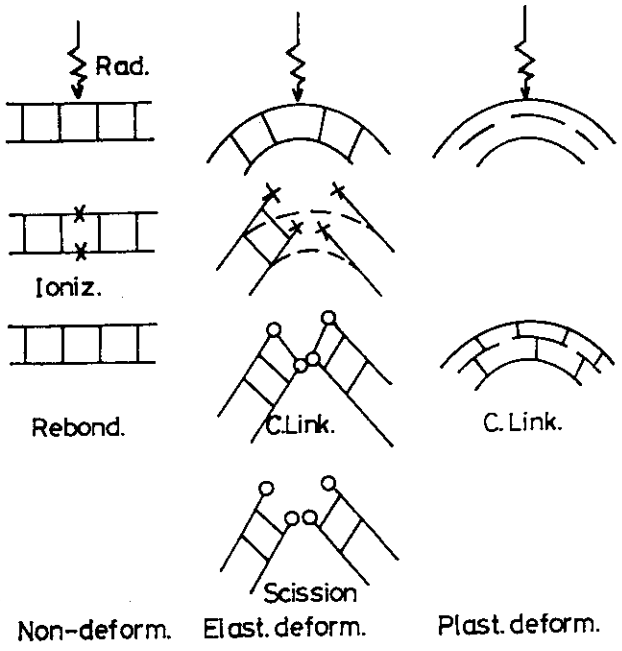

Fig. 14. Effects of stress on the deformation of the resin during irradiation.

12. Structural Changes of Organic Solids Caused by Irradiation: Raman Study at Very Low Temperatures.

Hirotomo Hase, Kunie Ishioka[1] and Yoko Miyatake[2]

Research Reactor Institute, Kyoto University, Kumatori-cho, Sennan-gun, Osaka, 590-04 Japan,
[1]National Research Institute for Metals, Tsukuba, Ibaraki, 305 Japan,
[2]Department of Mechanical Engineering, Faculty of Engineering Science, Osaka University, Toyonaka, Osaka, 560, Japan

I INTRODUCTION

Upon irradiation of organic solids, a variety of ionic species, free radicals and molecular products is generated and some of them are stably trapped in matrices at low temperatures and are normally detected by ESR and optically spectroscopic methods. However, molecular products trapped in low temperature matrices are scarcely detected, since they are neither paramagnetic nor uv-vis (250-800 nm) absorbing species. We have been aware of the utility of Raman spectroscopy for detecting molecular products as well as ionic species and free radicals, since most of them are Raman active. We have also realized that this method can shed light on structural changes caused in irradiated organic solids by observing spectral changes in intra- and intermolecular vibration modes.

It is instructive to note that the vibrational modes of a disordered medium obey Bose-Einstein statics, so that the correction for the observed Raman spectra is usually made with use of the so called Bose-Einstein factor, $f_{BE} = \{1 - \exp(h\nu/kT)\}$, where ν is the Raman shift in wavenumber and T is the temperature of the sample. The factor depends on both frequency and temperature, e.g. at 77 K f_{BE} = 0.372 and 0.976 at 25 and 200 cm^{-1}, respectively, but becomes independent of frequency at very low temperatures, i.e. $f_{BE} \approx 1.00$ for all frequencies at 5 K. This convinces one that Raman spectroscopy at very low temperatures is indispensable for measurement of organic solid, particularly in the low frequency region.

In reality, however, the focusing of an intense laser beam on the surface of a sample causes a considerable rise of the local temperature. This makes Raman scattering measurements at low temperatures very difficult if the sample is mounted in a conventional conduction-tail cryostat. Furthermore, this type of cryostat is not suitable for organic glass samples because mounting and handling of the glass samples without warming are required, otherwise the samples often change their thermodynamical properties or melt above certain temperatures.

Another type of cryostat is a flow-gas helium cryostat in which cold helium gas flows down, being directed onto the sample surface[1,2]. This type of cryostat may be more efficient for preventing the temperature rise of the sample than a conduction-tail cryostat, but still being not satisfactory for organic glass samples because of the difficulties mentioned above. Recently Weng *et al.*[3] reported Raman spectra of ethanol and deuterated ethanol glasses as a function of temperature above about 10 K with a flow-gas helium cryostat. This temperature is the lowest one reported for alcohols as far as we are aware.

In this paper we first describe a simple liquid helium cryostat and a device of making and mounting organic solid samples. We then present the Raman spectra for irradiated ethanol crystal that were obtained by using the new cryostat and demonstrate how the Raman method is useful for getting insight into structural changes of organic solids caused by irradiation.

II APPARATUS

The cryostat is made of an inner quartz vessel which is fixed in a cylindrical vacuum chamber of thin- walled stainless steel[4]. The details of the cryostat are shown in Fig. 1. A bottom window for the incident laser beam and a side window for the scattered light, both of which are of optical-quality Suprasil quartz, are attached onto the wall of quartz vessel (D), and outside of the vessel was aluminized to reduce radiation losses. The vessel is surrounded by a cylindrical

thin-walled stainless steel reservoir for liquid nitrogen (C). The bottom wall of the reservoir is in thermal contact with a copper radiation shield boot (G) which was holes for the optical windows (K). Vessel D and bath C hold 1.8 and 1.5 ℓ of liquid helium and liquid nitrogen, respectively, which enable us to carry out measurements for 2.5h under the irradiation of a typical Ar ion laser beam of 1.5W of the maximum output onto the organic solid samples through the bottom optical window.

The temperature of the organic solid samples under the irradiation of the laser beam of 1.5W was measured by a Au + 0.07% Fe vs. Cr thermocouple which was shallowly inserted in the organic solid samples at the irradiation point of the laser beam. Any change of the thermo-electric voltages on the irradiation of the laser beam was not detectable in the range of 5 μV in liquid nitrogen. The difference in liquid helium was not more than 10 μV. This indicates that the temperature of the sample does not exceed 5 K in liquid helium under the irradiation of the laser beam.

Another feature of the cryostat is worthy to note. If one wants to use the cryostat as a conduction-tail cryostat, the inner quartz vessel can be replaced by a conduction-tail vessel which is made of a thin-walled stainless steel with a copper conduction tail. A sample dish, which will be described later, is screwed into the top of the conduction tail and can be easily changed by removing flange H out of chamber B.

Disk samples of organic solids with a thickness of 0.4 cm and a diameter of 2 cm were made by dropping drops of solution on brass dishes which were kept at liquid nitrogen temperature. The cross-sectional view of the sample dish is shown in the insert of Fig. 1.

The sample making procedure is similar to the one reported previously[5] except for the brass dish employed in this apparatus instead of a washer-like brass ring. The sample dish is screwed into the stainless steel joint at the top of the glass fiber holder as shown in the insert of Fig. 1. The length of the holder and the angle of incidence of the reflected light to the optical window can be changed by turning a nut (A) outside the cryostat so that the maximum intensity of Raman scattering can be obtained.

It is worthy to note that the present cryostat has a remarkable advantage when it is used at liquid nitrogen temperature.

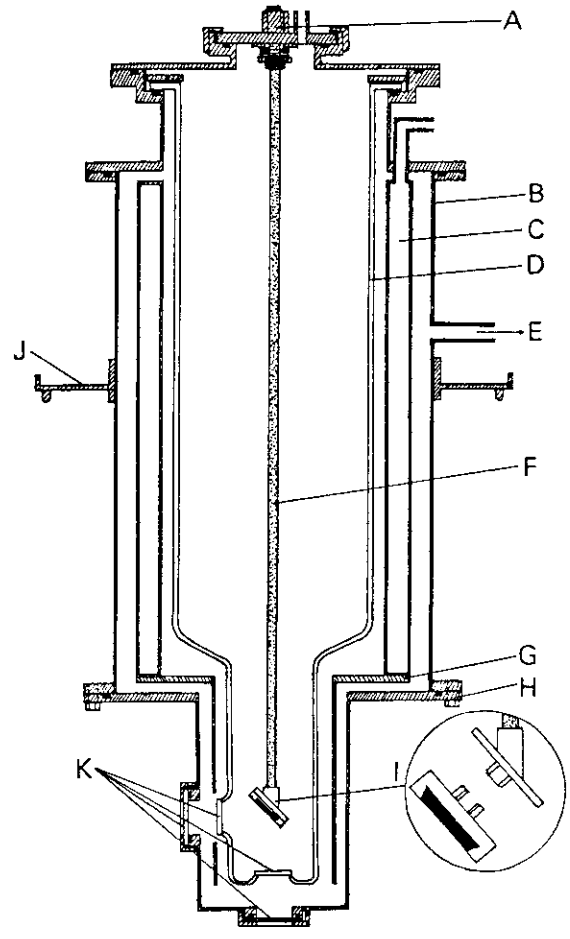

Fig.1 Cross-sectional view of the cryostat for Raman spectroscopy. A-Nut for adjusting the length of the glass fiber sample holder and changing the angle of incidence of the reflected light to the optical window; B-Thin-walled stainless steel cylinder of 15.5 cm i.d.; C-Stainless steel nitrogen reservoir; D-Quartz vessel of 9.6 cm i.d. for liquid helium; E-Vacuum pumping port; F-Glass fiber sample holder; G-Copper radiation shield boot; H-Removable flange; I-Brass sample dish and holder; J-Support flange; K-Optical quality window of Suprasil quartz.

It has been commonly recognized that the measurement of Raman scattering of samples inserted in liquid nitrogen is difficult because of the noise caused by irregular bubbles passing across the scattered light. With the present cryostat, however, no bubbles occur in liquid nitrogen of the inner vessel when the outer nitrogen bath is filled with liquid nitrogen. This allows us to measure Raman spectra with extremely reduced noise at liquid nitrogen temperature.

III EXPERIMENTAL

Regent grade ethanol was used without further purification. Ethanol crystal was prepared by annealing ethanol glass near the melting point for 40 min according to the recipe of Jönsson[6]. Irradiation with γ-rays was carried out at liquid nitrogen temperature. The total dose was 1130 kGy for ethanol crystal. The temperature of the disk samples in liquid helium did not exceed 5 K during the exposure to the laser beam of ~800 mW by the 514.5 nm line of a NEC argon-ion laser as an exciting source. Raman spectra were recorded with a JASCO NR-1100 spectrometer. The CCO symmetric stretching band of ethanol crystal at 891 cm^{-1} was used as an internal standard, on the basis of the assumption that the intensity of the skeletal stretching is hardly affected by the transformation of an ethanol molecule into an ion or a radical. In fact, Edwards *et al.*[7] showed evidence for the suitability of CCO stretching band as an internal standard of ethanol. Thus the relative intensities of the Raman bands before and after irradiation were determined respectively, and the intensity ratio was determined between them.

IV RESULTS AND DISCUSSION

Intermolecular vibration region

In the wavenumber region below 300 cm^{-1} of the ethanol crystal, the intermolecular vibration modes as well as the hydrogen bond stretching mode were observed[8]. This shown in Fig. 2.A. The spectra observed are in good accordance with those reported by Weng *et al* [3]. Assignment of peaks seems to be difficult, since the spectra are too complicated to be resolved and also some mixing of modes might be occurred. Weng *et al* [3] tried to assign the peaks by examining the frequency ratios for ethanol and deuterated ethanol and comparing them with the inertia ratios. According to their results, the peaks observed at 66, 89, 102 and 137 cm^{-1} are attributed to the translation, while the peaks at 56 and 120-126 cm^{-1} are attributed to the libration. We ascribe the band at 294 cm^{-1} to the hydrogen bond stretching as described previously[9].

After irradiation at 77 K, the intermolecular bands showed the drastic changes. This is demonstrated in Fig. 2B. It follows that the translation peaks shift towards the low wavenumber side by about 10 cm^{-1}, and increase in their intensities. The libration peaks, on the other hand, neither shift nor increase in the intensities.

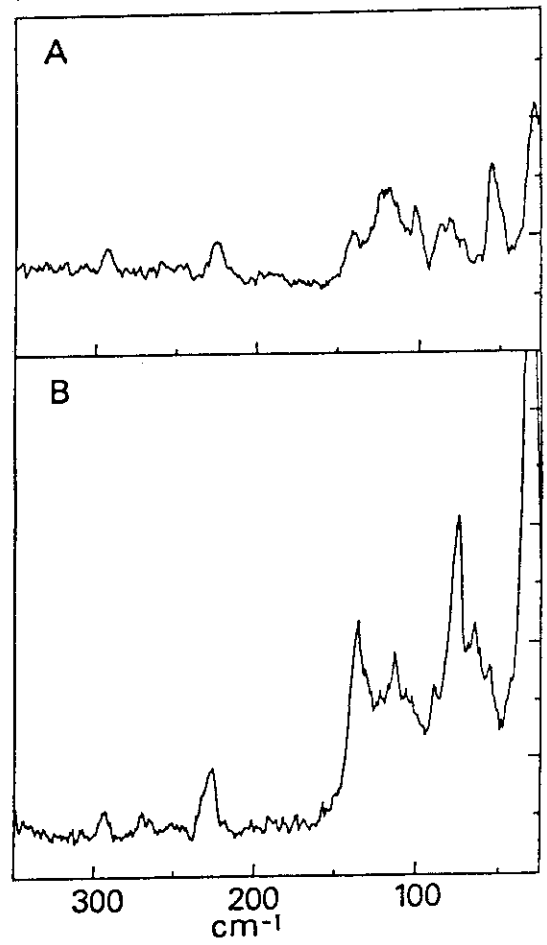

Fig.2 Raman spectra of ethanol crystal in the wavenumber region of the intermolecular vibration modes. The spectra were measured before(A) and after(B) irradiation at 77 K. The total dose was 1960 kGy.

It is inferred that some structural changes occur in such a way that freedom of the initial translational vibration is reduced, but that the population of the translational vibration is enhanced. We infer that radiation-produced species which are trapped in the interstitial sites of the crystal form additive hydrogen bondings to a chain of ethanol molecules. A most probable candidate of the species is hydrogen molecules. In fact the hydrogen bond stretching band at 294 cm^{-1} increased in intensity by about 30 % after irradiation.

Intramolecular bending region

The intense intramolecular modes including the CCO bending of ethanol molecules appear in the wavenumber region of 420-470 cm^{-1}, as shown in Fig. 3A. After irradiation at 77 K, a set of sharp bands was observed at 358 and 590

cm^{-1} [10]. This is shown in Fig. 3B.

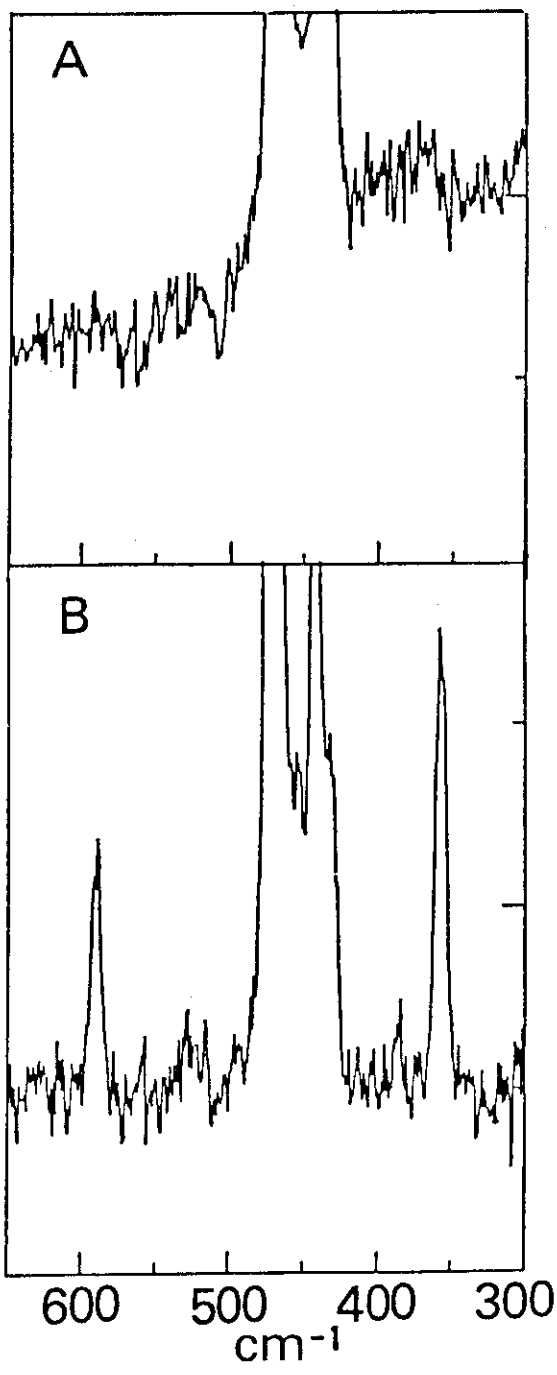

Fig.3 Raman spectra of ethanol crystal in the wavenumber region of intramolecular bending modes at 5 K. The spectra were measured before(A) and after(B) irradiation at 77 K. The total dose was 1130 kGy. The intense bands at 420-470 cm^{-1} are attributed to the intramolecular modes including CCO bending of ethanol molecules.

The wavenumbers observed are very compatible to those for compressed gaseous normal hydrogen, that is 355 and 588 cm^{-1} [11], and also those for solid normal hydrogen, that is 351 and 587 cm^{-1} [12]. These are assigned to the rotational bands of hydrogen molecules: The 358 cm^{-1} band is ascribed to $S_0(0)$ ($\Delta v=0$, $\Delta J=2$) transition and the 590 cm^{-1} band to $S_0(1)$ transition. We emphasize that this is the first and direct evidence that hydrogen molecules are produced and trapped in irradiated ethanol crystal.

It was well known at a quarter of a century before that a large yield, i.e. $G(H_2)=5$ of gaseous hydrogen is observed after melting solid ethanol which was previously irradiated at 77 K[13,14]. It was assumed that hydrogen atoms, which are not stably trapped in alcoholic solids, undergo the reaction of hydrogen molecule formation. The reaction was thought to occur through a tunneling abstraction at cryogenic temperatures such as 4 K.

Although there is convincing, indirect evidence that hydrogen molecules are formed in irradiated alcoholic solids at cryogenic temperatures, no direct observation of hydrogen molecules in solids has been reported so far. Since hydrogen molecules absorb light of the near u.v. region in the gas phase, it is almost impossible to apply ordinary optical absorption methods to detecting hydrogen molecules in alcoholic solids at cryogenic temperatures. Considering that hydrogen molecules are not infra-red active, but are Raman active, we can apply Raman spectroscopy as the unique, experimental technique to directly detect hydrogen molecules which are produced by irradiation and are trapped in solids. We have now demonstrated that this is the case.

OH stretching region

Shown in Fig. 4A is the OH stretching bands of ethanol crystal obtained at 5 K before irradiation. It is noted that the OH stretching bands of the crystal differ from those of glass. The former consists of two bands at 3144 and 3260 cm^{-1} and a small band at 3229 cm^{-1} and their contours fit Lorentzian, while those of glass fit Gaussian. Comparison of the spectral profiles of crystal and glass leads us to the conclusion that the hydrogen bond networks in the crystal are distinctly classified into two configurations, and that they are strengthened and homogenized much more than in glass. It is known from the X-ray work of Jönsson[6] that the infinite zigzag chain is formed through the hydrogen bond in ethanol crystal and that two kinds of hydrogen bond exist with the distance

of 2.716 and 2.730A. Recalling that the hydrogen bond distance of 0.014A yields a separation of 75 cm^{-1} [15], we attribute the bands at 3144 and 3260 cm^{-1} to OH stretching associated with short and long hydrogen bond, respectively. The small band at 3229 cm^{-1} might be due to a distribution of hydrogen bond length in consequence of a disordered configuration in the crystal.

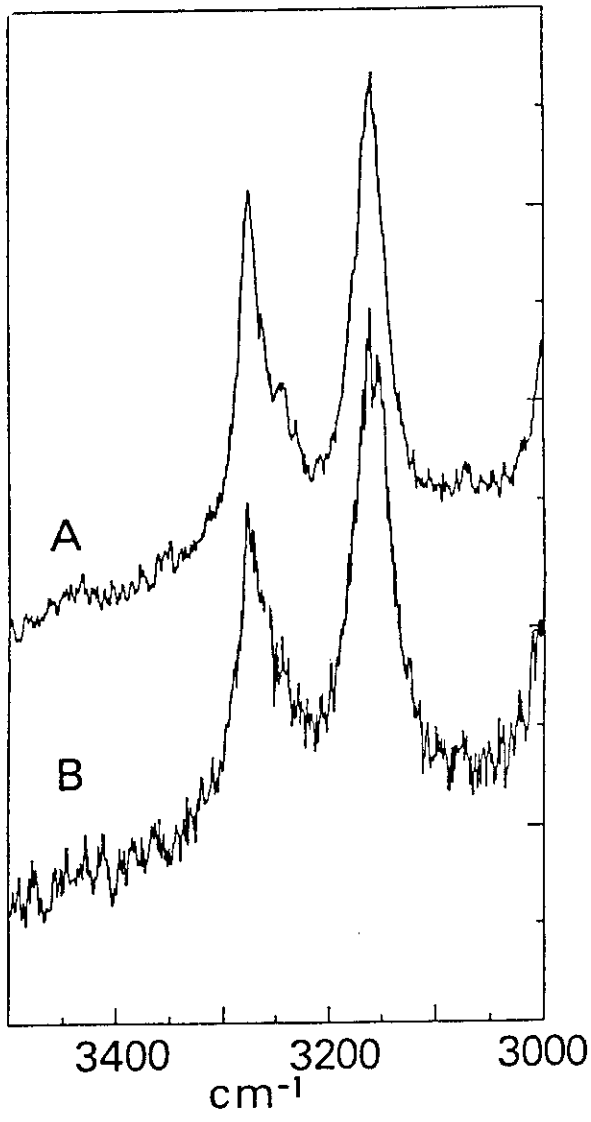

Fig.4 Raman spectra of ethanol crystal in the wavenumber region of the OH stretching modes at 5 K. The spectra were measured before(A) and after(B) irradiation at 77 K. The total dose was 1130 kGy .

After irradiation, the two main bands shifted slightly toward the high frequency, *ca* 5 cm^{-1}, but the shift of the 3225 cm^{-1} band is, if any, obscure[10]. This is shown in Fig. 4B. Note that after irradiation the 3260 band decreases while the 3144 cm^{-1} band increases in the intensity. The decrease of the weakly hydrogen-bonded OH oscillator and a concomitant increase of the strongly hydrogen-bonded OH oscillator imply that the intermolecular configuration is changed in such a way that additive intermolecular interaction, i.e. hydrogen bonding, is caused by irradiation. The spectral changes after irradiation observed in the intermolecular vibration region as well as the direct observation of the rotational bands due to hydrogen molecules accommodate the above interpretation.

Hydrogen molecule stretching region

In the wavenumber region greater than that of the OH stretching vibration, no spectrum was observed for ethanol crystal before irradiation, as shown in Fig. 5A. After irradiation the Raman spectra were observed at 4133(20) and 4153(10) cm^{-1} for glass and crystal, respectively, where numbers in parentheses are the values of FWHM[10, 16]. The spectrum for ethanol crystal provides a sub-band at 4159 cm^{-1} as shown in Fig. 5B. These peak wavenumbers are in good accordance with those of normal hydrogen compressed at 398 Amagat at 87 K[11] i.e. 4153 and 4158 cm^{-1} , but shift to the high frequency side by about 8 cm^{-1} from those of solid normal hydrogen at 2 K[12]. These peaks were ascribed to $Q_1(1)$ ($\Delta v=1$, $\Delta J=1$) and $Q_1(0)$ (($\Delta v=1$, $\Delta J=0$) transition, respectively. It should be noted that $Q_1(0)$ transition is characteristic of parahydrogen (p - H_2), while $Q_1(0)$ transition of orthohydrogen (o - H_2). The observed Q-branch spectrum for irradiated ethanol crystal can be resolved into two Lorentzian bands at 4153(6) and 4159(3.5) cm^{-1} with their intensity ratio of 3 where the numbers in parentheses are FWHM values. This ratio is much smaller than that for solid normal hydrogen at 2 K which is about 15.

It follows that the relative concentration of p-H_2 in irradiated ethanol is much larger than that for solid normal hydrogen at 2 K. At present three explanations are possible for the phenomenon: (1) a selectivity of the rotational quantum state for hydrogen molecule formation by radiolysis at low temperatures, (2) an exchange reaction of $H+o\text{-}H_2 - H+p\text{-}H_2$ caused by H atoms which are produced during radiolysis and (3) the conversion from $J=1$ to $J=0$ states during irradiation and storage of the sample at 77K. Further study should be carried out to elucidate the mechanism.

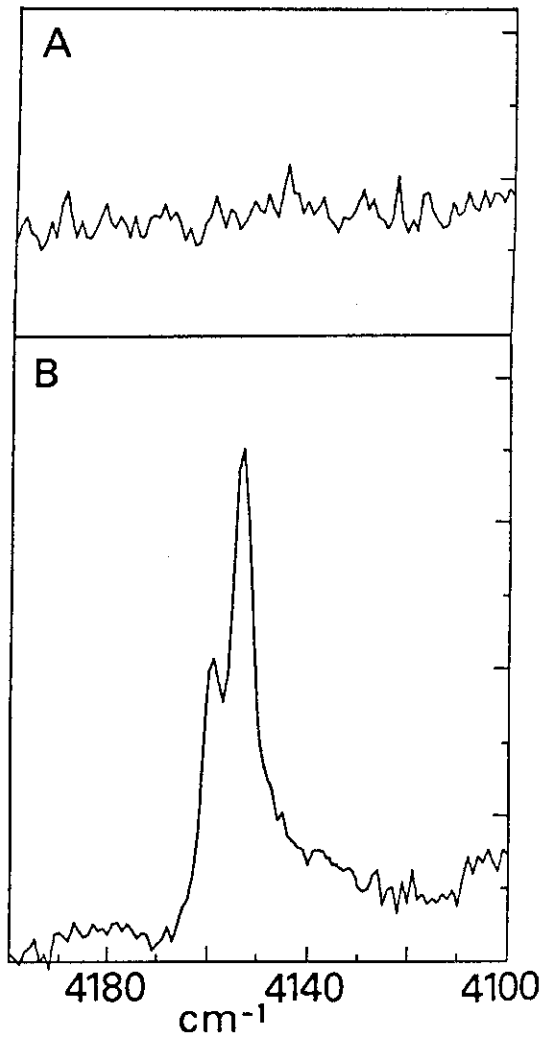

Fig.5 Raman spectra of ethanol crystal in the wavenumber region of the HH stretching of hydrogen molecules at 5 K. The spectra were measured before(A) and after(B) irradiation at 77 K. The total dose was 1130 kGy.

V CONCLUSION

We made a simple but very convenient cryostat for Raman scattering measurement at very low temperatures and used it for investigation of structural changes in ethanol crystal which were induced by irradiation.

The intermolecular vibration modes were affected by irradiation: translation modes enhanced and shifted to the low wavenumber side. This was tentatively interpreted in terms of additional hydrogen bonds formed between the hydroxyl groups and hydrogen molecules, the latter of which was produced by irradiation. The direct observation of hydrogen molecules produced and trapped in ethanol crystal was first successful in the measurements of the rotational and stretching modes. We emphasize from these results that the Raman scattering measurement at low temperatures is one of the most elegant, efficient techniques to investigate structural changes in organic solids which are induced by irradiation.

REFERENCES

1. R. Freeman, SPEX Speaker **16**, 9 (1971).
2. R. D. Kirby and J. R. Duffy, Rev. Sci. Instrum., **50**, 663 (1979).
3. S. X. Weng, J. Decker, B. H. Torrie and A. Anderson, Indian J. Pure Appl. Phys., **26**, 76 (1988).
4. H. Hase and K. Ishioka, Ann. Rep. Res. Reactor Inst., Kyoto University, **23**, 183 (1990).
5. H. Hase, M. Noda and T. Higashimura, J. Chem. Phys., **54**, 2975 (1971).
6. P. G. Jönsson, Acta Cryst., **B32**, 232 (1976).
7. H. G. M. Edwards, D. W. Farwell and A. Jones, Spectrochim. Acta, **45A**, 1165 (1989).
8. H. Hase, K. Ishioka and T. Higashimura, Radiat. Phys. Chem., **38**, 23 (1991).
9. H. Hase, K. Ishioka, Y. Miyatake, M. Kobayashi and M. Kobayashi, J. Phys. Chem., **95**, 8541 (1991).
10. H. Hase, K. Ishioka, Y. Miyatake, Bull. Chem. Soc. Jpn., **65**, 2526 (1992).
11. A. D. May, G. Varghese, J. C. Stryland and H. L. Welsh, Can. J. Phys., **42**, 1058 (1964).
12. S. S. Bhatnagar, E. J. Allin and H. L. Welsh, Can. J. Phys., **40**, 9 (1962).
13. R. H. Johnson, J. Phys. Chem., **65**, 2144 (1961).
14. J. W. Fletcher and G. R. Freeman, Can. J. Chem., **45**, 635 (1967).
15. K. Nakamoto, M. Margoshes and R. E. Rundle, J. Am. Chem. Soc., **77**, 6480 (1955).
16. H. Hase and K. Ishioka, Radiat. Phys. Chem., **39**, 329 (1992).

13. Photoinduced Oxygen-Atom Transfer from NO_2 to Alkenes, Alkynes, and Amines in Low-Temperature Argon Matrices

Munetaka NAKATA

Graduate school of Bio-Applications and Systems Engineering,
Tokyo University of Agriculture and Technology,
Saiwai-cho, Fuchu, Tokyo 183, Japan

The cryogenic-matrix technique is ideally suited for the study of photoinitiated bimolecular chemistry since the reactants of interest can be brought together as sustained pairs, and reaction can be followed in complete absence of diffusional processes that complicate elucidation of the reaction path in liquid-solution or gas phase. Photolysis wavelength dependence of the chemistry, both in terms of quantum efficiency and the course the reaction takes, can conveniently be determined by laser initiation in an inert, solid environment. Particularly useful for uncovering reaction pathways is the possibility to trap chemical intermediates. These advantages are fully exploited in the studies on visible-light induced photooxidation of alkenes, dienes, alkynes, and amines by NO_2.

(1) Ethylene

Chemical reaction has been observed upon irradiation of ethylene:NO_2 pairs in solid Ar with cw dye laser light at visible wavelengths as long as 574 nm, well below the 398 nm dissociation limit of isolated NO_2. Reaction products were acetaldehyde, oxirane, NO, and ethyl nitrite radical, as established by FT-infrared spectroscopy. Kinetic analysis of product absorbance growth showed the acetaldehyde is the prevalent final oxidation product of direct, single photon photolysis of ethylene:NO_2 pairs, while oxirane is exclusively produced by yellow and shorter wavelength induced photodissociation of trapped ethyl nitrite radical. Experiments with trans and cis CHD=CHD yielded nitrite radical CHD-CHD-ONO under retention of stereochemistry, but scrambling in the oxirane product. Based on these results and those on NO_2 photooxidation of cis and trans 2-butene, a reaction path is proposed that involves O atom transfer from NO_2 to the C=C bond to give a short lived singlet oxirane biradical. The photolysis wavelength dependence of the reaction quantum efficiency indicates that NO_2 reactant vibrational excitation plays an essential role, and opens a reaction path that is unique to visible light induced alkene + NO_2 chemistry in a matrix.

(2) trans 2-Butene

Reaction was induced between trans 2-butene and nitrogen dioxide by exciting trans 2-butene:NO_2 pairs, isolated in solid Ar at red, yellow, and green wavelengths. The chemistry was monitored by FT-infrared spectroscopy, and Ar ion and cw dye laser were used for photolysis. Products formed were 2,3-dimethyloxirane + NO, the former under complete retention of stereochemistry, and an addition product that was identified by ^{18}O

isotopic substitution as a butyl nitrite radical. Analysis of the photolysis wavelength dependence of the butyl nitrite radical and trans 2,3-dimethyloxirane (and NO) growth kinetics revealed that oxirane + NO is formed along two reaction pathways. The first gives trans 2,3-dimethyloxirane + NO and butyl nitrite radical upon absorption of a single photon by trans 2-butene:NO_2 pairs (one photon path). The second path is formation of trans 2,3-dimethyloxirane + NO by photodissociation of trapped butyl nitrite radical by a (second) red or shorter wavelength photon (two photon path). Two alternative transients are proposed for the one photon path, namely a hot butyl nitrite radical and an oxirane biradical, respectively.

(3) cis 2-Butene

As in the case of the trans 2-butene + NO_2 reaction, 2,3-dimethyloxirane was the only final oxidation product observed upon direct photolysis of reactant pairs. While in the case of the trans 2-butene reaction stereochemical retention was complete, it was found that in the cis case 85% of the oxirane with retained configuration when conducting the reaction at low matrix concentration. This fraction decreased with increasing reactant to matrix ratio. Infrared bands of two conformers of a butyl nitrite radical were observed concurrently with the oxirane, one with syn, the other with anti conformation about the central C-C bond (with respect to the CH_3 groups). A correlation was found between the syn to anti nitrite radical and the cis to trans oxirane ratios in the case of the cis 2-butene:NO_2 reaction, suggesting a common transient precursors. It is most probably an oxirane biradical, whose conformation determines the stereochemistry of the oxirane product.

(4) 2-Methylpropene

The structure and dynamics of an intermediate in the photooxidation of 2-methylpropene by nitrogen dioxide excited at visible wavelengths (610 - 570 nm) were studied by low-temperature matrix-isolation FT-infrared spectroscopy. The reaction intermediate showed the most intense bands at 1644 cm^{-1} and 754 cm^{-1}, which are assignable to be N=O stretching and O-N stretching bands of 2-methylpropyl nitrite radical, respectively. The first order rate constants, obtained from an analysis of time dependence of the infrared absorption, are compared with those for other butenes.

(5) 2,3-Dimethyl-2-butene

Red light-induced oxygen atom transfer from NO_2 to 2,3-dimethyl-2-butene has been investigated in a low-temperature argon matrix. The infrared spectra of a reaction intermediate identified as an alkyl nitrite radical and two final products, tetramethyloxirane and 3,3-dimethyl-2-butanone (pinacolone), were observed. From analysis of the absorbance growth of the infrared bands, first-order rate constants were determined by least-square fittings. A reaction mechanism is proposed that involves oxygen atom transfer from NO_2 to the C=C bond of 2,3-dimethyl-2-butene to give a short-lived singlet oxirane biradical. Alkyl nitrite

radical is produced by a recombination of the transient biradical with NO trapped in the cage of the matrix. Tetramethyloxirane and pinacolone emerge from secondary photolysis of the trapped alkyl nitrite radical.

(6) Butadiene, 2-Methylbutadiene, and 2,3-Dimethylbutadiene

Visible light induced oxygen atom transfer from NO_2 to conjugated dienes has been investigated in a low temperature Ar matrix, where the dienes are 1,3-butadiene, 2-methyl-1,3-butadiene, and 2,3-dimethyl-1,3-butadiene. In each diene/NO_2/Ar system, the corresponding nitrite radical, oxirane, aldehyde, and NO were obtained as the photochemical reaction products. The reactions are initiated by the formation of undetectable short-lived oxirane biradical and NO due to visible light induced oxygen atom transfer from NO_2 to the conjugated dienes. (1) The recombination of oxirane biradicals and neighboring NO gives the nitrite radicals as the photochemical intermediate. (2) The ring closure of the biradicals leads to the formation of oxiranes. (3) The intramolecular H atom transfer of biradicals leads to the formation of aldehydes. The visible photolysis of the nitrite radicals gives rise to oxirane, aldehyde, and NO. The reaction rates are derived by measuring the absorbance changes of the products upon the 582 nm irradiation. The methyl substituent effect on the reactivity is discussed.

(7) Propadiene (Allene) and 2-Butyne (2,3-Dimethylacetylene)

Oxygen atom transfer from NO_2 to allene and dimethylacetylene was observed upon excitation of reactant pairs in solid Ar at wavelength as long as 585 nm (NO_2 + allene) and 610 nm (NO_2 + dimethylacetylene). Continuous wave dye laser radiation was used to initiate reaction, and product growth was monitored by FT-infrared spectroscopy. In the case of the allene + NO_2 reaction 2-allyl nitrite radical was obtained as product, while excitation of dimethylacetylene:NO_2 pairs gave acetylmethyliminoxy radical and dimethylketene + NO. Structures of products were determined by ^{15}N and ^{18}O isotopic substitution and, in the case of allyl nitrite radical, by observation of photodissociation products allene oxide and cyclopropanone. The observed radicals constitute transient biradicals formed upon oxygen atom transfer that are chemically trapped by NO cage coproduct. Interpretation by aid of literature ab initio results indicates that in the case of allene + NO_2 the observed nitrite radical is 2-allenylidoxy biradical trapped in a B_1excited state. The iminoxy radical product of the dimethylacetylene photooxidation is a trapped singlet excited acetylmethylene biradical. This is the first insight into O atom transfer paths involving cummulene and CC triple bonds gained by chemical trapping of excited state biradicals.

(8) Methylamine

The visible light-induced reaction of NO_2 with methylamine in a cryogenic argon matrix has been investigated using an FT-infrared spectrometer. The photochemical products were identified as methyleneimine, water and nitric oxide. This photoin-

duced dehydrogenation reaction is interpreted by the following reaction sequence: (1) photoexcitation of NO_2, (2) oxygen atom transfer from excited NO_2 to methylamine and (3) isomerization from the methylamine N-oxide to methylhydroxylamine (intramolecular hydrogen atom migration), followed by (4) dissociation into methyleneimine and water. It was confirmed by the infrared spectrum that two of the dissociation products interact with each other in the matrix cage. This reaction mechanism is also supported by the formation of CD_2=NH:HDO in the CD_3NH_2:NO_2 system.

References

(1)"Vibronic excitation of O atom transfer from NO_2 to ethylene by long wavelength visible light in a cryogenic matrix", M. Nakata, K. Shibuya, and H. Frei, J. Phys. Chem., 94(21)8168-8175(1990).

(2)"Stereoselective photooxidation of trans 2-butene to epoxide by nitrogen dioxide excited with red light in a cryogenic matrix", M. Nakata and H. Frei, J. Am. Chem. Soc., 111(14)5240-5247 (1989).

(3)"Stereocontrol of the red light induced photo-epoxidation of 2-butenes by nitrogen dioxide in solid Ar", M. Nakata and H. Frei, J. Phys. Chem., 93(22)7670-7877(1989).

(4)"Stereoselective photooxidation of butenes by electronically excited NO_2: Structure and dynamics of intermediates", M. Nakata and H. Frei, J. Chem. Soc. Jpn., 1412-1417(1989).

(5)"Red light-induced reaction of NO_2 with 2,3-dimethyl-2-butene in a low-temperature Ar matrix", M. Nakata, Spectrochim. Acta, 50(8/9)1455-1465(1994).

(6)"Visible light induced reactions of NO_2 with conjugated dienes in a low-temperature Ar matrix", N. Tanaka, Y. Kajii, K. Shibuya, and M. Nakata, J. Phys. Chem., 97(27)7048-7053(1993).

(7)"Chemical trapping of electronically excited biradicals upon visible light-induced oxygen-atom transfer from NO_2 to allene and dimethylacetylene in a cryogenic matrix", M. Nakata and H. Frei, J. Am. Chem. Soc., 114(4)1363-1372 (1992).

(8)"Photoinduced dehydrogenation reaction of CH_3NH_2 by NO_2 in a cryogenic Ar matrix identification of the CH_2=NH:H_2O complex", N. Tanaka, J. Oike, Y. Kajii, K. Shibuya, and M. Nakata, Chem. Phys. Lett., 232,109-114(1995).

14. Study of Relaxation Processes Following Laser Irradiation of Small Molecules Doped in Rare Gas Low-Temperature Crystals

-Vibrational Reluxation of Ground State O_2 and related processes in low temperature rare gas crystals-

Hideo Kajihara and Seiichiro Koda

Department of Chemical System Engineering, Faculty of Engineering, The University of Tokyo, Hongo 7-3-1, Bunkyo-ku, Tokyo 113, Japan

Abstract

The UV absorption spectrum of O_2 doped in a low-temperature Ar crystal, when excited by ArF or KrF excimer laser, showed banded absorption lines. These lines were assigned to the transitions from vibrationally excited levels of ground state O_2(v"=4-12) to vibrational levels of B state(v'=0-6). The absorption intensity from higher vibrational levels decayed monotonically after interruption of laser irradiation, while some lower vibrational levels showed intensity increase followed by decrease. These time behaviors were interpreted by the mechanism incorporating the relaxation through X state vibrational manifold and cross-relaxation with absorption of the exciting laser light by the vibrationally and/or electronicallyexcited O_2 molecules. The vibrational relaxation rate is considerably slow with time constant of 10-200 seconds.

1. Introduction

In order to understand many-body interaction behavior in solids, we have studied relaxation processes of small molecules after laser excitation in low-temperature crystals (O_2 in Ar crystal[1], O_2 in N_2 crystal [2], O_2 in D_2 matrix[3], N_2 in N_2 crystal[4] and OCS in Xe crystal[5]). In the previous studies of the relaxation of O_2 [1,2], we have employed the fluorescence spectroscopy and analysed the time behavior of the electronically excited states after laser irradiation. In the present study following the previous preliminary report[6], we have adopted the UV absorption method in order to trace the vibrationally excited molecules in the ground electronic state. Absorption method is

favorable to obtain an absolute value of concentration. On the basis of time behavior of individual vibrational levels, the relaxation process of the excited O_2 by ArF or KrF excimer laser will be discussed.

2. Method

A free-standing Ar crystal containing small amount (0.16% or1%) of O_2 of a cubic structure of around $1cm^3$ and of a 1cm optical pass length was prepared according to the method of Schwentner and co-workers [7]. The latter method is adequate for preparing a free-standing crystal of a relatively large volume which is composed of constituent grains of several-100μm sizes.

The procedure for the preparation of a free standing crystal is as follows. A bottomless glass cup of $10x10x20mm^3$ of volume equipped with a gas inlet tube was pressed against a copper cryotip, which was kept at 16K (by a closed-cycle refrigerator) in a vacuum chamber. The crystal was grown in the cup for 20 min by deposition of the gas mixture of O_2 and Ar at a total pressure of 150-250 Torr. The deposition rate was ca. 1.6×10^{-3} mol min^{-1}. The gases were obtained commercially in cylinders: nominal O_2 purity, 99.999%; nominal Ar purity, 99.9999%. The required amount of O_2 was mixed to the gaseous Ar in advance.

The sample held at 16K was irradiated by ArF or KrF excimer laser (typical laser fluence, ArF:1 mJ $pulse^{-1}cm^{-2}$, KrF: 10 mJ $pulse^{-1}$ cm^{-2}, repetition rate, 10Hz) through a quartz window of the vacuum chamber. In order to obtain the absorption spectrum, the sample crystal was irradiated with a deuterium lamp from the perpendicular direction to the laser beam during and after the laser irradiation. Transmission light through the sample crystal was collected by quartz lenses, resolved by a monochromator (Nikon P-250) and detected by an appropriate photomultiplier (Hamamatsu Photonics R928, detection range: 185-850nm). The output signal from the photomultiplier was amplified and then treated by PC.

3. Result

A lot of sharp absorption lines were observed in the uv range when the sample crystal was under irradiation by ArF or KrF excimer laser as shown in Fig.1 for the case of ArF laser irradiation. The absorption intensity of these peaks reached almost constant values after continuous laser irradiation for several minutes. Comparing the absorption peak wavelengths with those deduced using molecular constants of the ground state O2[8] and also those of the B state O_2 [9,10] in Ar, these lines were assigned to the transitions from vibrationally excited levels (v"=4-12) of $X(^3\Sigma g^-)$ state to vibrational levels(v'=0-6) of $B(^3\Sigma u^-)$ state. The absorption lines from X(v"=9) to B state could not be observed.

The time evolution of the absorption intensity of individual lines after the interruption of laser light was pursued. The values of ln(I0/I) for several vibrational levels, which are proportional to the population are plotted against the elapsed time after the interruption of the laser irradiation in Figs.2 and 3. While the population of most of the higher vibrational levels monotonically decreased, some lower vibrational levels showed the intensity increase followed by decrease. In the case of higher vibrational levels, the decrease curve approximately obeyed a single-exponential decay. In most of the other cases, the time behavior could be analysed by emplying two exponential terms (one is rising, and the other is decaying). The obtained decay-time constants with some rise-time constants are tabulated in Table 1.

The decay-time constants of the vibrationally excited levels are surprisingly long. Both of the decay- and rise-time constants of lower vibrational levels are larger than those of higher vibrational levels. It is also important to note that the rise-time constant of a v-1 level is usually smaller than the decay-time constant of the higher v level.

4. Discussion

4.1 Processes for populating X, a and b electronic states

We have previously observed A'-X and c-a emissions from O_2

molecules diluted in a low-temperature Ar crystal, being irradiated with an ArF excimer laser[1]. The relaxation process of O_2 was considered as follows. When O_2 is excited by the ArF excimer laser light at 193 nm whose energy is larger than the dissociation energy, most of the excited molecules dissociate along the repulsive curves (Schmann-Runge predissociation and/or Herzberg continuum). While the produced $O(^3P)$ atoms depart permanently in the gas phase, they are recombined in the crystal after being repelled at the cage wall to form the A, A' or c states, though the branching fractions into the individual Herzberg state are not determined. Correspondingly, strong uv-vis emission bands were observed, which were assignable to A'(v'=0)-X and c(v'=5)-a transitions. The lifetime of the emissions were 80μs and 80 ns, respectively. On the other hand, under the KrF excimer laser irradiaiton at 248 nm, the O_2 molecules absorb the laser light to reach the v'=9 level of Ω= 1 component and/or the v'=10 level of Ω= 3 component of A' state. The nascent population of c state is considered to be much smaller in the KrF laser than ArF excimer laser irradiation. Indeed, the difference was reflected to the stronger c-a emissions observed in the ArF excimer laser irradiation.

As mentioned above, O_2 molecules irradiated with 193nm and/or 248nm light are considered to relax to the X and a, and probably to b electronic state from the A', A and c Herzberg manifolds mainly via radiative process within 1 ms. In fact, the emissions assignable to a-X and b-X were observed in previous literatures [8], the lifetimes of which were 79s and 24.5ms, respectively.

By using the estimated absorption coefficients for the B-X transitions, the concentrations of v=6 and 7 levels are estimated from the absorption intensity observed in Fig. 2 to be in the order of 10^{14} molecules cm^{-3} under the ArF excimer laser irradiation (1 mJ $pulse^{-1}$, 10 Hz repetition). At the same time, almost equal or larger population than the A' levels are expected to exist steadily in lower vibrational levels of a state.

4.2 Time evolution of vibrationally excited levels of X state

In order to explain why some intermediate vibrational levels of X state showed the intensity increase followed by decrease after the interruption of the laser irradiation, we take into account the possibility that some levels of the O_2 molecules in X and/or a states are absorbing the excitation laser during the irradiation. If the level is absorbing the laser light and being depleted to some extent due to the absorption during the irradiation, the population of the level is expected to increase at first after the interruption of the laser irradiation, because the feed from higher levels (radiatively or non-radiatively) still exist but the depletion due to the laser absorption is now stopped. In this mechanism, the rise-time corresponds to the decrease of the population of the higher levels. Cosidering the favorable Franck-Condon factors of the B-X transition for higher vibrational levels of X state, efficient absorption of the excimer laser lights via B-X transiton is plausible. Transitions from a state to Herzberg continuum may also occur to some extent.

The important fact to note is that the rise-time constant of a v-1 level does not coincide with the decay-time constant of the v level. This fact denies the exclusive contribution of the sequential relaxation which loses a single vibrational quantum step-wise in the X electronic state. Some interstate cascading from a state to X state may be opperative above the v=0 level of a state, in order to explain the faster population feed than the decay of the vibrational level of higher quantum number by one.

It is interesting to note that absorption lines from the v=9 level of X state are not observed. This lack is considered to be caused by the population transfer from X state to b state at this particular level. The energy levels are very close to each other between X(v=9-11) and b(v=0-2) levels. Although the energy of X(v≥10) state is lower than that of b(v≥1) state, the energy level of X (v=9) are 42cm^{-1} higher than the b (v=0) level [8]. Thus the X(v=9) level can't have a long lifetime because of rapid population transfer.

4.3 Vibrational relaxation rate

Time resolved relaxation measurement of the absorption intensity after the interruption of the laser irradiation shows an extremely slow vibrational relaxation in the ground state. We have not yet analysed the network of the vibrational relaxation taking into account all possible elementary relaxation processes including vibration-vibration energy transfer between O_2 molecules. Thus the tabulated decay-time constants should not be taken as the intrinsic lifetime of individual levels. Salloum and Dubost [11] have also obtained similar relaxation time constants. In their experiments, they have adopted vibratinal energy transfer from vibrationally excited CO to O_2 in order to prepare higher vibrational levels of O_2. Thus their solids always contain CO, which may make the total network analysis more formidable.

Two reasons for the slow relaxation are: 1) the very large difference between the phonon energy of Ar lattice and vibrational quantum, from which the rate of phonon assisted radiationless relaxation is expected to be very slow, 2) no dipole allowed radiative transition in O_2.

5. Conclusions

When O2-doped Ar crystal was irradiated by ArF or KrF excimer laser, absorption lines which were assigned to the transitions from highly vibrationally excited levels(v"=4-12) of ground state to electronically excited B state were observed in UV absorption spectra. Time resolved measurement of absorption intensity showed that vibrational relaxation of ground state was very slow due to the very large difference between the vibrational quantum and the phonon quantum of Ar lattice. Absorption of laser light not only by the initial O_2 but also by O_2 in excited levels is considered to be important in order to explain the initial intensity rise in some vibrationally excited levels after the interruption of the laser irradiation.

Acknowledgment

This work was supported by the Grant-in-Aids from the Minisitry of Education, Science and Culture of Japan (No. 05044080) , which is greatly appreciated. H. K is also grateful to the support by the Research Fellowship of the Japan Society for the Promotion of Science for Young Scientists.

References

[1] F. Okada, H. Kajihara and S. Koda, Chem. Phys. Lett. 192, 357 - 361(1992).

[2] H. Kajihara, T. Okamura, F. Okada and S. koda, Laser Chemistry, 15, 83-92 (1995).

[3] A. V. Danilychev, V. E. Bondybey, V. A. Apkarian, S. Tanaka, H. Kajihara, and S., Koda, J. Chem. Phys., in press (1995).

[4] H. Kajiahra, F. Okada, and S. Koda, Chem. phys., 186, 395-400 (1994).

[5] S. Tanaka, H. Kajihara, S. Koda, and V. A. Apkarian, Chem. Phys. Lett., 233, 555-558 (1995).

[6] H. Kajihara, T. Okamura, and S. Koda, "Proceeding of Yamada Conference XLIII on Structures and Dynamics of Clusters", Shimoda, Shizuoka, Japan (1995), in press.

[7] N. Schwentner, O. Doessel and H. Nahme, in: Laser techniques for extreme ultraviolet spectroscopy, AIP Conf. Proc., 90 (1982), p.163.

[8] A. C. Becker, U. Schrath, H. Dubost and J. P. Galoup, Chem. Phys. 125, 321 (1988)

[9] A. M. Bass and H. P. Broida, J. Mol. Spec. , 12, 221 (1964).

[10] E. Boursey, J. Roncin and N. Damany, Chem. Phys. Lett., 5, 584- (1970).

[11] A. Salloum and H. Dubost, Chem. Phys. 189, 179 (1994)

Table 1 The decay time constants and rise time constants of vibrationally excited O2

Concentration	O2/Ar:1/600		O2/Ar:1/100
Excitation	ArF(193nm)		KrF(248nm)
v″	τ (decay)/s	τ (rise)/s	τ (decay)/s
12	15		6
11	27		11
10	33		35
9	-		-
8	69		41
7	94	16	44
6	106	27	63
5	114	43	72
4			97

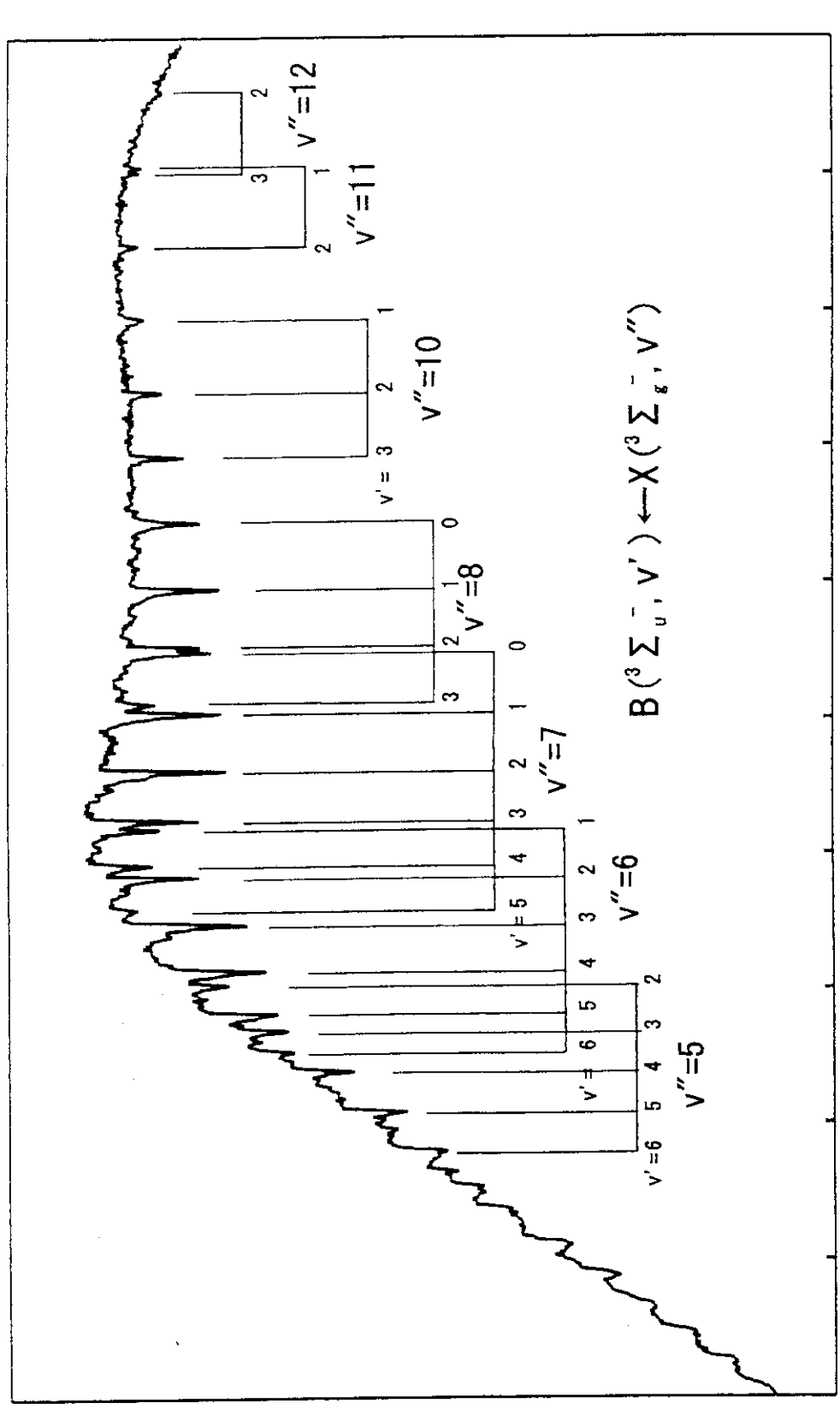

Fig. 1 Absorption spectra of O_2 excited by ArF excimer laser in Ar solid

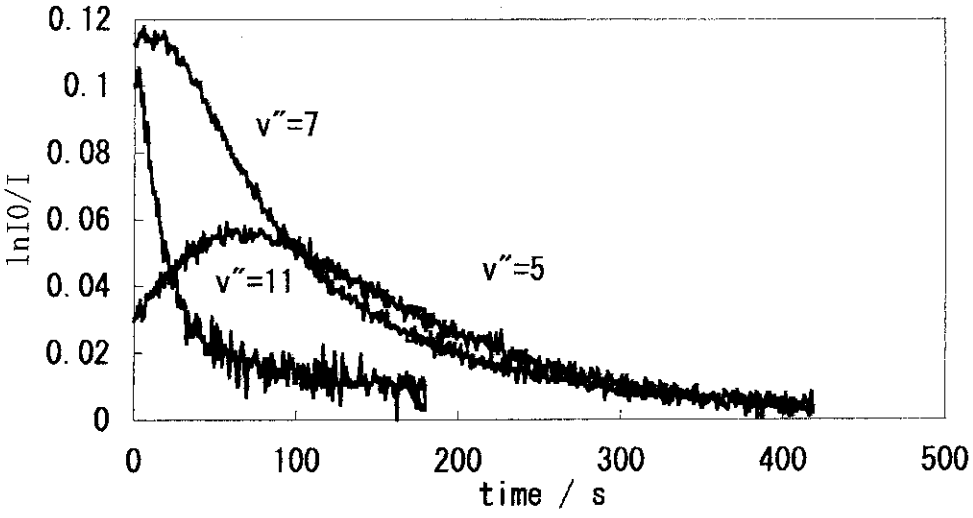

Fig.2 Time evolution of populations of individual levels after the interruption of ArF laser light

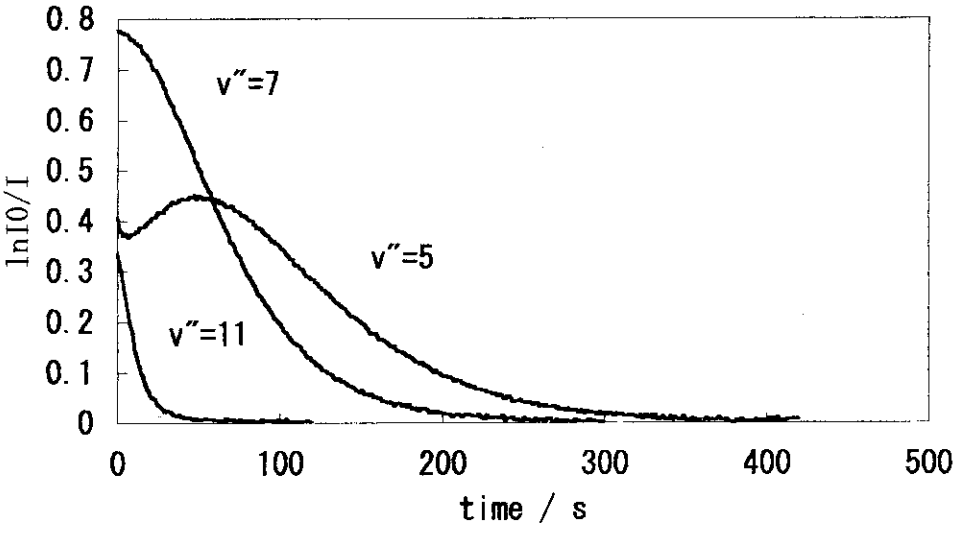

Fig.3 Time evolution of population of individual levels after the interruption of KrF laser light